AD-A120 952 LOCALIZED IMPACT DAMAGE IN CERAMICS(U) CERAMIC FINISHING CO STATE COLLEGE PA H P KIRCHNER ET AL. 31 AUG 82 N00014-74-C-0241 1/2

UNCLASSIFIED F/G 11/2 NL

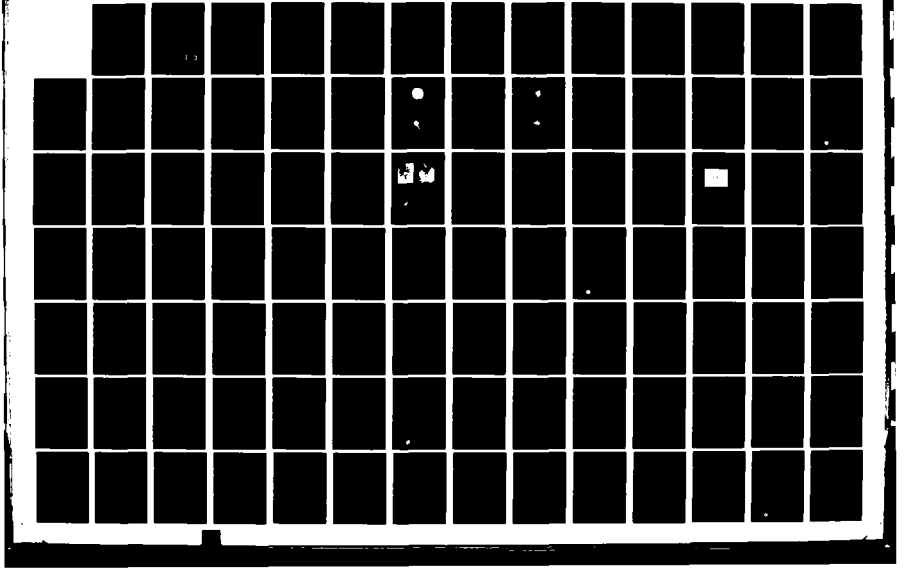

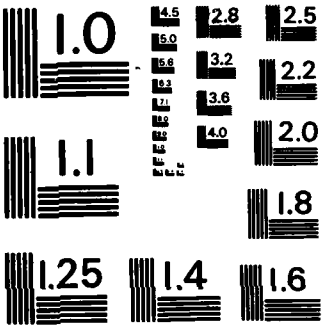

CERAMIC FINISHING COMPANY

State College, Pennsylvania

FINAL REPORT

LOCALIZED IMPACT DAMAGE IN CERAMICS

Contact Damage in Hot Pressed and CVD Zinc Sulfide
Comparisons of Static and Impact Loading Damage in Zinc Sulfide
Load-Radial Crack Length Relations for Spherical Indentations in Hot Pressed ZnS
Elastic Recovery at Static Loading and Impact Indentations in MgF_2
Effect of Mechanical Impedance Ratio on the Distribution of Stress Wave Energy During Particle Impact

August, 1982

Prepared by: H. P. Kirchner
D. M. Richard
T. J. Larchuk
J. A. Tiracorda
J. A. Ragosta
C. S. Cannon

Prepared under Contract No. N00014-74-C-0241 for the Office of Naval Research, Department of the Navy Requisition No. NR032-545/12-17-73 (471)

SECURITY CLASSIFICATION OF THIS PAGE (When Data Entered)

REPORT DOCUMENTATION PAGE

READ INSTRUCTIONS BEFORE COMPLETING FORM

1. REPORT NUMBER	2. GOVT ACCESSION NO. AD-A120952
3. RECIPIENT'S CATALOG NUMBER	
4. TITLE (and Subtitle) LOCALIZED IMPACT DAMAGE IN CERAMICS	5. TYPE OF REPORT & PERIOD COVERED Technical Report Feb. 1, 1980 - Aug. 31, 1982
	6. PERFORMING ORG. REPORT NUMBER
7. AUTHOR(s) H. P. Kirchner, D. M. Richard, T. J. Larchuk, J. A. Tiracorda, J. A. Ragosta, C. S. Cannon	8. CONTRACT OR GRANT NUMBER(s) N00014-74-C-0241
9. PERFORMING ORGANIZATION NAME AND ADDRESS Ceramic Finishing Company P. O. Box 498 State College, Pa. 16801	10. PROGRAM ELEMENT, PROJECT, TASK AREA & WORK UNIT NUMBERS
11. CONTROLLING OFFICE NAME AND ADDRESS Office of Naval Research (Code 471) Department of the Navy Arlington, Virginia 22217	12. REPORT DATE August 31, 1982
	13. NUMBER OF PAGES 132
14. MONITORING AGENCY NAME & ADDRESS(if different from Controlling Office)	15. SECURITY CLASS. (of this report) Unclassified
	15a. DECLASSIFICATION/DOWNGRADING SCHEDULE

16. DISTRIBUTION STATEMENT (of this Report)

Distribution of this document is unlimited

17. DISTRIBUTION STATEMENT (of the abstract entered in Block 20, if different from Report)

18. SUPPLEMENTARY NOTES

19. KEY WORDS (Continue on reverse side if necessary and identify by block number)

ceramics, stress waves, elastic recovery, localized impact damage, radial cracks, lateral cracks, magnesium fluoride, zinc sulfide, glass, mechanical impedance, residual stresses, fracture

20. ABSTRACT (Continue on reverse side if necessary and identify by block number)

The following topics are covered in this report:

1. Contact Damage in Hot Pressed and CVD Zinc Sulfide,
2. Comparisons of Static and Impact Loading Damage in Zinc Sulfide,
3. Load-Radial Crack Length Relations for Spherical Indentations in Hot Pressed ZnS,

DD FORM 1 JAN 73 1473 EDITION OF 1 NOV 65 IS OBSOLETE

SECURITY CLASSIFICATION OF THIS PAGE (When Data Entered)

4. Elastic Recovery at Static Loading and Impact Indentations in MgF_2, and

5. Effect of Mechanical Impedance Ratio on the Distribution of Stress Wave Energy During Particle Impact.

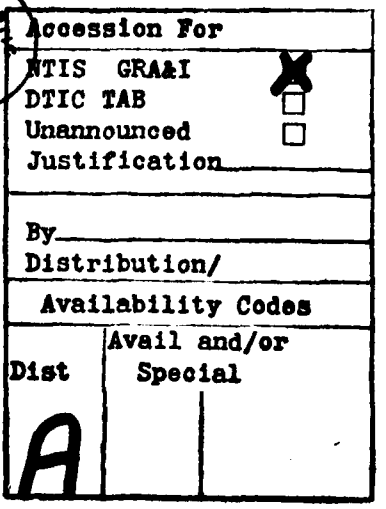

Ceramic Finishing Company
State College, Pennsylvania

FINAL REPORT

LOCALIZED IMPACT DAMAGE IN CERAMICS

Contact Damage in Hot Pressed and CVD Zinc Sulfide
Comparisons of Static and Impact Loading Damage in Zinc Sulfide
Load-Radial Crack Length Relations for Spherical Indentations in Hot Pressed ZnS
Elastic Recovery at Static Loading and Impact Indentations in MgF_2
Effect of Mechanical Impedance Ratio on the Distribution of Stress Wave Energy During Particle Impact

August, 1982

Prepared by: H. P. Kirchner
D. M. Richard
T. J. Larchuk
J. A. Tiracorda
J. A. Ragosta
C. S. Cannon

Prepared under Contract No. N00014-74-C-0241 for the Office of Naval Research, Department of the Navy
Requisition No. NR032-545/12-17-73 (471)

TABLE OF CONTENTS

FOREWORD

This summary report describes research performed on a program sponsored by the Office of Naval Research, Department of the Navy, under contract N00014-74-C-0241. The research was performed under the general technical direction of Dr. Robert Pohanka and Dr. Arthur M. Diness, Metallurgy Branch, Office of Naval Research.

The report covers work performed during the period of February 1, 1980 to August 31, 1982. The writers are pleased to acknowledge the contributions of their associates at Ceramic Finishing Company.

I. INTRODUCTION

Research on this contract which extended from 1974 to 1982 has included the following topics related to localized impact damage:

1. Development of a comprehensive analytical model for elastic-plastic impact by particles for calculating the contact radius, indentation radius, impact force, penetration time, depth of damage, remaining strength, contact time and coefficient of restitution.
2. Localized impact damage in stressed members consisting of glass, alumina and silicon nitride.
3. Branching of Hertzian cracks.
4. Energy loss mechanisms during impact.
5. Impact on a viscous medium (glass).
6. Impact damage in transformation toughened zirconia.
7. Comparison of static and impact damage in ZnS.
8. Load-radial crack size relations in ZnS.
9. Comparisons of contact damage in hot pressed and CVD ZnS.
10. Elastic recovery at static loading and impact indentations in MgF_2.
11. Effect of mechanical impedance on the distribution of stress wave energy during impact.

12. Methods of improving the impact damage resistance of ceramics including low elastic midulus surface layers, friable surface layers and compressive surface layers (silicon nitride, silicon carbide, alumina, stc.).

In addition to the above topics which directly involve contact damage, the following supporting research topics were investigated:

1. Crack branching in ceramics.
2. Strengthening by heat treatments.
3. Strengthening by compressive surface stresses including preparation of a monograph on this topic.
4. Comparisons of flaws at fracture origins in various ceramics.
5. Crack growth from small flaws in larger grains in alumina.

The results of these investigations show that, at least in some cases, reasonable predictions of crack propagation and strength degradation are possible. The impact damage resistances of a variety of ceramics can be improved by surface treatment. Increasing the fracture toughness (K_{IC}) of the underlying material is also effective. The roles of hardness and Young's modulus are more complex in the impact case compared with the static case because of the effect of these properties on the impact load and stress wave energy.

The present report consists of five papers which are presented as separate sections. A list of papers, reports and presentations follows.

LIST OF PAPERS, REPORTS AND PRESENTATIONS

H. P. Kirchner, R. B. Gruver and W. A. Sotter, "Use of Fracture Mirrors to Interpret Impact Fractures in Brittle Materials," Presented at the Annual Meeting, American Ceramic Society (May, 1974) J. Amer. Ceram. Soc. 58 (5-6) 188-191 (May-June 1975).

H. P. Kirchner and W. A. Sotter, "Comparisons of Fracture Mirrors in Flint Glass Fractured Under Various Loading Conditions," Ceramic Finishing Company Technical Report No. 1, Contract N00014-74-C-0241 (May, 1974).

H. P. Kirchner and J. Seretsky, "Improving Impact Resistance by Energy Absorbing Surface Layers," Bull. Amer. Ceram. Soc. 54 (6) 591-592 (June, 1975). (Partially supported by NASA).

H. P. Kirchner, W. A. Sotter and R. M. Gruver, "Strengthening Hot Pressed Si_3N_4 by Heating and Quenching," Presented at the Fall Meeting, Basic Science Division, American Ceramic Society (October, 1974). J. Amer. Ceram. Soc. 58 (7-8) 353 (July, August, 1975). Partially supported by NASA.

H. P. Kirchner, R. M. Gruver and W. A. Sotter, "The Variation of Fracture Mirror Radius with Fracture Stress for Polycrystalline Ceramics under Various Loading Conditions." Ceramic Finishing Company Technical Report No. 2, Contract N00014-74-C-0241 (November, 1974).

R. M. Gruver and H. P. Kirchner, "Effect of Leached Surface Layers on Impact Damage and Remaining Strength of Silicon Nitride," Presented at the Annual Meeting, American Ceramic Society (May, 1975). J. Amer. Ceram. Soc. 59 (1-2) 85-86 (January, February, 1976).

H. P. Kirchner, R. M. Gruver and W. A. Sotter, "Fracture Stress-Mirror Size Relations for Polycrystalline Ceramics," Presented at the Annual Meeting, American Ceramic Society (May, 1975), Phil. Mag. 33 (5) 775-780 (1976).

H. P. Kirchner, R. M. Gruver and W. A. Sotter, Comparisons of Flaws at Fracture Origins in Various Ceramics." Presented at the Annual Meeting, American Ceramic Society (May, 1975). Mater. Sci. Eng. 22, 147-156 (1976). (Partially supported by NASC).

H. P. Kirchner, "Strength Degradation of Polycrystalline Ceramics Caused by Localized Impact Damage," Presented at ONR Contractors Meeting, LaJolla 23, 24, July, 1975.

H. P. Kirchner, R. M. Gruver and C. S. Miller, "Localized Impact Damage in Hot Pressed Si_3N_4 and SiC," Presented at the Fall Meeting, Basic Science Division, American Ceramic Society (September, 1975).

H. P. Kirchner, "Localized Impact Damage and Other Impact Responses of Ceramics," Presented at the Graduate Seminar in Ceramics, Penn State University (October 24, 1975).

H. P. Kirchner and R. M. Gruver, "Localized Impact Damage in Ceramics," Ceramic Finishing Company Technical Report No. 4, Contract N00014-74-C-0241 (June, 1976).

H. P. Kirchner, "Criteria for Fracture Mirror Boundary Formation in Ceramics," Presented at the Second International Conference on Mechanical Behavior of Materials, Boston (August, 1976). Published in the proceeding of the conference, pages 1317-1321.

H. P. Kirchner and R. M. Gruver, "Localized Impact Damage in Glass," Presented at the Annual Meeting American Ceramic Society, May 5, 1976, Mater. Sci. Eng. 28 (1) 153-160 (1977).

H. P. Kirchner and R. M. Gruver, "Branching of Hertz Cracks," Presented at the Fourth International Conference on Fracture, Waterloo, Canada (June, 1977), Fracture 1977, Volume 3, Pages 959-964.

H. P. Kirchner and R. M. Gruver, "Localized Impact Damage in Stressed Members," Mater. Sci. Eng. 28 (2) 249-255 (1977).

H. P. Kirchner and R. M. Gruver, "Localized Impact Damage on Ceramics," Ceramic Finishing Company Technical Report No. 5, Contract N00014-74-C-0241 (January, 1977).

H. P. Kirchner, "Crack Branching in Ceramics," Seminar presented at Alfred University (October, 1977).

H. P. Kirchner, "Analysis of Localized Impact Damage in Biaxially Stressed Glass Plates," Presented at the Annual Meeting, American Ceramic Society (April, 1977), J. Amer. Ceram. Soc. 61 (3-4) 161-163 (1978).

H. P. Kirchner and R. M. Gruver, "The Effect of Localized Damage on Energy Losses During Impact," Presented at the Annual Meeting, American Ceramic Society (April, 1977), Mater. Sci. Eng. 33, 101-106 (1978).

H. P. Kirchner and R. M. Gruver, "Localized Impact Damage in a Viscous Medium (Glass)," Presented at the International Symposium on Fracture Mechanics of Ceramics, Penn State University (July, 1977), Fracture Mechanics of Ceramics, Vol. 3, Edited by R. C. Bradt, F. F. Lange and D. P. H. Hasselman, Plenum, New York (1978), p. 365-377.

H. P. Kirchner, "The Strain Intensity Criterion for Crack Branching in Ceramics," Engineering Fracture Mechanics 10, 283-288 (1978).

H. P. Kirchner and R. M. Gruver, "Localized Impact Damage in Stressed Al_2O_3 and Si_3N_4," Mater. Sci. Eng. 34, 25-31 (1978).

H. P. Kirchner and J. W. Kirchner, "Fracture Mechanics of Fracture Mirrors," Presented at the Fall Meeting, Basic Science Division, American Ceramic Society (September, 1977), J. Amer. Ceram. Soc. 62 (3-4) 198-202 (1979).

D. B. Marshall, B. R. Lawn, H. P. Kirchner and R. M. Gruver, "Contact Induced Strength Degradation in Thermally Treated Al_2O_3," J. Amer. Ceram. Soc. 61 (5-6) 271-272 (1978).

H. P. Kirchner, R. M. Gruver and J. W. Kirchner, "Localized Impact Damage in Ceramics," Ceramic Finishing Company Technical Report No. 6, Contract N00014-74-C-0241 (January, 1978).

H. P. Kirchner, R. C. Garvie, R. M. Gruver and D. M. Richard, "Localized Impact Damage in Transformation Toughened Zirconia," Presented at the Annual Meeting, American Ceramic Society (1978), Mater. Sci. Eng. 40, 49-57 (1979).

H. P. Kirchner, R. M. Gruver, M. V. Swain and R. C. Garvie, "Crack Branching in Transformation Toughened Zirconia," Presented at the Fall Meeting, Basic Science Division, American Ceramic Society, (1979). J. Amer. Ceram. Soc. 64 (9) 529-533 (1981).

D. M. Richard and H. P. Kirchner, "Theory of Elastic-Plastic Impact on Ceramics," Presented at the Conference on Erosion by Liquid and Solid Impact, Cambridge University (September 3-6, 1979). Published in the proceedings of the conference, pages 27-1 through 27-10.

H. P. Kirchner, "Strengthening of Ceramics: Treatments, Tests, and Design Applications," Marcel Dekker, New York (1979).

H. P. Kirchner, R. M. Gruver, D. M. Richard and R. C. Garvie, "Localized Impact Damage in Ceramics," Ceramic Finishing Company Technical Report No.7, Contract N00014-74-C-0241 (January, 1979).

H. P. Kirchner and J. M. Ragosta, "Crack Growth from Small Flaws in Larger Grains in Alumina," Presented at the Fall Meeting, Basic Science Division, American Ceramic Society (October, 1979). J. Amer. Ceram. Soc. 63 (9-10) 490-495 (1980).

D. M. Richard and H. P. Kirchner, "Theory of Elastic-Plastic Impact," Presented at the ONR Contractors Meeting, National Bureau of Standards (June 26-27, 1979).

H. P. Kirchner and T. J. Larchuk, "Radial Crack Propagation During Contact Fracture of Zinc Sulfide," Presented at the Annual Meeting, American Ceramic Society (April 30, 1980).

H. P. Kirchner, T. J. Larchuk and J. M. Ragosta, "Localized Impact Damage in Ceramics," Ceramic Finishing Company Technical Report No. 8, Contract N00014-74-C-0241 (February, 1980).

H. P. Kirchner and T. J. Larchuk, "Localized Impact Damage in Ceramics: Comparisons of Recent Experiments and Theoretical Calculations," Ceramic Finishing Company Informal Report, Contract N00014-74-C-0241 (July, 1980).

H. P. Kirchner and T. J. Larchuk, "Comparisons of Static and Impact Loading Damage in Zinc Sulfide." Submitted for Publication.

H. P. Kirchner and T. J. Larchuk, "Load-Radial Crack Size Relations for Static Indentations in Zinc Sulfide," J. Amer. Ceram. Soc. 64 (2) C27,28 (1981).

H. P. Kirchner and T. J. Larchuk, "Variation of Crack Length with Load and K_{IC} for Spherical Indentations in Transformation Toughened Zirconia," Presented at the International Symposium on Fracture Mechanics of Ceramics, July 17, 1981, To be published in the proceedings of the symposium.

H. P. Kirchner, J. A. Tiracorda and T. J. Larchuk, "Comparisons of Contact Damage in CVD and Hot Pressed Zinc Sulfide," Presented at the Annual Meeting, American Ceramic Society (1981), Submitted for publication.

H. P. Kirchner, "Applications of Contact Fracture Mechanics to Particle Impact and Grinding Damage," Seminar presented at Penn State University (November 5, 1981).

H. P. Kirchner, J. A. Ragosta and C. S. Cannon, "Load-Radial Crack Length Relations for Spherical Indentations in Hot Pressed ZnS," Submitted for publication.

H. P. Kirchner, J. A. Tiracorda and T. J. Larchuk, "Elastic Recovery at Static Loading and Impact Indentations in MgF_2," Submitted for publication.

D. M. Richard and H. P. Kirchner, "Effect of Mechanical Impedance on the Distribution of Stress Wave Energy During Particle Impact," To be submitted for publication.

CONTACT DAMAGE IN HOT PRESSED AND CVD ZINC SULFIDE

by

H. P. Kirchner
J. A. Tiracorda
T. J. Larchuk

ABSTRACT

Hot pressed zinc sulfide was indented by spherical indenters under static and impact loading. The static and impact damage characteristics were compared with earlier results for CVD zinc sulfide showing that hot pressed zinc sulfide is less resistant to contact damage than CVD zinc sulfide.

Polycrystalline zinc sulfide can be prepared in a transparent form suitable for use in optical components by at least two methods, hot pressing (HP ZnS) and chemical vapor deposition (CVD ZnS). Evans and Wilshaw[1] characterized static contact damage at spherical indentations in CVD ZnS and other ceramics and determined that crack extension depends primarily on the indentation radius and the ratio of hardness to toughness. Shockey, Dao, and Curran[2] characterized the impact damage at spherical indentations in CVD ZnS and correlated the damage with the plastic impression strain. Kirchner, Richard and Larchuk[3-5] characterized static and impact damage at spherical indentations in CVD ZnS and used the resulting data to evaluate a theory of elastic-plastic impact, to correlate the radial crack length with load and indentation radius, and to demonstrate the importance of strain rate effects. Van der Zwaag, Hagan and Field[6] investigated deformation mechanisms at static contacts in CVD ZnS. Other investigators[7-10] have studied water drop impact on ZnS. In these investigations, contact damage in HP and CVD ZnS has not been compared.

The HP ZnS* was purchased as a cylindrical plate 3 in. diam. x 6mm thick. This plate was indented on the large surfaces which are perpendicular to the hot pressing direction by static and impact loading using spherical glass indenters, 3mm in diameter**. The static loads ranging from 111-890N were applied by an Instron testing machine. The HP ZnS plate was placed on the load cell and the spheres were fastened to the crosshead. A compressed gas (N_2) gun was used to accelerate the spheres for the impact tests. The plate was mounted perpendicularly to the path of the sphere. The impact and rebound velocities were measured from multiple images of

---

* IRTRAN 2, Eastman Kodak Co., Rochester, N.Y. 14650
** Glass spheres, No. 3000, Walter Stern, Inc., Port Washington, N.Y.

the sphere on a photograph obtained by illuminating the sphere at known time intervals using a stroboscope and recording the images using a camera with an open shutter. The velocities of the glass spheres ranged from 18-73 $m \cdot s^{-1}$.

The damage was characterized by optical and scanning electron microscopy and the results were compared with earlier results obtained for CVD ZnS indented on the surface perpendicular to the deposition direction.

Comparison of microstructure and properties of HP and CVD Zns

The microstructures of HP and CVD ZnS differ because of the differences in the forming method. The HP ZnS has a grain size of 1-5 μm which does not vary significantly with orientation in the plate. The CVD ZnS is deposited in the form of columnar grains oriented roughly parallel to the deposition direction. These grains have an aspect ratio of 8:1 and are up to perhaps 50 μm in length. In the plane perpendicular to the deposition direction the grain size is quite variable ranging from about 1-20 μm and the grains are approximately equidimensional.

The properties of the HP and CVD ZnS are compared in Table I using data from various sources. The K_{IC} of the HP ZnS was measured by the single edge notched beam method for a crack propagating parallel to the hot pressing direction yielding 0.44 $MPam^{\frac{1}{2}}$, a value substantially lower than the literature values for CVD ZnS. This result suggests that cracks will propagate farther in HP ZnS than in CVD ZnS. This crack propagation direction is relevant to propagation of the radial and median cracks. Comparisons of the diameters of static indentations in the HP and CVD ZnS show that the hardnesses are approximately equal (1.9 GNm^{-2}).

TABLE I

Comparison of Properties of HP and CVD ZnS

	HP ZnS*	CVD ZnS**
Microstructure		(c,d,e,see note ***)
Grain size, μm	1-5	2-5 in growth plane
		9-30 ⊥ " "
Crystal habit	-	columnar grains
Crystal symmetry	cubic[a]	cubic
Critical stress intensity factor, MPa $m^{\frac{1}{2}}$	0.44 ± 0.08****	1 [f]
		0.75[g]
		0.67[c]
Density, $g \cdot cm^{-3}$	4.09[b]	4.08[e]
Elastic properties		
Young's modulus, MPa	96,550[b]	74,500[e]
Shear modulus, MPa	-	41,000[f]
Poisson's ratio	-	0.30[c] in growth plane
		0.35 ⊥ " "
Modulus of rupture at 25°C, MPa	97.2[b]	110.3[e]

* IRTRAN 2, Eastman Kodak Co., Rochester, N.Y. 14650.
** RAYTRAN ZnS, Raytheon Research Division, Waltham, Mass. 02154.
*** References d and e indicate wider ranges than those listed.
**** Average of two values.

(a) Personal communication with Eastman Kodak Co. (Mr. Fairbanks).

(b) Manufacturer's literature, Eastman Kodak Co.

(c) J. M. Wimmer, "Mechanical and Physical Properties of Chemically Vapor-Deposited (CVD) Zinc Sulfide," Air Force Materials Laboratory Report AFML-TR-79-4013 (1979).

(d) D. A. Shockey, K. C. Dao and D. B. Curran, "Nucleation and Growth of Cracks in CVD ZnS under Particle Impact," SRI International Annual Report Part II, Contract N00014-76-C-0657 (April, 1979).

(e) Manufacturer's literature, Raytheon Co.

(f) A. G. Evans and T. R. Wilshaw, "Quasi-Static Solid Particle Damage in Brittle Solids I. Observations, Analysis and Implications," Acta Met. 24,939-956 (1976).

(g) S. van der Zwaag, J. T. Hagan and J. E. Field, "Studies of Contact Damage in Polycrystalline Zinc Sulfide," J. Mater. Sci. 15 (12) 2965-2972 (1980).

Comparison of static and impact loading damage in HP and CVD ZnS

The expected load (P) dependence of the radial crack length (c) in the elastic-plastic case is described by $P \propto dc^{\frac{1}{2}}$ where d is a contact dimension[4]. Several mechanisms can give rise to this relation including line contact loading or wedging where d is the length of the contact[11,12], the existence of an irreversibly deformed zone under the contact where d is the depth of this zone[13,14] and the existence of residual stresses where d is the length subject to stress[15]. In addition, Niihara, Morena and Hasselman[16] have proposed that a $P \propto c^{\frac{1}{2}}$ relation applies for Palmquist cracks.

Indentations and cracks formed by static loading in HP and CVD ZnS are compared in Figure 1, which shows that, compared at approximately equal indentation radii, the cracks are slightly longer in HP ZnS than in CVD ZnS and also shows the presence of a lateral crack (the circular shadow) in the HP ZnS. The load threshold for lateral crack formation is lower in HP ZnS than in CVD ZnS. Loads of 500-600N are required to cause lateral cracking in CVD ZnS.

The extent of radial cracking in HP and CVD ZnS is compared in Figure 2. The plots show that the variations of crack length with load in both materials are equally well represented by $P \propto d_i c^{\frac{1}{2}}$ where d_i is the indentation diameter and that, when compared on this basis, the cracks are longer in HP ZnS than in CVD ZnS. At high loads the radial cracks in HP ZnS are about 30% longer than those in CVD ZnS.

Impacts using the glass spheres yielded damage that was similar in magnitude to the damage induced by static loading as shown in Figure 3. For specimens impacted at approximately equal velocities, the radial cracks are longer in HP ZnS than in CVD ZnS as was the case for static loading.

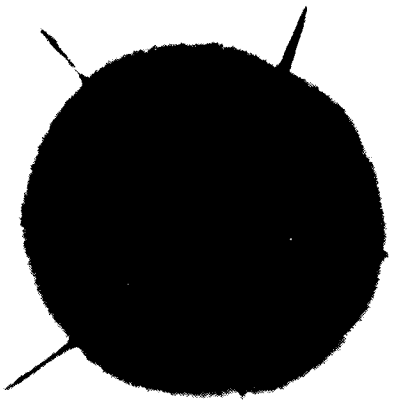

HP ZnS (334N Load, r_i = 250 μm, c_r = 660 μm, c_l = 385 μm)

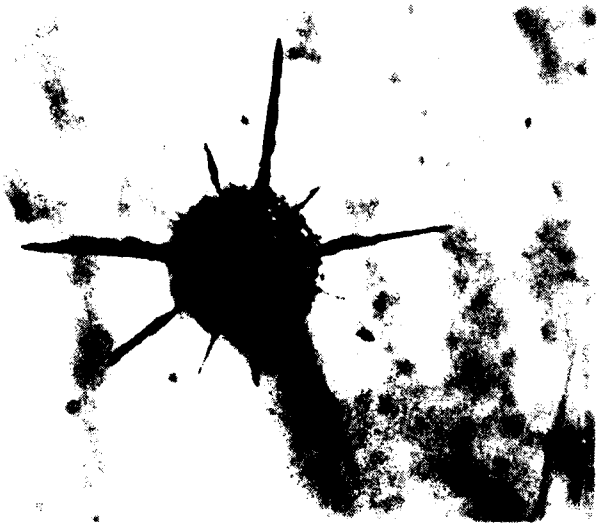

CVD ZnS (343N Load, r_i = 254 μm, c_r = 585 μm, c_l = 0 μm)

Figure 1. Damage induced by static loading, 39X (HP ZnS and CVD ZnS plates with 3 mm glass spheres).

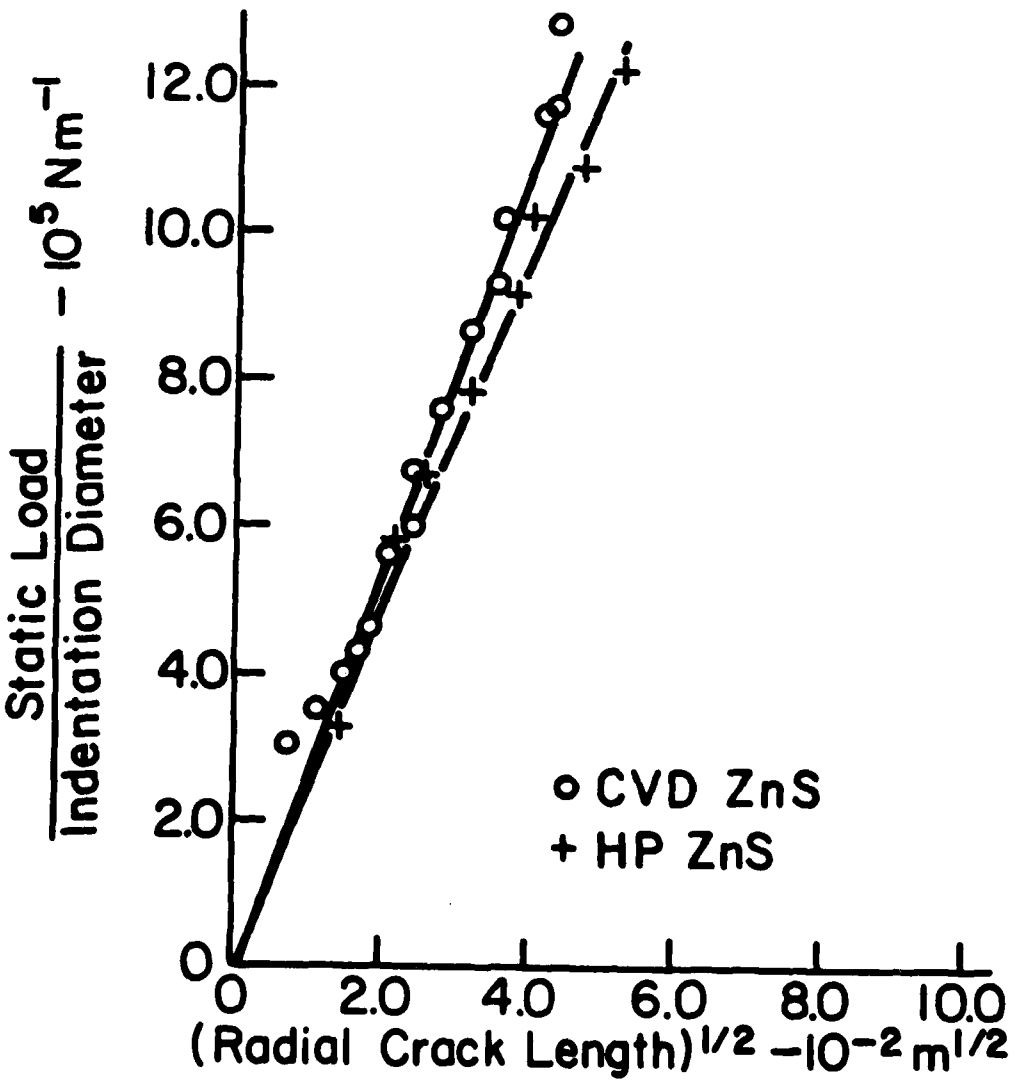

Figure 2. Static load divided by indentation diameter vs square root of maximum radial crack length (for both CVD ZnS and HP ZnS statically loaded with 3 mm diameter glass spheres).

HP ZnS (impact velocity = 27 $m \cdot s^{-1}$, r_i = 286 μm, c = 792 μm, c_l = 276 μm)

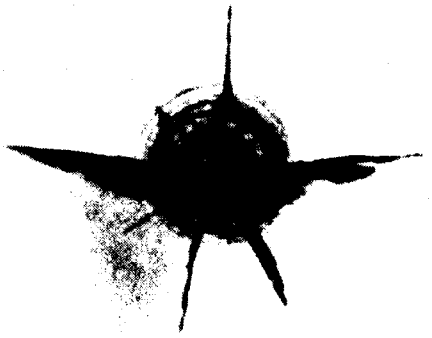

CVD Zns (impact velocity = 28.1 $m \cdot s^{-1}$, r_i = 276 μm, c_r = 600 μm, c_l = 82 μm)

Figure 3. Damage induced by impact loading, 39X (HP ZnS and CVD ZnS plates with 3 mm glass spheres).

The HP ZnS specimen in Figure 3 also shows a partial lateral crack. The differences in the radial crack lengths were not consistent throughout the velocity range. In some cases the radial crack lengths in HP ZnS were much longer than would normally be expected.

The circumferential cracks formed in the impact indentations are much better defined than those in the static indentations.

The coefficients of restitution (the ratios of the rebound velocities to the impact velocities) were calculated. These values were only slightly different for the two materials and ranged from a maximum of about 0.94 at the low end of the velocity range to a minimum of about 0.76 at the high end of the velocity range. The variations of the kinetic energy loss with impact velocity were compared. Because of the importance of plastic deformation as an energy absorption mechanism, differences in kinetic energy loss are expected to indicate differences in the relative dynamic hardnesses of the materials. The slightly higher energy losses in HP ZnS indicate that the dynamic hardness of HP ZnS may be slightly lower that that of CVD ZnS.

The log-log plots of the kinetic energy loss vs. impact velocity for both HP and CVD ZnS are essentially linear with slopes of 2.75 and 2.92 respectively. These slopes can be compared with a value of 2.6 predicted for elastic impacts by Hunter[17]. This result provides additional evidence that the presence of impact damage, including plastic deformation at indentations, does not substantially affect these slopes except at transitions where new energy loss mechanisms become important.

Therefore, it is concluded that at static spherical indentations in HP ZnS, the variation of the radial crack length with load is well represented by $P \propto d_i \, c^{\frac{1}{2}}$. The region in which this relation provides a good

fit extends to c/r_i ratios as great as 7.3, much larger values than would have been expected based on previous investigations using Vickers indenters[18] which suggests that further investigations of indenter shape and stiffness might be fruitful. At high static loads the maximum radial crack lengths in HP ZnS are about 30% longer and the numbers of radial cracks are greater than in CVD ZnS. The threshold loads for lateral crack formation are much lower in HP ZnS than in CVD ZnS.

Under comparable impact conditions the radial crack lengths are greater and the cracks are more numerous in HP ZnS than in CVD ZnS. Also, crushing is more extensive in HP ZnS. The kinetic energy losses during impact are only slightly greater in HP ZnS than in CVD ZnS.

Observations of longer radial cracks, larger numbers of radial cracks, a lower threshold load for lateral crack formation and increased crushing in HP ZnS indicate that HP ZnS is more susceptible to contact damage than CVD ZnS. This difference is attributable, at least in part, to the difference in the K_{IC} values.

ACKNOWLEDGEMENTS

The writers are pleased to acknowledge the contributions of D. A. Sentner who measured the K_{IC} of HP ZnS, J. C. Conway, Jr., R. M. Gruver, helpful discussions with E. R. Fuller and K. Niihara, and the sponsorship of the Office of Naval Research.

REFERENCES

1. A. G. Evans and T. R. Wilshaw, "Quasi-Static Solid Particle Damage in Brittle Solids, I. Observations, Analysis and Implications," Acta Met. 24, 939-958 (1976).

2. D. A. Shockey, K. C. Dao and D. R. Curran, "Nucleation and Growth of Cracks in CVD ZnS under Particle Impact," SRI Annual Report, Part II, Contract N00014-76-C-0657 (April, 1979).

3. D. M. Richard and H. P. Kirchner, "Theory of Elastic-Plastic Impact on Ceramics," Proc. Fifth International Conference on Erosion by Liquid and Solid Impact, Cavendish Laboratory, Cambridge U. (September, 1979) pages 27-1 to 27-10.

4. H. P. Kirchner and T. J. Larchuk, "Load-Radial Crack Size Relations in Zinc Sulfide," Communications Amer. Ceram. Soc. 64 (2) C27,28 (1981).

5. H. P. Kirchner and T. J. Larchuk, "Comparisons of Static and Impact Loading Damage in Zinc Sulfide," Submitted for publication.

6. S. van der Zwaag, J. T. Hagan and J. E. Field, "Studies of Contact Damage in Polycrystalline Zinc Sulfide," J. Mater. Sci. 15 (12) 2965-2972 (1980).

7. J. V. Hackworth and L. H. Kocher, "Behavior of Infrared Window Materials Exposed to Rain Drop Environments at Velocities to 2000 FPS (610 M/S)," Bell Aerospace Textron Technical Report AFML-TR-78-184, Contract F33615-77-C-5069 (September, 1978).

8. J. E. Field, M. Mathewson and S. van der Zwaag, "Liquid Impact Erosion Mechanisms in Transparent Materials," University of Cambridge Technical Report AFWAL-TR-80-4057, Contract AFOSR-78-00125 (November, 1979).

9. W. F. Adler, J. C. Botke and T. W. James, "Response of Infrared-Transparent Materials to Raindrop Impacts," Effects Technology, Inc. Technical Report AFML-TR-79-4151 (October, 1979).

10. W. F. Adler and T. W. James, "Localized Deformation and Fracture of Transparent Ceramics," Effects Technology, Inc. Technical Report CR80-758, Contract N00014-76-C-0744 (March, 1980).

11. B. R. Lawn and D. B. Marshall, "Contact Fracture Resistance of Physically and Chemically Tempered Glass Plates: A Theoretical Model," Phys Chem. Glasses 18 (1) 7-18 (1977).

12. H. Tada, P. Paris and G. Irwin, "The Stress Analysis of Cracks Handbook," Del Research Corp., Hellertown, Pa. (1973).

13. B. R. Lawn and M. V. Swain, "Microfracture Beneath Point Indentations in Brittle Solids," J. Mater. Sci. 10, 113-122 (1975).

14. J. C. Conway, Jr. and H. P. Kirchner, "The Mechanics of Crack Initiation and Propagation Beneath a Moving Sharp Indenter," J. Mater. Sci. 15, 2879-2883 (1980).

15. H. P. Kirchner and E. D. Isaacson, "Residual Stresses in Hot Pressed Si_3N_4 Grooved by Single-Point Grinding," J. Amer. Ceram. Soc. 65 (1) 55-60 (1982).

16. K. Niihara, R. Morena and D. P. H. Hasselman, "Evaluation of K_{IC} of Brittle Solids by the Indentation Method with Low Crack to Indent Ratios," J. Mater. Sci. Letters 1,13 (1982).

17. S. C. Hunter, "Energy Absorbed by Elastic Waves During Impact," J. Mech. Phys. Solids 5, 162-171 (1957).

18. A. G. Evans and E. A. Charles, "Fracture Toughness Determination by Indentation," J. Amer. Ceram. Soc. 59 (7-8) 371-372 (1976).

COMPARISONS OF STATIC AND IMPACT LOADING DAMAGE IN ZINC SULFIDE

by

H. P. Kirchner

T. J. Larchuk

CERAMIC FINISHING COMPANY

P. O. Box 498, State College, Pa. 16801

ABSTRACT

Contact damage was induced in CVD zinc sulfide by static and impact loading using glass spheres. Calculations based on the relationship between the residual depth of the indentation and the ratio of the hardness to Young's modulus were used to estimate the dynamic hardness and impact load. Comparisons of applied loads, threshold loads for crack formation and crack lengths for static and impact indentations at equal indentation radii show that predictions of impact damage using data from static loading are inadequate.

I. INTRODUCTION

A common approach to investigation of localized impact damage has been to characterize the damage at static indentations induced by various loads and to use the results of these observations to predict the type and extent of impact damage, assuming that, at equal loads, identical damage is induced irrespective of the method of loading.[1-5] Evaluation of this assumption is handicapped by the difficulty in measuring the impact load. However, the validity of the assumption can be evaluated indirectly by comparing damage at static and impact indentations that have an equal measurable characteristic such as the indentation radius. Presumably, if the response of the material depended only on the maximum load and not on the loading rate, each characteristic of the damage observed at equal indentation radii will be the same for both static and impact loads. The extent of the observed differences will indicate the degree to which the response differs from the assumption.

The details of the damage induced during impact are important because of the differing roles of the various types of cracks in the performance of the material. For example, radial cracks are considered to control the strength degradation. Lateral cracks control the degradation of optical transmission and, combined with crushing, control the erosion rate.

II. PROCEDURES

When a sufficiently high load is applied to a sphere pressed against a flat plate, the yield point of the plate material will be exceeded and a permanent indentation is induced (Figure 1). As the load is removed, some of the elastic deformation is recovered while the remainder is constrained by the irreversibly deformed material resulting in residual stresses.

In this investigation, zinc sulfide plates (25x25x7mm) were indented by glass spheres, 3mm diameter, under various loads using an Instron testing machine. The materials are identified and the properties of the plates and spheres are given in Table I. The zinc sulfide consists of columnar grains with a high degree of preferred orientation[4]. The observed grain size ranges from one to 40 μm depending especially on the orientation relative to the deposition direction. The indentation radius (r_i) was measured in the plane of the surface as indicated in Figure 1. The indentation radii, numbers of radial cracks and maximum radial and lateral crack lengths were measured, using a calibrated eyepiece in an optical microscope for the load range of 84 to 1059 N.

Similar plates were impacted at velocities ranging from 19 to 65 $m \cdot s^{-1}$ by glass spheres accelerated by a gas gun using compressed N_2 gas. The impact and rebounding velocities were measured using photographs with multiple stroboscopic images of the glass spheres. The spheres were coated with a thin layer of aluminum to improve their reflectivity. The impact damage was characterized as described above for the static indentations. In some cases the profiles of the static and impact indentations were compared, using a profilometer. The results were analyzed and are presented in the following section.

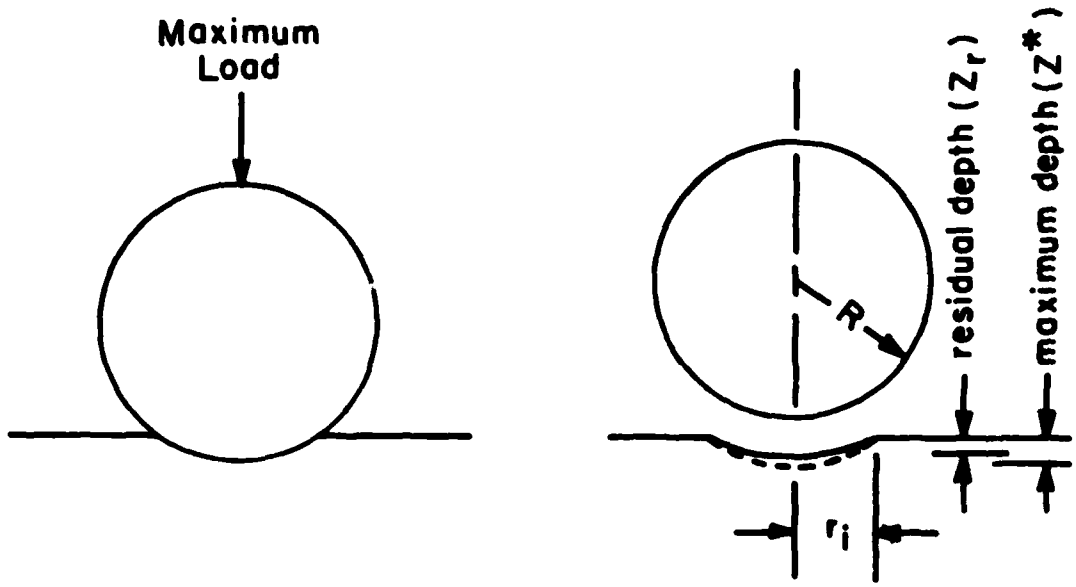

Figure 1. Indentation after loading and unloading.

Table I

Material Properties

Property	Material	
	Glass*	ZnS**
Young's Modulus MPa	70,000 [9]	74,100 [6]
Poisson's Ratio	---	0.30 [6] (in plane of plate)
Density Kgm^{-3}	2,500	4,090 [6]
Critical Stress Intensity Factor $MPam^{\frac{1}{2}}$	0.7	1 [2] 0.75 [8] 0.67 [6]
Hardness GPa	5.3 [7]	1.9 [2]
Average Grain Size μm	---	30 [2]

* Glass spheres, No. 3000, Walter Stern, Inc., Port Washington, N.Y.

** Chemical vapor deposited zinc sulfide plates, Raytheon Co., Waltham, Mass.

III. RESULTS AND DISCUSSION

The response of the ZnS plates to static and impact loading was elastic-plastic, yielding permanent indentations with the indentation radii increasing with the maximum loads. Ring cracks, radial cracks and lateral cracks were observed for both static and impact loading as shown in Figure 2 where the lateral cracks appear as the shaded areas between the radial cracks. When the damage was observed in cross section, a clear zone was observed beneath the contact. This zone is relatively transparent because of the absence of large-scale cracks. However, this zone contains dispersed spots that have been identified as pores[4].

At static indentations, the load thresholds were 84 N for radial crack formation and 899 N for lateral crack formation. In the impact tests measurable indentations, radial cracking, and evidence of lateral cracking were observed at the lowest velocity tested and all higher velocities.

Damage at static and impact sites was compared at approximately equal indentation radii (Figure 2). When the indentation radii are relatively small, as in Figures 2A (static) and 2B (impact), the radial cracks formed at the impact sites are fewer in number and smaller than those formed at the static sites. However, in the impact case, lateral cracks initiate at smaller indentation radii as indicated by the lighter area to the left of the indentation. Also, the ring cracking is much more visible at the impact site. At larger indentation radii, as shown in Figure 2C (static) and 2D (impact), both the radial cracks and the lateral cracks are larger at the impact site than at the comparable static site. The lateral cracking at the impact site has produced chipping to the right

A. Static Loading, $r_i \cong 260\mu m$ (39X)

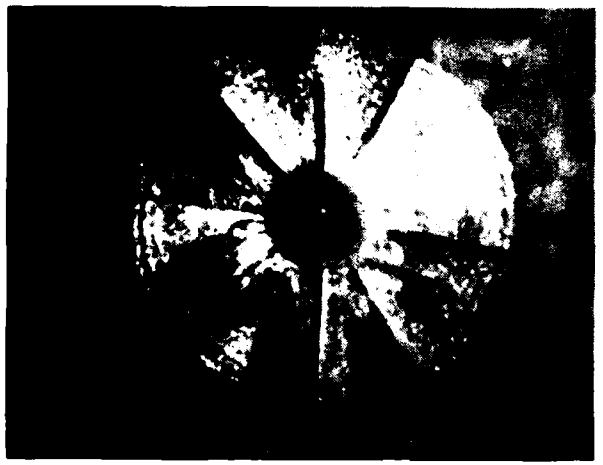

C. Static Loading, $r_i \cong 400\mu m$ (19X)

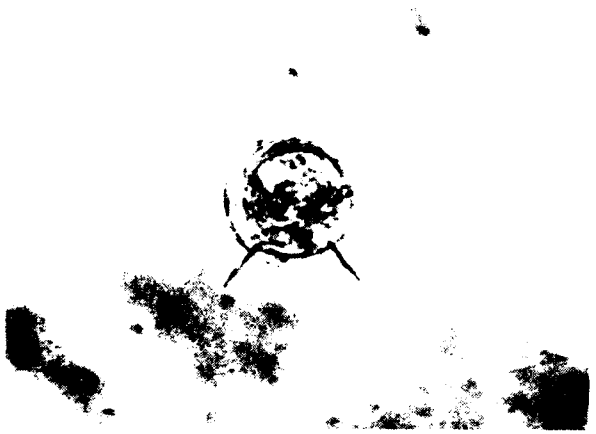

B. Impact Loading, $r_i \cong 260\mu m$ (39X)

D. Impact Loading, $r_i \cong 400\mu m$ (19X)

Figure 2. Damage induced by static and impact loading (3mm diameter glass spheres on ZnS plates).

of the indentation. Also, the ring cracking within the impact indentations has become much more pronounced, causing the contours of these indentations to appear somewhat irregular, compared with the static indentations.

The irregularities observed in the impact indentations were investigated by profilometer measurements. Figure 3 shows the diametral profiles of static and impact indentations, compared at approximately equal indentation radii. It should be noted that the vertical scale is ten times the horizontal scale. The distinguishing features are:

1. The impact indentation is much shallower than the static indentation.
2. The center of the impact indentation is separated from the outer rim by substantial circumferential (ring) cracks, one of which is visible at the boundary of the dark central area in Figure 2D.
3. The central area of the impact indentation has been pushed down, apparently as a result of shear failure at the circumferential cracks.
4. The outer portions of the impact profile form a rim with a much lower slope than that of a comparable static indentation.

These features indicate that, mechanically, the formation of impact indentations is much more complex than the formation of static indentations.

The above results, together with recent equations of Lawn and Howes[9], were used to estimate the dynamic hardness and the maximum impact load for this impact. Lawn and Howes expressed the elastic recovery for elastic-plastic indentations by Vickers indenters in terms of the hardness to Young's modulus ratio (H/E) obtaining the relation

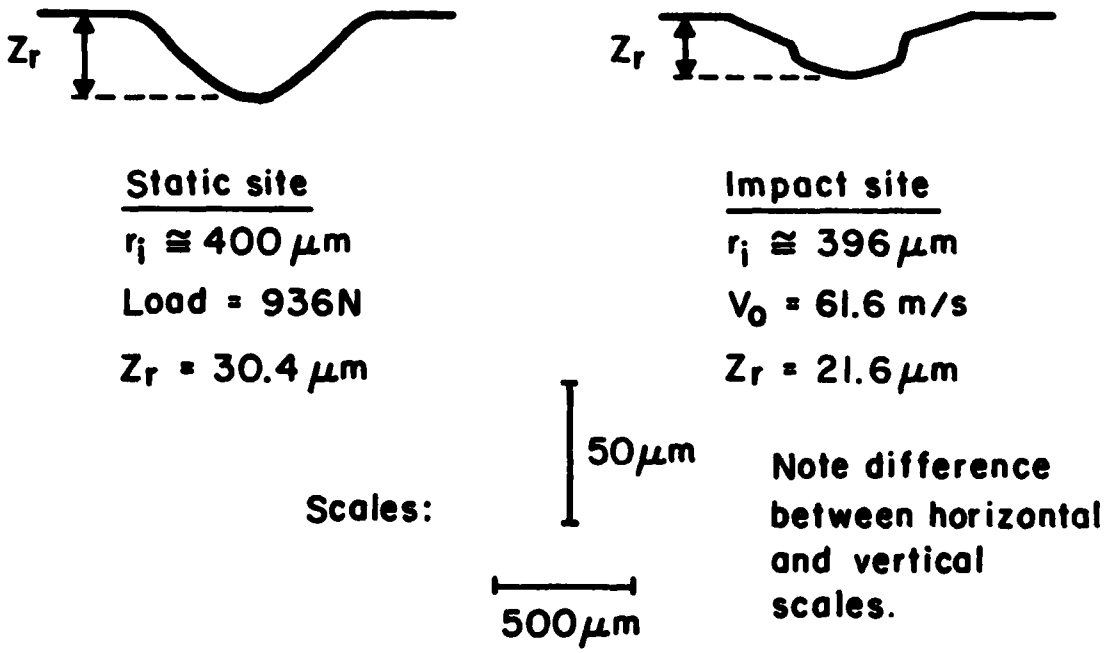

Figure 3. Diametral profilometer traces of static and impact indentations (ZnS, 3 mm diameter glass spheres).

$$\left(\frac{Z_r}{Z^*}\right)^2 = 1 - \left[2(1-\nu^2)\left(\frac{\gamma_E}{\gamma_H}\right)^2 \tan \Psi\right] \frac{H}{E} \qquad (1)$$

where Z^* is the maximum penetration under load, Z_r is the depth of the indentation after unloading, H is the hardness, E is Young's modulus, ν is Poisson's ratio, Ψ is the indenter angle and γ_E and γ_H are geometrical factors. In the case of Vickers indenters Ψ is fixed by the pyramidal shape and the rigidity of the diamond. The above equation might be expected to apply to glass spheres as indenters, despite the different shape and the elastic deformation if an appropriate value of tan Ψ can be estimated in each particular case. Also, Z^* cannot be estimated directly from the spherical geometry of the indenter and the indentation radius (r_i) because of the elastic deformation. However, Z^* for the impact case in Figure 3 can be estimated from measured values of the coefficient of restitution (e) using[9]

$$e = \left[\frac{1 - \frac{3Z_r^2}{Z^{*2}} + \frac{2Z_r^3}{Z^{*3}}}{\left(1 - \frac{Z_r^2}{Z^{*2}}\right)}\right]^{1/2} \qquad (2)$$

In this case e = 0.79[5] and Z^* = 40.75 μm. Then, noting that r_i is approximately the same in both the static and impact cases, it can be assumed that Z^* is approximately the same in both cases, and that $\gamma_E \simeq \gamma_H$ so that tan Ψ can be estimated from equation (1) for the static case yielding $\Psi = 83.8^\circ$ where Ψ in this case is an apparent indenter angle. Then, assuming that tan Ψ is approximately the same in both the static and impact cases the

dynamic hardness can be estimated from equation (1) for the impact case yielding 3.1 GPa. This dynamic hardness implies an impact load of 1500 N which can be compared with the static load of 936 N at approximately the same indentation radius and an impact load of 1800 N estimated previously[10] using the Hertzian equations that assume elastic conditions. Because the plastic deformation reduces the maximum load one would expect the load in the elastic-plastic case to be less than that in the elastic case as is indicated above.

One can speculate that the boundary formed by the wide circumferential crack represents a boundary between a central region in which forces tending to cause radial flow of the ZnS along the interface between the ZnS and glass are insufficient to overcome the frictional forces[11] and a circumferential band in which the frictional forces are overcome so that there is movement of ZnS radially along this interface.

The extent of damage under the surface was observed in detail by viewing the damage through the polished sides of the plates as shown in Figure 4 in which the radial cracks are evident. The sketches in Figure 5 present details of cracks observed in this manner. Out-of-plane radial cracks were omitted for clarity. The pairs of static and impact specimens have comparable indentation radii and are arranged in order of increasing indentation radius. The cross-section in Figure 5A represents damage at a small static indentation. The damage consists of radial (Palmquist) cracks extending from the edges of the indentation and a clear, irreversibly deformed zone under the indentation. The radial cracks to not

Figure 4. Side view of damage under the surface at a static indentation (load = 708 N, r_i = 348 μm).

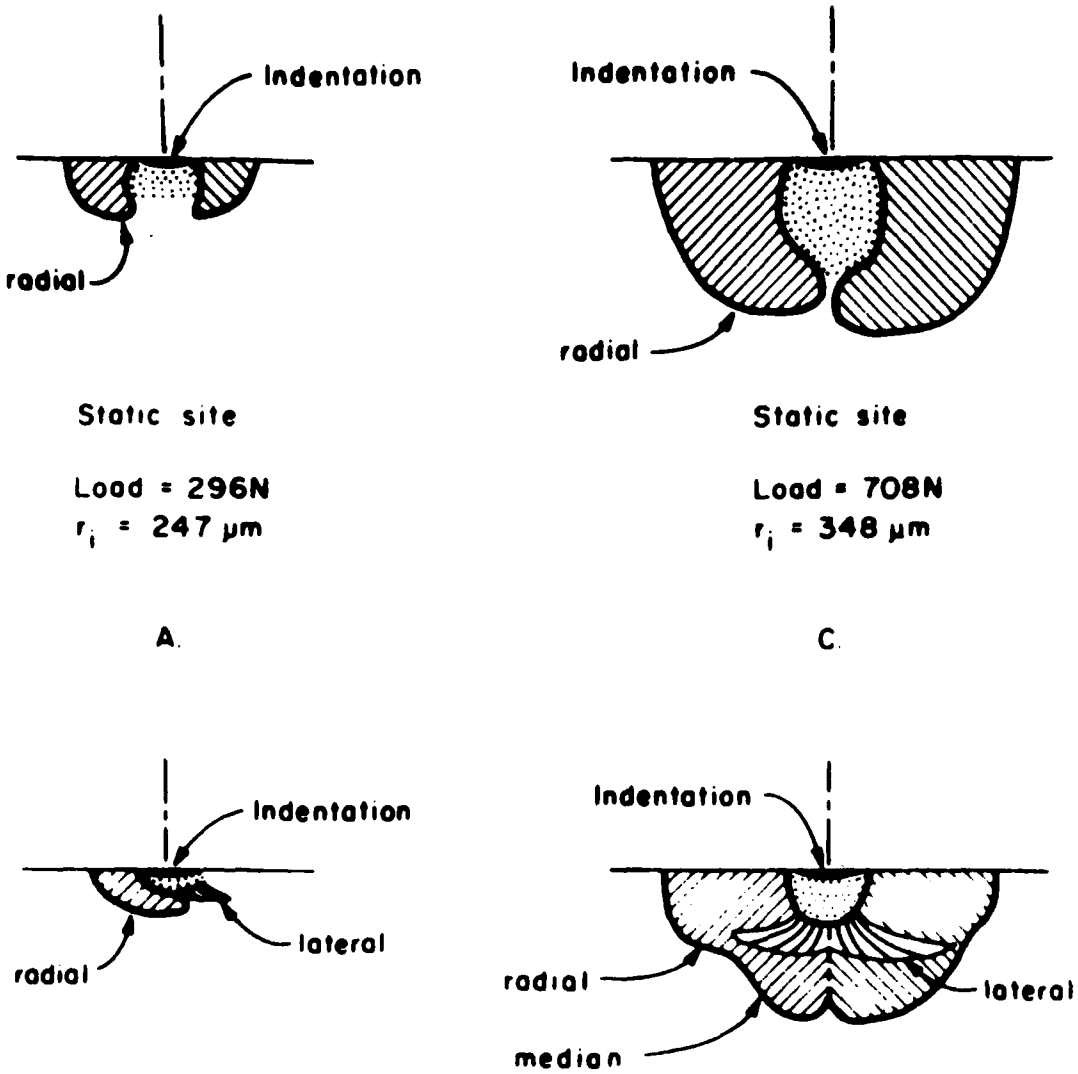

Figure 5. Comparisons of cracks formed at static and impact sites with comparable indentation radii (ZnS, 3 mm diameter glass spheres).

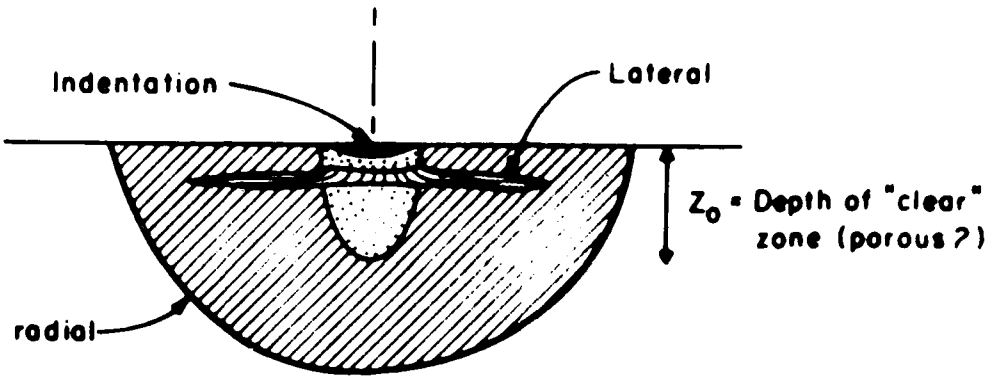

Static Site

Load = 936N Δ = 30 4 μm
r_i = 400 μm

E

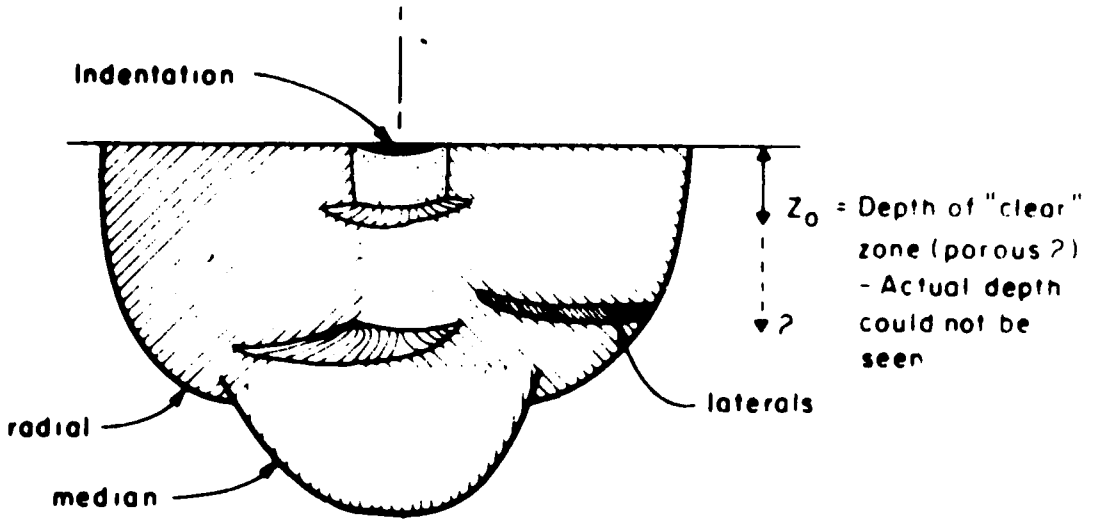

Impact site

V_0 = 61.6 m/s Δ = 21 6 μm
r_i = 396 μm

F

Figure 5. (continued)

extend downward into the plate appreciably until they are beyond the irreversibly deformed zone. The radial cracks are not necessarily coplanar and they do not bridge the gap under the indentation.

Evans and Wilshaw[2] observed that radial cracks form on loading in ZnS. This observation is confirmed by observation of radial cracks that extend into the indentation (Figure 2A). If the radial cracks formed on unloading, as a response to the residual stresses, the radial cracks would originate at the boundary of the irreversibly deformed zone.

The Boussinesq and Michell stress distributions for a point load and the Hertzian stress distribution for a blunt load at the surface show that, in the absence of plastic deformation, the out-of-plane hoop stresses are compressive[12,13]. However, Perrott[14] has shown that when the plastic zone radius is 1.65 times the indentation radius the out-of-plane hoop stresses at the boundary of an indentation become tensile at the surface. Also, for an extreme case in which a rigid sphere is pressed to the depth of its radius into zinc sulfide, numerical analysis of the elastic stress field by Evans and Wilshaw[2] has shown that the out-of-plane hoop stresses are tensile. Therefore, the observation that radial cracks form on loading in zinc sulfide can be attributed to the extensive plastic deformation of this relatively soft material.

The impact site (Figure 5B) differs from the comparable static site in several ways. The impact site has only one radial crack, which is smaller than the largest radial crack at the static site. Also, lateral cracking is present and the irreversibly deformed zone is smaller. These

observations are consistent with the earlier observation that the impact indentations are shallower than static indentations at comparable indentation radii. Therefore, one would expect lower tensile out-of-plane hoop stress during loading and lower residual stresses during unloading which would result in fewer and smaller radial cracks. Also, because the dynamic hardness is greater than the static hardness in ZnS, the presence of lateral cracking at the impact site is consistent with the observation of Evans and Wilshaw[2] that lateral cracking is more extensive in harder materials.

At the next larger indentations (Figures 5C,D), the radial cracks at the static indentation are much larger than those in Figure 5A, and they have extended so that they almost meet under the indentation. Otherwise, the damage is similar to that in Figure 2A. The impact damage shows larger radial and lateral cracks, as expected. In addition, under the clear zone, there are cracks extending deeper into the ZnS perpendicular to the surface that have been labelled as median cracks. These cracks are not coplanar and the vertical line extending along the impact axis represents the intersection of the cracks. Median cracks are frequently observed at static indentations under sharp indenters. As the load is removed, radial cracks may extend in response to residual stresses and merge with existing median cracks. Apparently, this has occurred in the present case.

At the largest indentations (Figure 5E,F), the radial cracks at the static indentation are even larger and they have extended under the indentation to completely close the gap to form an approximately semicircular

crack. A large lateral crack was observed close to the surface. The impact damage shows larger non-coplanar radial cracks and larger lateral cracks compared with those in Figure 5D. Again, median cracks have merged with radial cracks. Lateral cracks are observed at several levels, all farther from the surface than the lateral crack at the comparable static site.

The numbers and lengths of radial cracks in static and impact loaded specimens are compared in Figures 6 and 7. Radial cracks at static indentations are observed at smaller indentation radii and larger numbers of radial cracks are formed at a given indentation radius than at impact indentations (Figure 6). Apparently, the more extensive irreversible deformation at the static indentations changes the sign of the out-of-plane hoop stresses from compressive to tensile at smaller indentation radii than in the impact case leading to greater tensile hoop deformation and the greater number of cracks. Also, the extensive irreversible deformation may induce substantial residual stresses.

Radial cracks at static indentations are longer than those at impact sites for indentation radii up to about 400 μm (Figure 7). At greater radii the radial cracks at impact sites are longer. Apparently, at small indentation radii, the deeper indentations and greater irreversible deformation observed at the static sites changes the sign of the out-of-plane hoop stresses at lower loads and results in greater residual stresses leading to longer radial cracks than those at comparable impact indentations. However, at large indentation radii, the larger loads resulting from increased dynamic hardness during impact become dominant and the cracks become larger than those at comparable static indentations.

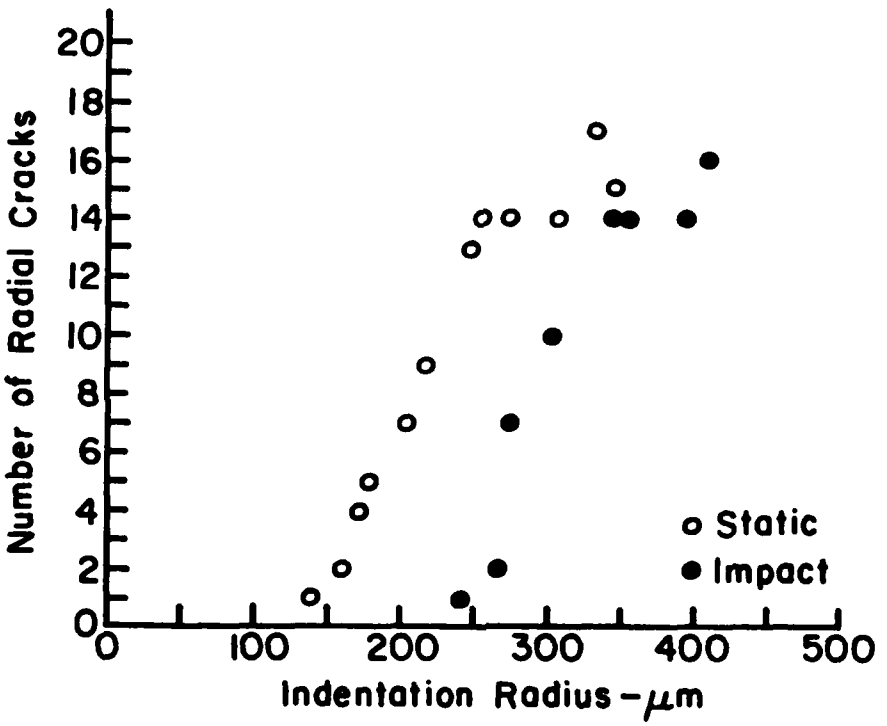

Figure 6. Number of radial cracks vs. indentation radius for static and impact loading (ZnS, 3mm diameter glass spheres).

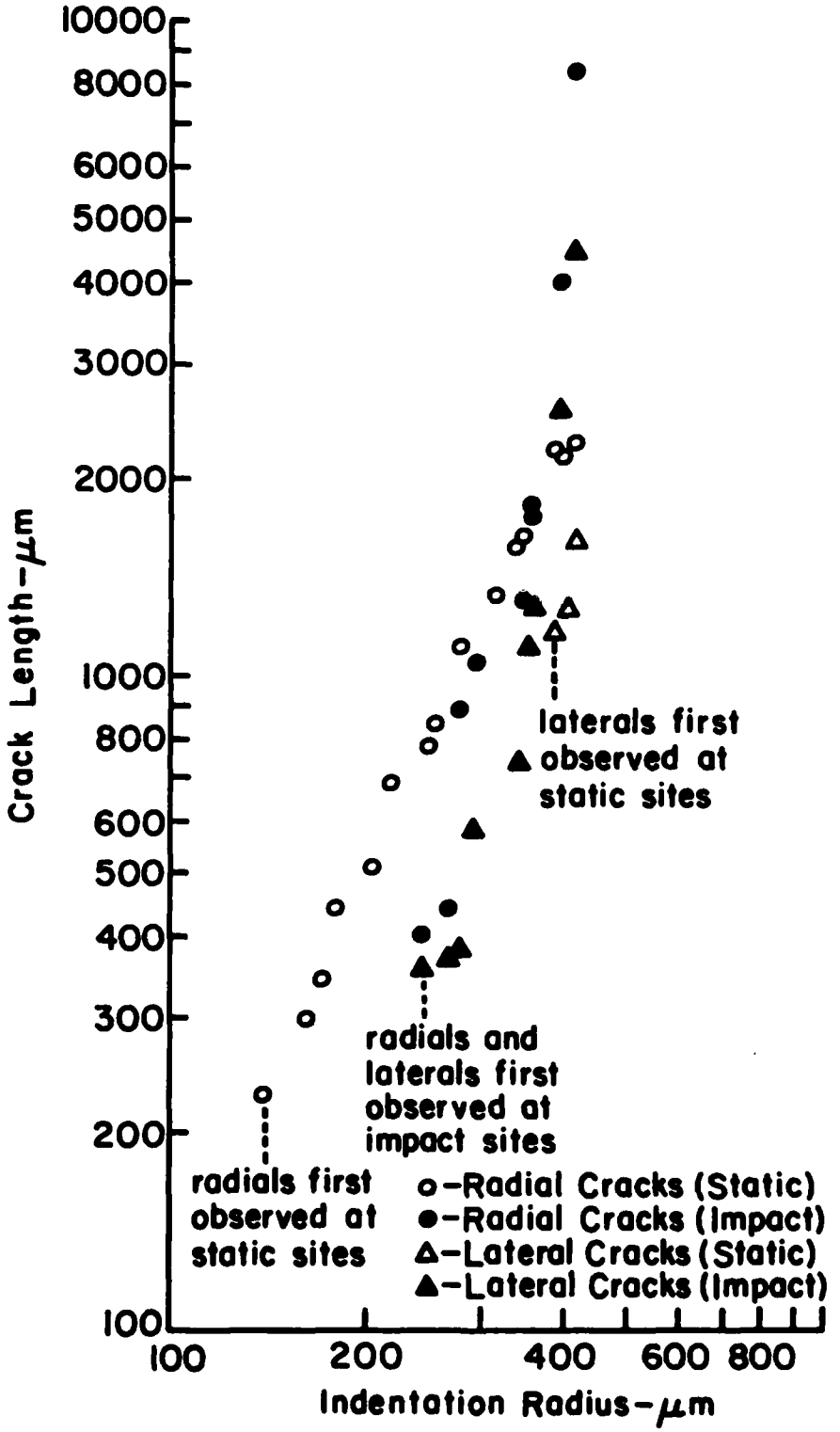

Figure 7. Crack lengths for static and impact radial and lateral cracks vs. indentation radius (ZnS, 3 mm diameter glass spheres).

IV. SUMMARY AND CONCLUSIONS

ZnS plates were statically indented under various loads and impacted at various velocities using 3mm diameter glass spheres. The contact damage was characterized and the damage at the static and impact sites was compared yielding the results described in the previous section. The results show that when compared at equal indentation radii, there are substantial differences between static and impact damage.

Damage at the static and impact indentations included the irreversibly deformed zone directly under the indentation and ring, radial, and lateral cracks. The scale of the damage at the static indentations increased with increasing loads on the glass spheres. An overall comparison of the static and impact damage at approximately equal indentation radii shows that the scale of the overall impact damage is approximately the same as that of the static indentation damage. If one assumes that the sizes of the cracks mainly depend on the maximum loads applied at the contact, this observation appears to justify the assumption of equal loads at equal indentation radii for static and impact indentations. However, the calculations and microscopic observations show that, at equal indentation radii the impact loads are substantially higher than the static loads and there are substantial differences in the indentation radius thresholds for crack formation and the numbers and sizes of the various types of cracks at static and impact indentations. These differences are important in the performance of the material. For example, predictions based on the static damage may overestimate the extent of radial cracking and strength degradation at low impact velocities. Also, they may underestimate the extent of lateral cracking and, therefore, underestimate the degradation of optical transmission and erosion rate.

ACKNOWLEDGEMENTS

The writers are pleased to acknowledge the contributions of their associates at Ceramic Finishing Company, including J. C. Conway, and the sponsorship of the Office of Naval Research.

REFERENCES

1. A. G. Evans, "Strength Degradation by Projectile Impacts," J. Amer. Ceram. Soc. 56 (8) 405-409 (1973).

2. A. G. Evans and T. R. Wilshaw, "Quasi-Static Solid Particle Damage in Brittle Solids, I. Observations, Analysis and Implications," Acta Met. 24, 939-958 (1976).

3. S. M. Wiederhorn and B. R. Lawn, "Strength Degradation of Glass Resulting from Impact with Spheres," J. Amer. Ceram. Soc. 60 (9-10) 451-458 (1977).

4. D. A. Shockey, K. C. Dao and D. R. Curran, "Nucleation and Growth of Cracks in CVD ZnS Under Particle Impact," SRI International Annual Report, Part II, Contract N00014-76-C-0657 (April, 1979).

5. D. M. Richard and H. P. Kirchner, "Theory of Elastic-Plastic Impact on Ceramics," Proc. Fifth International Conference on Erosion by Liquid and Solid Impact, Cavendish Laboratory, Cambridge U. (September, 1979) pages 27-1 to 27-10.

6. W. J. Adler, T. W. James, "Localized Deformation and Fracture of Transparent Ceramics," Effects Technology, Inc., Technical Report, March 1980, ONR Contract N00014-76-0744 NR 032-565.

7. R. W. Rice, "Correlation of Hardness with Mechanical Effects in Ceramics," from The Science of Hardness Testing and Its Research Applications, Edited by J. H. Westbrook and H. Conrad, American Society for Metals (1973), p. 117-133.

8. D. A. Shockey, D. J. Rowcliffe, and K. C. Dao, "Fracture Toughness of CVD ZnS," Stanford Research Institute Topical Report, Contract N00014-76-C-0657 (March, 1977).

9. B. R. Lawn and V. R. Howes, "Elastic Recovery at Hardness Indentations," J. Mater. Sci. 16, 2745-2752 (1981).

10. H. P. Kirchner and T. J. Larchuk, "Localized Impact Damage in Ceramics: Comparisons of Recent Experiments and Theoretical Calculations," Ceramic Finishing Company Special Report, Contract N00014-74-C-0241 (July, 1980).

11. A. G. Evans, J. C. Chestnutt and H. Nadler, "Quasi-Static Solid Particle Damage in Brittle Solids, Part II. Indentation Friction," Acta Met. 24, 867-870 (1976).

12. B. R. Lawn and R. Wilshaw, "Indentation Fracture: Principles and Applications," J. Mater. Sci. 10, 1049-1081 (1975).

13. J. C. Conway and H. P. Kirchner, "The Mechanics of Crack Initiation and Propagation Beneath a Moving Sharp Indenter," J. Mater. Sci. 15, 2879-2883 (1980).

14. C. M. Perrott, "Elastic-Plastic Indentation: Hardness and Fracture," Wear 45, 293-309 (1977).

LOAD-RADIAL CRACK LENGTH RELATIONS FOR SPHERICAL INDENTATIONS IN HOT PRESSED ZnS

by

Henry P. Kirchner
John A. Ragosta
Christopher S. Cannon

CERAMIC FINISHING COMPANY
P. O. Box 498, State College, Pa. 16801

ABSTRACT

HP ZnS was indented by spherical indenters of various radii. The relationship of the load (P) and radial crack length (c_r) was better modeled by $P \propto d_i \, c_r^{1/2}$ where d_i is the indentation diameter than by $P \propto c_r^{3/2}$.

I. INTRODUCTION

Elastic[1,2] and elastic-plastic[2-6] analyses have been used to relate the extent of crack propagation to the applied load at contacts with various types of indenters. The resulting relations can be used to estimate the extent of crack propagation, strength degradation and erosion resulting from damage induced during static indentation[1-4,7], localized impact[8,9] and grinding[5,6,10-12]. The available relations differ mainly in the extent to which they take account of the characteristics of the particular contact, including the effect of residual stresses. In the region far removed from the contact (the far field), the effects of the particular contact characteristics are negligible and relations of the form load $P \propto c^{3/2}$ where c is the crack dimension can be used. However, in a wide range of cases, the effects of the contact characteristics are important and must be accounted for. The contact characteristics may be important when the contact area is large, when there is extensive irreversible deformation at the contact, in the presence of residual stresses, and in cases of line contact loading or wedging. In this investigation, the indenter radii and applied loads were varied and the resulting observations were used to evaluate the effect of contact characteristics associated with indenter radius on the extent of crack propagation in zinc sulfide.

The original elastic relation for the far field was derived by Roesler[1,2] for the case relating a load on a flat punch to the radius (R) of the base of a cone crack propagated from the contact leading to

$$P = \frac{K_{IC}}{(B(\nu))^{1/2}} R^{3/2} \qquad (1)$$

where K_{IC} is the critical stress intensity factor and B is a dimensionless constant uniquely determined by the Poisson's ratio (ν) so that, for a particular material, $P \propto R^{3/2}$. Cone crack diameters five times greater than the punch diameters were necessary to assure far field conditions.

Analogous $P \propto c^{3/2}$ relations are frequently applied in the case in which the contact is elastic-plastic, for example in contacts involving sharp indenters[2,9,10]. Other types of cracks including median, radial and lateral cracks are formed reflecting the different stress distributions in this case. Lawn and Fuller[2] have shown that wedging forces and friction can modify the crack lengths, with the wedging forces depending on the indenter angle. Also, residual stresses at contacts can cause crack growth, especially near the surface where the sign of the out-of-plane hoop stresses may be reversed from compressive to tensile on unloading[13].

In the case of line contact loading, $P \propto Lc^{1/2}$ where L is the length of contact. It is clear that in other cases in which applied loads or residual stresses act over an extended region, a similar relation must control crack propagation near the contact.

In cases in which there is irreversible deformation at the contact, one can proceed as did Lawn and Swain[3] and Conway and Kirchner[5] on

the basis that when shear failure occurs under the contact, the out-of-plane hoop tensile stresses are relaxed to zero in the plastic zone. In this case the function representing the radial dependence of the prior out-of plane hoop stress is substituted into a standard fracture mechanics equation and integrated over the region from the irreversibly deformed zone (Z_o) to the tip of a median crack of depth (c_m) leading to

$$P = \frac{2^{1/2}\,\pi^{5/2}\,K_{IC}\,Z_o\,c_m^{1/2}}{(1 - 2\nu)} \qquad (2)$$

assuming $c_m >> Z_o$. For $\nu = 0.25$

$$P = 49.5\,K_{IC}\,Z_o\,c_m^{1/2} \qquad (3)$$

Furthermore, based on the theory of hardness testing [3] $Z_o \propto P^{1/2}$ so that, for a particular material, one might expect to observe $P \propto c_m$. Therefore, theoretically at least, the contact characteristics have a definite effect on the load dependence of the crack length in this case leading to $P \propto c$ rather than $P \propto c^{3/2}$.

If one assumes that the irreversibly deformed zones are geometrically self-similar for various loads, which is reasonable in many cases, other contact dimensions such as the indentation radius (r_i) or diameter (d_i) can be substituted for Z_o in equation (3). For spherical indenters, the assumption of self-similarity is a reasonable approximation at high loads where there is substantial penetration of the surface. It should be noted that a wide range of mechanisms including line contact loading, wedging and residual stresses can also lead to $P \propto d_i\,c^{1/2}$ relations, especially in the near field. Therefore, experimental agreement with $P \propto d_i\,c^{1/2}$ does not necessarily identify the mechanism controlling crack propagation.

II. PROCEDURES

The HP ZnS* was purchased as a cylindrical plate 3 in. diameter x 6 mm thick. This plate was indented on the large surfaces which are perpendicular to the hot pressing direction, by static loading using spherical indenters. The indenters included relatively large compliant indenters of glass+ (3 mm diameter) and smaller, more rigid indenters of tungsten carbide† with diameters ranging from 0.36 to 1.59 mm. The loads which ranged from 9-890N were applied and measured using a standard testing machine$^{\phi}$ and a crosshead speed of 2 $\mu m \cdot s^{-1}$. The HP ZnS plate was placed on the load cell and the spheres were fastened to the crosshead.

The damage was characterized by optical and scanning electron microscopy. The indentation radius and the length of the longest radial crack at each indentation were measured along the specimen surface using the grid in the eyepiece of the optical microscope. Polarized light was used to improve the visibility of the tips of the cracks during the crack length measurements. Lateral cracking and chipping around the indentations were also characterized.

The results were plotted as suggested by the relations $P \propto c_r^{3/2}$ and $P \propto d_i \, c_r^{1/2}$ where c_r is the radial crack length. Coefficients of determination were calculated and used to evaluate these relations. The results are discussed in terms of the similarities and differences in the stress distributions beneath blunt and sharp indenters.

---

* IRTRAN 2, Eastman Kodak Co., Rochester, N.Y. 14650
\+ Glass spheres, No. 3000, Walter Stern, Inc. Port Washington, N.Y.
† Tungsten carbide spheres, Ultraspherics, Inc., Saulte Ste. Marie, MI. 49783
ϕ Instron Corp., Canton, Mass. 02021

III. RESULTS AND DISCUSSION

Relationship of load and radial crack length

In the range of loads used in this investigation, the spherical indenters induce permanent indentations in the HP ZnS. Radial cracks, lateral cracks and chipping were observed at the indentations. The lengths of the radial cracks and lateral cracks increased with increasing load. Evidence presented previously includes descriptions of these features including the radial cracks[14,15]. Among other characteristics, these cracks originate at the edge of the indentation where they form as shallow (Palmquist) cracks; that is, as radial cracks that do not penetrate very far below the surface. As the indentation spreads, it covers the original segments of these cracks. The fact that these cracks are observed within the indentation which is in compression indicates that these cracks grew during loading when each segment was not yet under the indenter. At higher loads the cracks extended to greater depths so that they approximated quarter penny-shaped cracks surrounding the irreversibly deformed zone. Unlike cracks formed under Vickers indenters where the edges control crack locations, each individual crack does not usually extend on both sides of the indentation.

As shown previously[14,15] the number of cracks formed increases strongly with increasing load, approaching 20 at high loads. A wide range of crack lengths is observed at each indentation.

Figure 1 shows that, for the six glass and tungsten carbide indenters, the average indentation pressure remains approximately constant with increasing load indicating the relative absence of work hardening in the HP ZnS. This result is consistant with recent observations of Chiang, Marshall and Evans[16] for ZnS of unspecified type and conflicts with

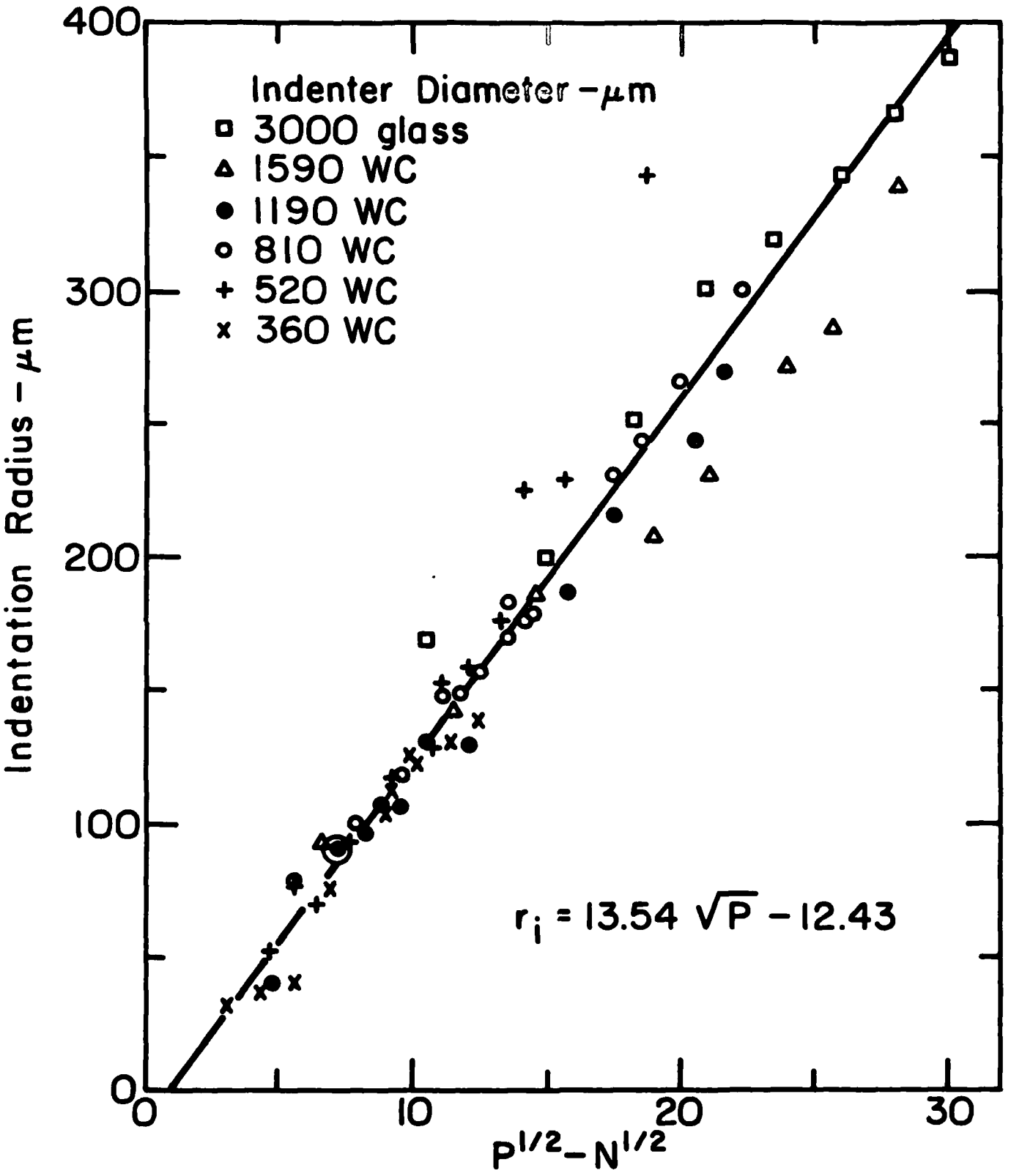

Figure 1. Indentation radius vs. $P^{\frac{1}{2}}$ for spherical indenters of various radii (HP ZnS).

earlier observations of Evans and Wilshaw[4] for CVD ZnS. Work hardening would be indicated by higher loads than predicted by the linear relation, at the larger indentations. The present average indentation pressure is approximately 1.9 GNm^{-2} which is consistant with the results of Chiang, Marshall and Evans[16] for fully developed indentations.

The data are plotted in terms of the relations $P \propto c_r^{3/2}$ and $P \propto d_i\, c_r^{\frac{1}{2}}$ where c_r is the length of the longest radial crack in Figures 2 and 3, for the two largest indenters which were 3 mm diameter glass spheres and 1.59 mm diameter tungsten carbide spheres. The $P \propto c_r^{3/2}$ results using the 3 mm diameter glass spheres (open circles in Figure 2) yield a curved plot rather than a straight line showing that the response of the material is non-linear in terms of the $P \propto c_r^{3/2}$ relation. This result indicates that another factor must be taken into account.

The $P \propto d_i\, c_r^{\frac{1}{2}}$ results are represented by x in Figure 2 yielding a straight line. This result suggests that this relation is a good model for the variation of load with radial crack length under these conditions.

The solid line through the data points represents crack lengths calculated using equation (3). To do this calculation it was first necessary to calculate Z_o. This was done by the method indicated by Conway and Kirchner[6] for glass using

$$Z_o = \zeta P^{\frac{1}{2}} \tag{4}$$

where ζ is a proportionality factor that varies from one material to another. $Z_o = \beta a$ where a is the indentation radius and β is a dimensionless geometrical factor determined by the plastic zone. For circular indentations and constant contact pressure, substituting for (a) yields

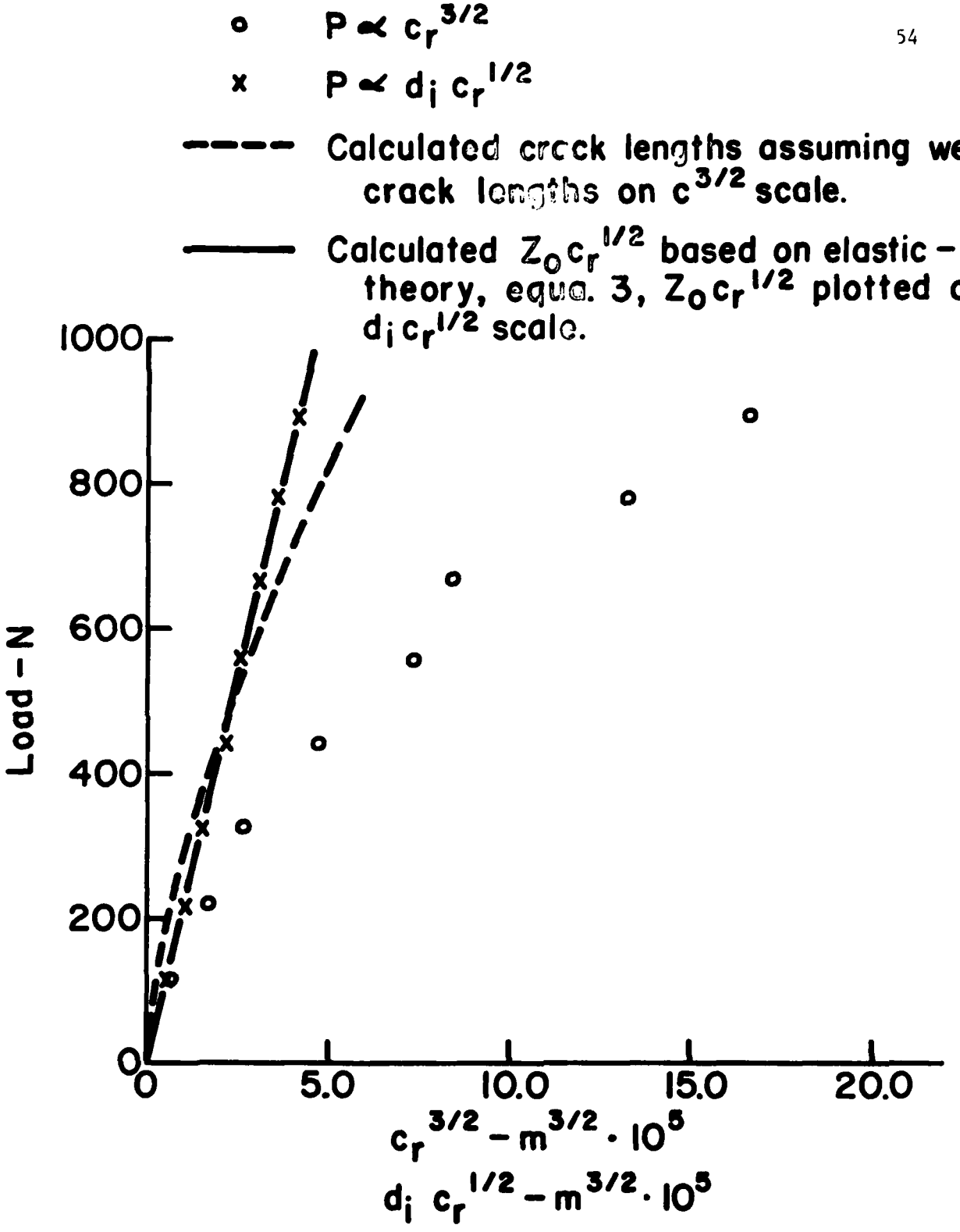

Figure 2. Comparison of data based on P ∝ $c_r^{3/2}$ and P ∝ $d_i c_r^{1}$ relations for 3 mm diameter glass spheres in HP ZnS (c_r measured from center of indentation).

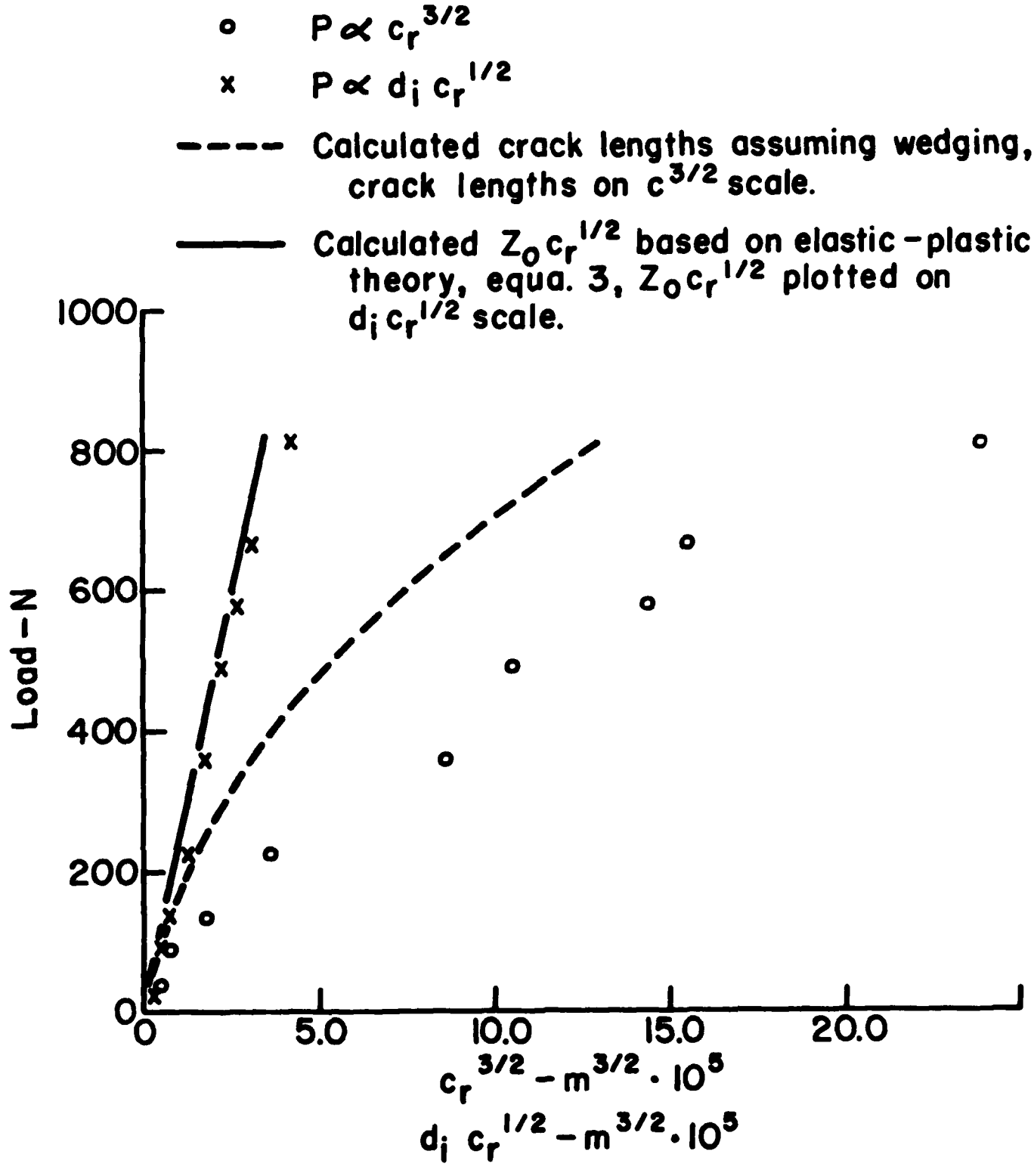

Figure 3. Comparison of data based on $P \propto c_r^{3/2}$ and $P \propto d_i c_r^{1/2}$ relations for 1.59 mm diameter tungsten carbide spheres on HP ZnS (c_r measured from center of indentation).

$$Z_o = \frac{\beta P^{1/2}}{(2\pi H)^{1/2}} \qquad (5)$$

where H is the hardness. Assuming approximate self-similarity and β constant for various materials indented by spherical indenters, ζ for ZnS was estimated by multiplying the earlier value determined for glass which was 15×10^{-6} $N^{-1/2}m$,[6] by the square root of the ratio of the hardness of glass (5.6 GPa) to the hardness of ZnS (1.9 GPa) yielding 25.8×10^{-6} $N^{-1/2}m$. The Z_o values were then calculated and substituted in equation (3) together with $K_{IC} = 0.44$ MPa $m^{1/2}$ [14] to calculate the curve represented by the solid line. The agreement between the data points and the calculated curve is remarkable considering the crudeness of the assumptions.

A second theoretical curve indicated by the dashed line was calculated using the method of Lawn and Fuller[2] based on the assumption that wedging controlled the extent of crack growth. Because the wedging angle Ψ of a sphere is not a fixed value, it was assumed in each case that the wedging angle was the angle between the tangent to the sphere at the edge of the contact and the perpendicular to the surface for each indentation. This assumption tends to maximize the calculated crack length. The crack lengths are plotted on the $c_r^{3/2}$ scale and by comparison with the experimental data (open circles) show that the calculated crack lengths are much smaller than the experimental values. This result indicates that the experimental crack depths are not controlled by wedging in this case.

Similar results are given in Figure 3 for the 1.59 mm diameter tungsten carbide indenter. Again, the experimental data plotted on the $c_r^{3/2}$ scale are nonlinear. The experimental data plotted on the $d_i\, c_r^{1/2}$ scale are essentially a straight line indicating good agreement with $P \propto d_i\, c_r^{1/2}$. The calculated crack lengths based on equation (3) yielded a straight line with the calculated crack lengths slightly smaller than the experimental values, and the wedging predictions yielded smaller crack lengths than the experimental values, as before.

Comparing the $P \propto c_r^{3/2}$ curves in Figures 2 and 3 reveals that in each case there is a non-linear region near the origin but that, as the sphere radius decreases, the region of greatest non-linearity moved closer to the origin. This trend continued at still smaller sphere radii so that at very small sphere radii these curves form reasonably straight lines, despite the fact that they tend to intersect the load axis at positive loads. Therefore, as the spheres tend toward sharp indenters, the $P \propto c_r^{3/2}$ relation becomes a somewhat better model than it is in the case of indenters with larger radii.

Based on the above comparisons, the experimental results obtained using indenters with six different diameters are given in terms of $P \propto d_i\, c_r^{1/2}$ in Figure 4. The results show approximately linear variation of $d_i\, c_r^{1/2}$ with increasing load and slightly decreasing slopes (increasing radial crack length) with decreasing sphere diameter. Apparently, as the sphere diameter decreases there is an increasing contribution to crack growth due to another mechanism such as wedging or residual stresses. In some cases in which there were data points indicating less crack growth than expected based on the general trend of the data for a

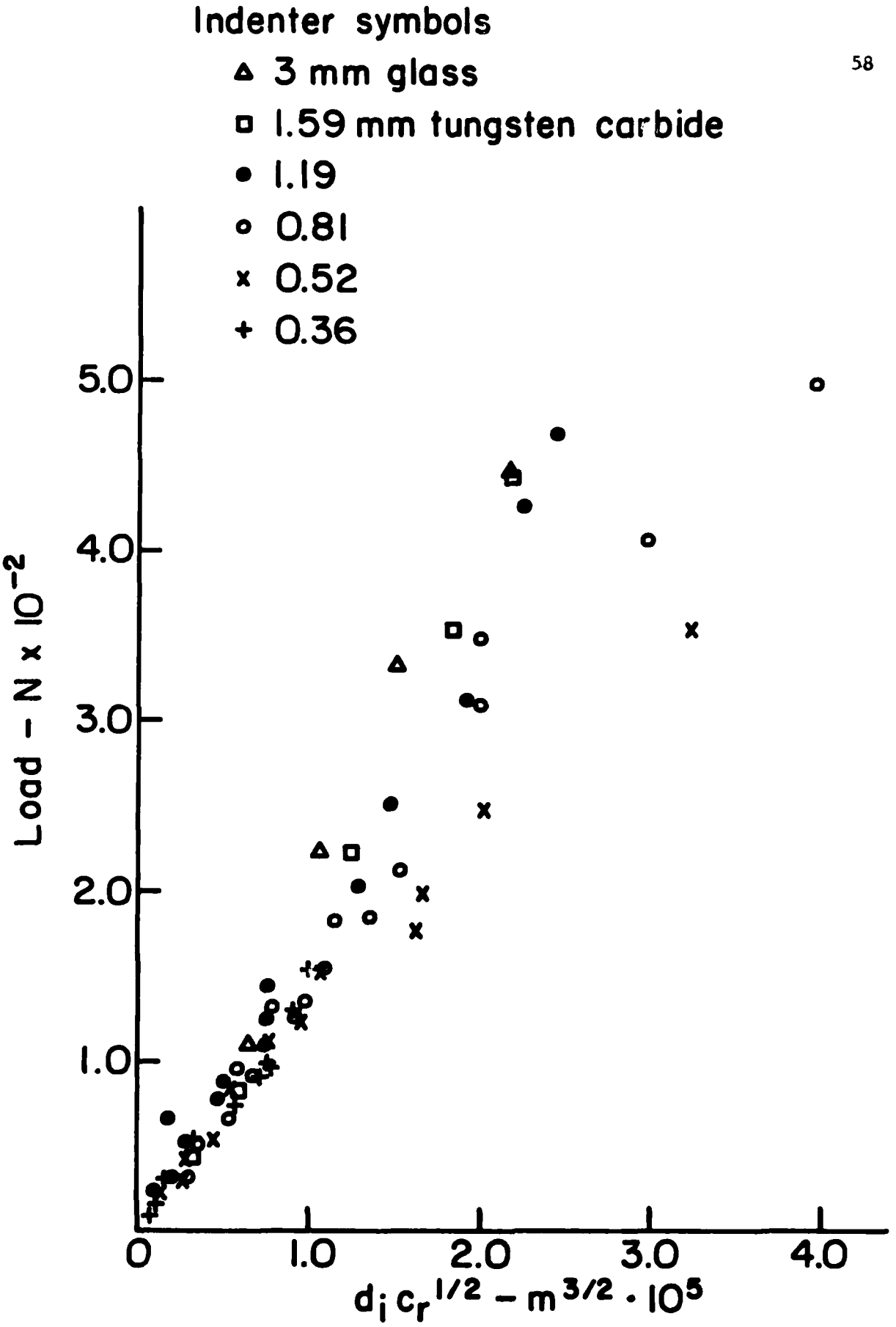

Figure 4. Load vs. $d_i c_r^{\frac{1}{2}}$ for spherical indenters of various diameters.

particular sphere radius, extensive chipping was observed at the indentations. In these cases, the residual stresses may have been relieved to some degree by chipping so that they contributed less to crack growth. In relation to the possibility of an added wedging contribution to crack growth, it should be pointed out that the ratio of the maximum contact radius to the sphere radius increased from 0.26 for the 3mm spheres to 0.77 for the .36mm spheres so that, in general, the contact angle varies with sphere radius in the direction expected to result in an increased wedging effect.

Statistical comparison of the $P \propto c_r^{3/2}$ and $P \propto d_i\, c_r^{1/2}$ relations

The suitability of the above relations was evaluated by comparing the coefficients of determination. When these measures were originally calculated, the scatter introduced by errors in the measurement of d_i was observed to effect the results. The d_i values are subject to error because the indentations are small and not well defined, in part because of chipping. Therefore, the coefficients of determination were recalculated using smoothed d_i values from Figure 1. These results are given in Table I. The coefficients of determination show that the data plotted according to the $P \propto d_i\, c_r^{1/2}$ relation are essentially linear and there is little scatter about the fitted line. The calculated intercepts of the six lines on the load axis are small, ranging from +34 to -5.4 N. The coefficients of determination for $P \propto c_r^{3/2}$ show poorer correlations. Also, the calculated intercepts are larger, consistantly positive and more scattered ranging from 10.4 to 178.6 N. These larger intercepts are not unexpected based on the strong (almost parabolic) curvature evident in Figures 2 and 3. Considering all of this evidence, it is clear that the data fits the $P \propto d_i\, c_r^{1/2}$ relation better than the $P \propto c_r^{3/2}$ relation.

TABLE I

Coefficients of determination of data
in terms of the $P \propto c_r^{3/2}$ and $P \propto d_i c_r^{1/2}$ models

Indenter Description	Coefficient of Determination	
	$P \propto d_i c_r^{1/2}$ model	$P \propto c_r^{3/2}$ model
3 mm glass	0.995	0.941
1.59 mm tungsten carbide	0.997	0.975
1.19 mm " "	0.998	0.960
0.81 mm " "	0.909	0.851
0.52 mm " "	0.972	0.832
0.36 mm " "	0.997	0.990

Effect of the stress distribution on crack propagation

The fact that radial cracks have been observed to form on loading in zinc sulfide[4] means that, at the surface, the out-of-plane hoop stresses in the elastic stress field are tensile under these elastic-plastic conditions rather than compressive as indicated by the theoretical elastic stress distribution for blunt indenters (Figure 5). Evans and Wilshaw[4] have shown numerically that, for the case of a sphere pressed into the surface under elastic-plastic conditions, to the point that the indentation radius equalled the sphere radius, the out-of-plane hoop stresses are tensile. Given the fact that these stresses are the result of a central load accompanied by an elastic-plastic disturbance, it is reasonable to assume that this stress field varies inversely as the square of the radius from the center of the contact as in the case of the out-of-plane hoop stresses directly under the indenter[5]. Furthermore, because the magnitudes of these stresses are fixed by the yield stress at the elastic-plastic boundary and the elastic stress fields scale with the radius of the yield zone[4], it is reasonable to assume that the stress distributions along the surface and under the contact are approximately equal in magnitude and vary similarly except to the extent that the stresses along the surface are affected by free surface effects and friction. Therefore, it is reasonable to apply equation (3) to the present radial cracks in addition to the median cracks for which it was derived.

As shown in Figure 5, near the surface under a blunt indenter subject only to elastic deformation, the stress is compressive as one would expect because ring cracks usually form instead of radial cracks. The sign of the stress changes to tensile between one

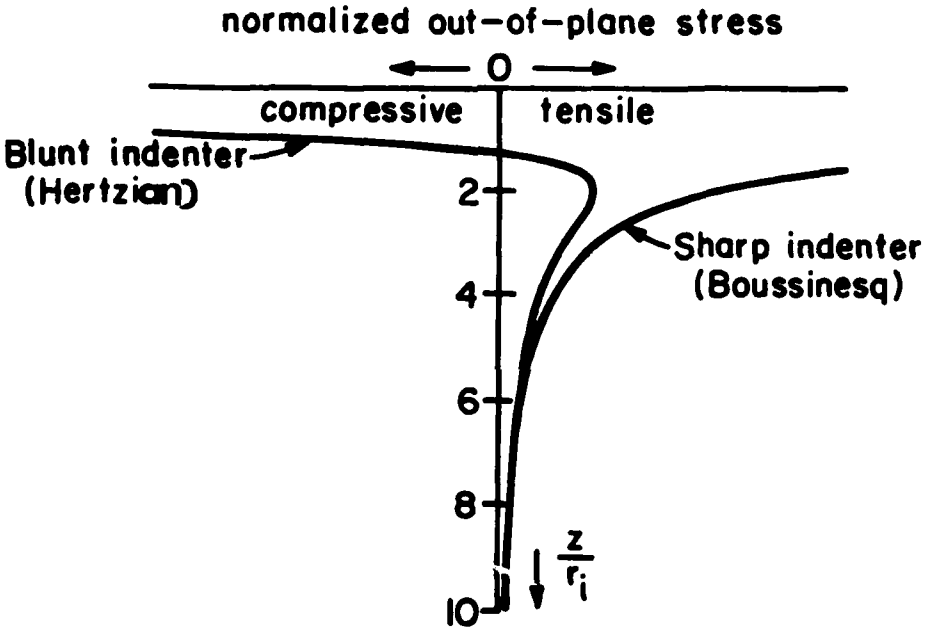

Figure 5. Comparison of normalized out-of-plane stress distributions for blunt and sharp indenters.

and two contact radii below the surface. At greater depths the stress passes through a peak and then decreases slightly more than linearly until it merges with the inverse square distribution in the far field. On the other hand the stress distribution under the sharp indenter decreases inversely with the square of the normalized depth. At first glance it might seem that because of the large difference in these stress distributions the shift from one of these distributions toward the other might lead to large differences in crack propagation. However, in ZnS there is substantial irreversible deformation under all of the spherical indenters. Z_o ranges approximately from one to two contact radii in depth. If we assume as we did previously that the out-of-plane hoop stresses are relaxed by the irreversible deformation, it is clear that the stress intensity factors will not be very different because the stress distributions are much less dissimilar at greater depths.

The nature of the near field-far field problem can be better understood with the aid of Figures 5 and 6. Figure 6 is a plot of the load versus the normalized crack length (c_r/r_i). The data are plotted in this way because the boundary between the near field and the far field is usually expressed in terms of c_r/r_i. It has been common in the case of sharp indenters to consider that the transition from the near field to far field behavior occurs at $c_r/r_i \approx 3$[17]. In Figure 6 this transition should be evidenced by a smaller load dependence of the crack length in the far field.

Beginning with Figure 5, one can see that at $z/r_i > 6$ the stress distributions due to the two types of indenters become identical. However, it would be a mistake to conclude that the resulting crack lengths become the same at this point because the stress intensity factor at the crack

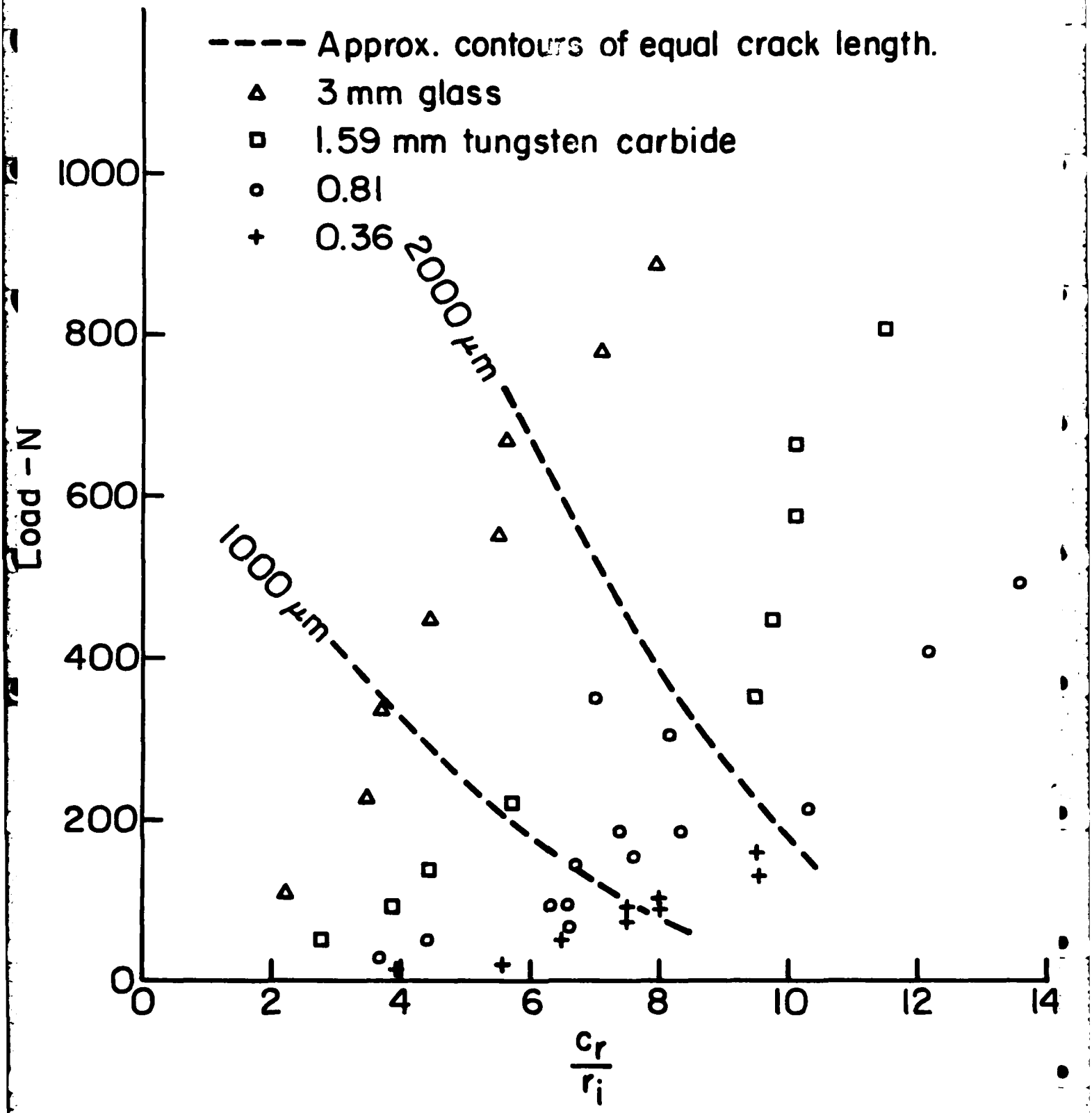

Figure 6. Load vs. c_r/r_i for spherical indenters of various diameters.

tip depends on these stresses integrated from Z_o to c. Therefore, the effect of differences in contact characteristics can extend even farther into the specimen. Turning to Figure 6, it is clear that there is no change in slope or discontinuity in the data obtained using the 3 mm glass spheres. The data from the smaller tungsten carbide indenters are somewhat scattered so that the results are less clear but there appears to be a gradual change in slope at $c_r/r_i \approx 6$ which may indicate a transition from near field to far field behavior. This result is consistent with Roesler's observations for cone cracks and with expectations based on the stress distribution in Figure 5.

IV. CONCLUSIONS

1. For HP ZnS indented by spheres of various radii, the radial crack length data plotted based on $P \propto d_i\, c_r^{1/2}$ yielded essentially linear plots. Theoretical curves based on equation (3) yielded good estimates of the radial crack lengths.

2. Data obtained using the larger indenters and plotted based on $P \propto c_r^{3/2}$ yielded plots with substantial nonlinearity showing that this is not a good model of the response of the material in these cases.

3. Small decreases in the slopes of the P vs. $d_i\, c_r^{1/2}$ curves with decreasing indenter radius may occur as a result of increasing contributions of wedging or residual stresses.

4. The experimental evidence suggests that for the largest diameter spheres the observed cracks propagated in the near field. For smaller diameter spheres both near field and far field propagation may be represented. However, the $P \propto d_i\, c_r^{1/2}$ relation fits the data very well in both cases.

ACKNOWLEDGEMENTS

The writers are pleased to acknowledge the contributions of their associates at Ceramic Finishing Company including T. J. Larchuk and J. A. Tiracorda who made some of the original measurements, and J. C. Conway for helpful discussions, and the sponsorship of the Office of Naval Research.

REFERENCES

1. F. C. Roesler, "Brittle Fractures Near Equilibrium," Proc. Phys. Soc. (London) B69, 981-992 (1956).

2. B. R. Lawn and E. R. Fuller, "Equilibrium Penny-like Cracks in Indentation Fracture," J. Mater. Sci. 10, 2016-2024 (1975).

3. B. R. Lawn and M. V. Swain, "Microfracture Beneath Point Indentations," J. Mater. Sci. 10, 113-122 (1975).

4. A. G. Evans and T. R. Wilshaw, "Quasi-static Solid Particle Damage in Brittle Solids I. Observations, Analysis and Implications," Acta Met. 24, 939-956 (1976).

5. J. C. Conway, Jr. and H. P. Kirchner, "The Mechanics of Crack Initation and Propagation Beneath a Moving Sharp Indenter," J. Mater. Sci. 15, 2879-2883 (1980).

6. J. C. Conway, Jr. and H. P. Kirchner, "Shear Flow and Fracture Beneath Sharp Indentations in Soda-Lime Glass," To be published in the proceedings of the Third International Symposium on Fracture Mechanics of Ceramics.

7. H. P. Kirchner and T. J. Larchuk, "Load/Radial Crack Size Relations for Static Indentations in Zinc Sulfide," Communications Amer. Ceram. Soc. 64 (2) C-27,28 (1981).

8. D. M. Richard and H. P. Kirchner, "Theory of Elastic-Plastic Impact on Ceramics," Proc. Fifth International Conference on Erosion by Solid and Liquid Impact, Cambridge, England (1979) pages 27-1 to 27-10.

9. J. E. Field, S. van der Zwaag and J. T. Hagan, "Liquid Impact Erosion Mechanisms in Transparent Materials," Cavendish Laboratory Report, AFWAL-TR-81-4026 (May, 1981).

10. H. P. Kirchner, R. M. Gruver and D. M. Richard, "Fragmentation and Damage Penetration During Abrasive Machining of Ceramics," from the Science of Ceramic Machining and Surface Finishing II, Edited by B. J. Hockey and R. W. Rice, National Bureau of Standards Publication 562 (1979) Pages 23-42.

11. H. P. Kirchner and E. D. Isaacson, "Residual Stresses in Hot-Pressed Si_3N_4 Grooved by Single Point Grinding," J. Amer. Ceram. Soc. 65 (1) 55-60 (1982).

12. H. P. Kirchner and E. D. Isaacson, "Contact Damage and Residual Stresses Induced During Single Point Grinding of Various Ceramics," To be published in the proceedings of the Third International Symposium on Fracture Mechanics of Ceramics.

13. B. R. Lawn, A. G. Evans and D. B. Marshall, "Elastic/Plastic Indentation Damage in Ceramics: The Median/Radial Crack System," J. Amer. Ceram. Soc. 63 (9-10) 574-581 (1980).

14. H. P. Kirchner and T. J. Larchuk, "Comparisons of Static and Impact Loading Damage in Zinc Sulfide," Submitted for publication.

15. H. P. Kirchner, J. A. Tiracorda and T. J. Larchuk, "Contact Damage in Hot Pressed and CVD Zinc Sulfide," Submitted for publication.

16. S. S. Chiang, D. B. Marshall and A. G. Evans, "The Response of Solids to Elastic-Plastic Indentation. I. Stresses and Residual Stresses," J. Appl. Phys. 53(1) 298-311 (1982).

17. A. G. Evans and E. A. Charles, "Fracture Toughness Determinations by Indentation," J. Amer. Ceram. Soc. 59(7-8) 371-372 (1976).

ELASTIC RECOVERY AT STATIC LOADING AND IMPACT INDENTATIONS IN MgF_2

by

H. P. Kirchner
J. A. Tiracorda
T. J. Larchuk

CERAMIC FINISHING COMPANY
P. O. Box 498, State College, Pa 16801

ABSTRACT

The extent of elastic recovery at spherical indentations in MgF_2 indented by static and impact loads was analysed. The fraction of the indentation depth that was recovered decreased with increasing static load. Similar results were observed for impact loads. The kinetic energy losses increased with a velocity exponent of 2.61, close to the value 2.6 predicted by Hunter for elastic impacts, despite substantial variations in the contributions of various loss mechanisms over the range of velocities for which measurements were made. Apparently the losses are partitioned among the various loss mechanisms that derive their energy from the elastic field.

I. INTRODUCTION

Elastic recovery at elastic-plastic contacts is responsible for residual stresses at indentations and controls the rebounding velocities of impacting particles[1-4]. The residual stresses are an important factor in the propagation of radial and lateral cracks and in determining the strength and erosion rate. The rebounding velocities are sensitive indicators of energy absorption during impact. For these reasons, understanding of elastic recovery is essential to understanding of mechanisms causing damage at contacts.

Lawn and Howes[4] recently extended an earlier analysis of elastic recovery at conical indentations by Stillwell and Tabor[5], introducing the hardness/elastic modulus (H/E) parameter for convenience in materials evaluation and incorporating a residual load term to account for the residual stresses necessarily induced as a result of the post indentation configuration that departs significantly from the initial flat surface. However, in many important cases, contact damage is induced by blunt rather than sharp indenters. Therefore, in the present investigation the Lawn and Howes approach has been used in an attempt to analyse elastic recovery at spherical indentations. This problem is complicated by the fact that, for spheres, the contact angle varies over the surface of the contact rather than remaining constant as in the case of cones or pyramids. This necessitates the use of assumptions the significance of which must be evaluated by comparing predictions with experimental results. The present problem is further complicated by the fact that, for spherical indenters, the initial response of the indented material is elastic in the low load range instead of elastic-plastic as in the case of sharp

indenters. Therefore, a model that accounts for only the elastic-plastic response can be expected to yield good approximations only at higher loads where the initial elastic response is only a small fraction of the total. However, at these higher loads, radial and lateral crack formation, crushing, chipping or pore formation under the indentation may disrupt the simple indentation geometry observed at low loads.

Despite the fact that Lawn and Howes restricted their experiments to loads less than the threshold for crack formation, it is clearly of interest to determine the applicability of their approach to greater loads such as those important in investigations of localized impact damage and erosion. This is one objective of the present investigation.

II. ANALYSIS

When a rigid spherical indenter is pressed into a flat surface of an elastic-plastic material, the initial deformation is elastic but at some load plastic deformation initiates within the plate, spreads with increasing load until it reaches the sphere-plate interface and then along that interface until it reaches the edge of the contact or beyond[6]. The loading tends to depress the edge of the contact below the original surface of the plate but, depending on friction and other factors, plastic flow toward the surface may form a ring-like hump surrounding the contact. Although the profile of this hump can be measured after unloading, little is known about the time dependence of this process during static and impact loading. Therefore, it is assumed in the present case that these effects offset each other so that, as shown in Figure 1a,

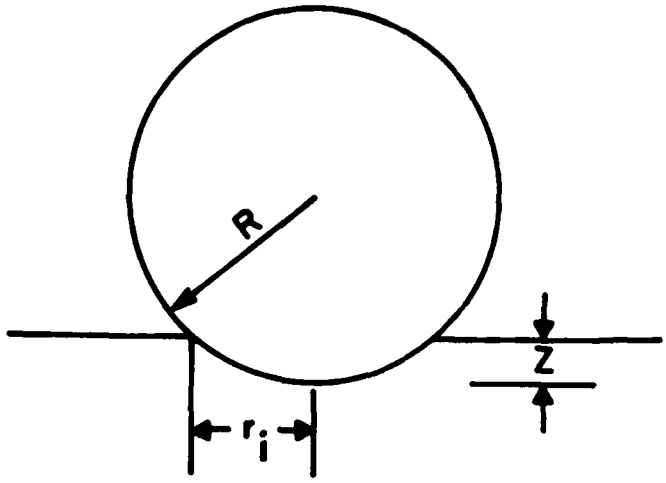

a. Sphere indenting flat surface

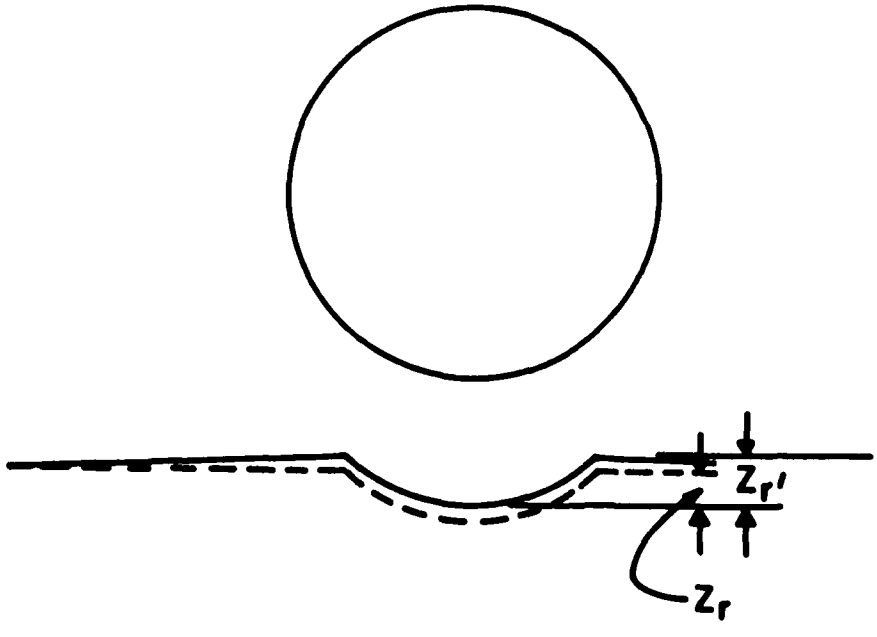

b. Surface after unloading showing elevation caused mainly by lateral cracking

Figure 1 Indentations during loading and after unloading.

the depth of the indentation Z can be measured from the original flat durface.

Loading

Assuming as Lawn and Howes did that the loading half cycle is mainly an elastic-plastic process, the load P is

$$P = p_o \cdot \pi r_i^2 \tag{1}$$

where p_o is the average pressure on the projected area of the indentation and r_i is the radius of the indentation. However, $r_2^2 = 2RZ - Z^2 \simeq 2RZ$ for shallow indentations where R is the sphere radius so that

$$P \simeq 2\pi H R Z \tag{2}$$

where the hardness (H) is taken equal to p_o.

Unloading

During unloading the material in the plate pushes against the indenter so that elastic energy is recovered from the plate. However, as unloading progresses, residual stresses are induced in the region near the indenter as the elastically deformed material relaxes against the irreversibly deformed material under the indentation. Therefore, only part of the stored elastic energy is recoverable during unloading. During subsequent loading cycles, the load path is retraced with only small deviations as long as the maximum load P^* is not exceeded[4]. In the absence of cracking and other complications, unloading can be considered to be mainly an elastic process.

As indicated by Johnson[7], the stresses in the surface of an elastic, semi-infinite solid indented by a rigid sphere are (for small strains)

$$p_o = \frac{4}{3\pi} \frac{E(r_i/R)}{(1-\nu^2)} \tag{3}$$

where ν is poisson's ratio. Therefore the load is

$$P = \frac{8\sqrt{2}}{3} \frac{E R^{1/2} Z^{3/2}}{(1-\nu^2)} \tag{4}$$

in the absence of residual stresses. However, at each point during recovery

$$P = P_E - P_r \tag{5}$$

where P_E and P_r are the elastic and residual loads respectively. Therefore,

$$P = \frac{8\sqrt{2}}{3} \frac{E R^{1/2}}{(1-\nu^2)} (Z^{3/2} - Z_r^{3/2}) \tag{6}$$

At the end of the loading cycle and the beginning of the unloading cycle the indenter loads (P^*) and depths (Z^*) are necessarily equal so that equating (2) and (6),

$$\frac{Z^{*3/2} - Z_r^{3/2}}{Z^*} = \left(\frac{6\pi(1-\nu^2) R^{1/2}}{8\sqrt{2}}\right) \frac{H}{E} \tag{7}$$

and assuming $\nu = 0.3$

$$\frac{Z^{*3/2} - Z_r^{3/2}}{Z^*} = 1.52 R^{1/2} \frac{H}{E} \tag{8}$$

so that as one might expect when H is large relative to E, $\frac{Z^{*3/2} - Z_r^{3/2}}{Z^*}$ is large and Z_r is small (shallow indentation). If Z^* and Z_r can be measured or estimated it should be possible to estimate the dynamic hardness during impact using equations (7) or (8).

Kinetic energy

In the impact case, the kinetic energy is reduced to zero during the loading half cycle so that the work done on the plate (W_i) is

$$W_i = \int_0^{Z^*} P(Z)\, dZ \tag{9}$$

$$W_i = \pi H R Z^* \tag{10}$$

Therefore, comparing the kinetic energy of the sphere with the work done during impact is another means to evaluate this approach.

III. EXPERIMENTAL RESULTS AND DISCUSSION

An MgF_2 plate[Δ] was subjected to static and impact loading using 1.59 mm diameter tungsten carbide spheres[†] as described in more detail elsewhere[8,9]. The contact damage was characterized by optical microscopy and profilometry. Good indentations were observed at all static loads in the load range investigated. Except at the lowest loads, radial and lateral cracks were observed. In the impact specimens, the lateral crack lengths were greater than the radial crack lengths. In many cases these cracks extended to the surface causing extensive chipping. Because these chips include a segment of the surface of the indentation, extensive chipping interfered greatly with determination of the indentation dimensions.

Static loading

Based on measurements of the indentation radii after unloading, the average pressure on the projected area of the indentation is approximately constant for the range of loads used as shown in Figure 2 and Table I. The average of these average pressures was 7.86 GPa. This value is slightly higher than available hardness values, for example 7.3 GPa[4], for this material. These constant pressures support

---

Δ IRTAN 1, Eastman Kodak Co., Rochester, N. Y.
† Ultraspherics, Inc., Saulte Ste. Marie, Michigan.

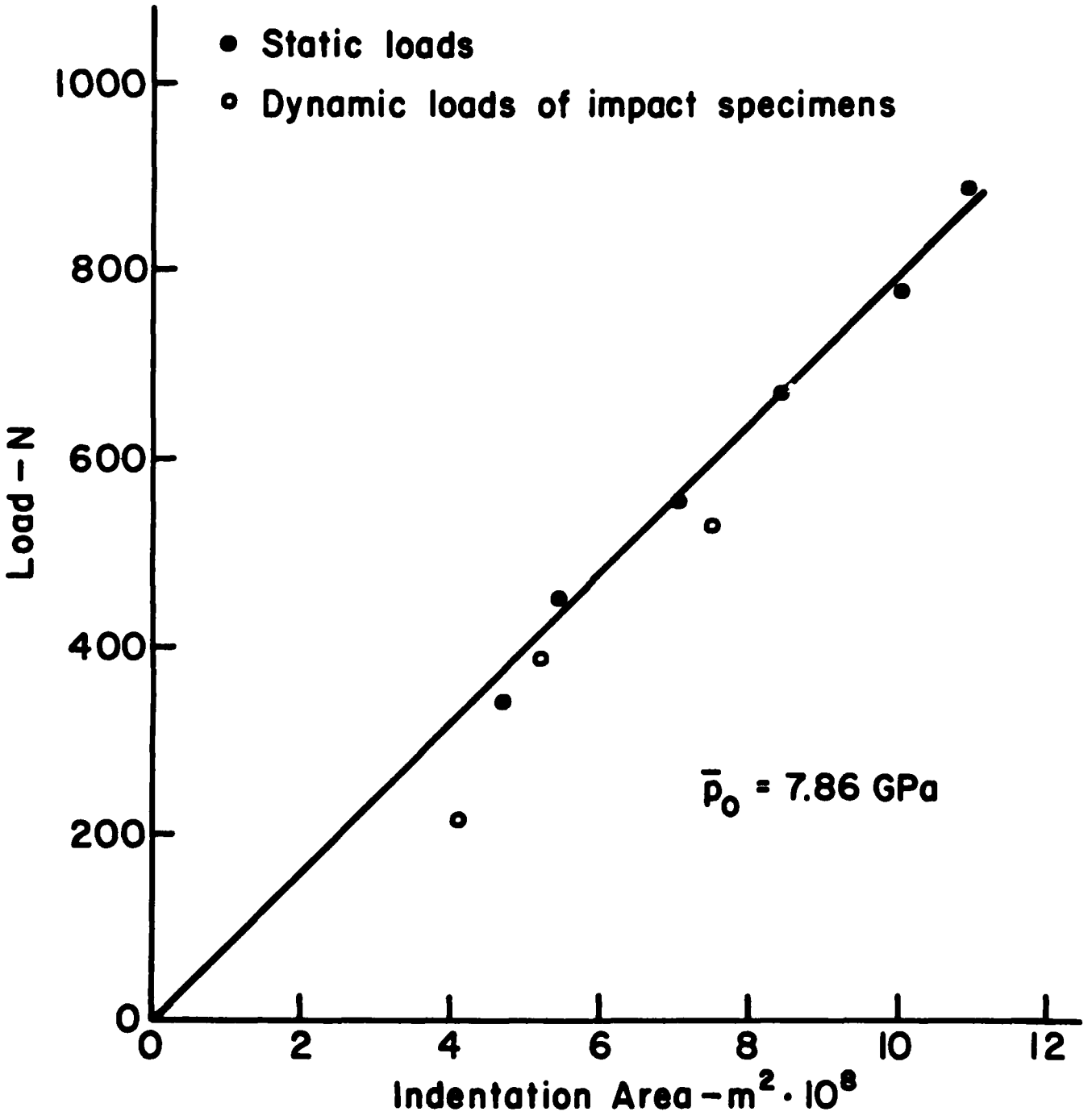

Figure 2 Load vs Indentation Area for static and impact loading of 1.59 mm diam. tungsten carbide spheres on MgF_2.

TABLE I

Indentation Depths at Maximum Load and After Recovery

Site No.	Load	Impact Velocity	Indent. Radius	Indentation Depth at Max. Load	Depth Recovered	at Depth	Fraction Recovered	Hardness
	P	V_o	r_i	Z^*	Z_r	Z_r'	$\frac{Z^* - Z_r}{Z^*}$	H
Static Loading	N	$m \cdot s^{-1}$	μm	μm	μm	μm		GPa
4	445	--	132	11.0†	4	5	.64	8.1
5	556	--	150	14.2†	6	8	.58	7.9
6	668	--	164	16.9†	8	10	.53	7.9
7	779	--	179	20.2†	10	14	.51	7.7
8	890	--	186	21.8†	14	22	.36	8.2
Impact Loading								
8	208†	13.3	114	8.2	4	6	.51	5.1†
10	387†	15.8	129	10.5	3	7	.71	7.4†
1	521†	21.5	154	14.9	[illegible]	11	.56	7.0†

† calculated values

the assumption of constant pressure as a function of Z in equation (2), at least for this particular range of loads.

The indentation depth at each maximum load (Z*) was calculated from the recovered indentation radii assuming that the indenter remained spherical and using E = 115 GPA.

The recovered indentation depths (Z_r) were measured by profilometry. These results are also presented in Table I and show that the recovered depth ranges from about 1/3 to 2/3 of the depth at maximum load and that the fractional extent of recovery decreases with increasing load. This variation is different from the constant Z_r/Z^* predicted by Lawn and Howes for pyramidal indentations in particular materials and it appears to arise from the lack of a constant indenter angle in the case of spherical indentations.

The theoretical predictions and experimental data for the fraction of Z* recovered are compared in Figure 3 and show reasonable agreement. At low values of contact radius the hardness is not exceeded at any point under the contact so an indentation is not observed. However, as the load and contact radius increase, the maximum pressure will, at some point, exceed the hardness under the center of the indentation. If one assumes that a permanent indentation can be formed at this load it is clear that the radius of such an indentation would be small relative to the total contact so that the assumptions relating the load and the average pressure in equation (1) and substitution of the hardness for the average pressure in equation (2) are not justified at low loads. The arrows in Figure 3 indicate the Z* values at which the maximum pressure at the center of the contact and the mean pressure reach 7.86 GPa. Because permanent

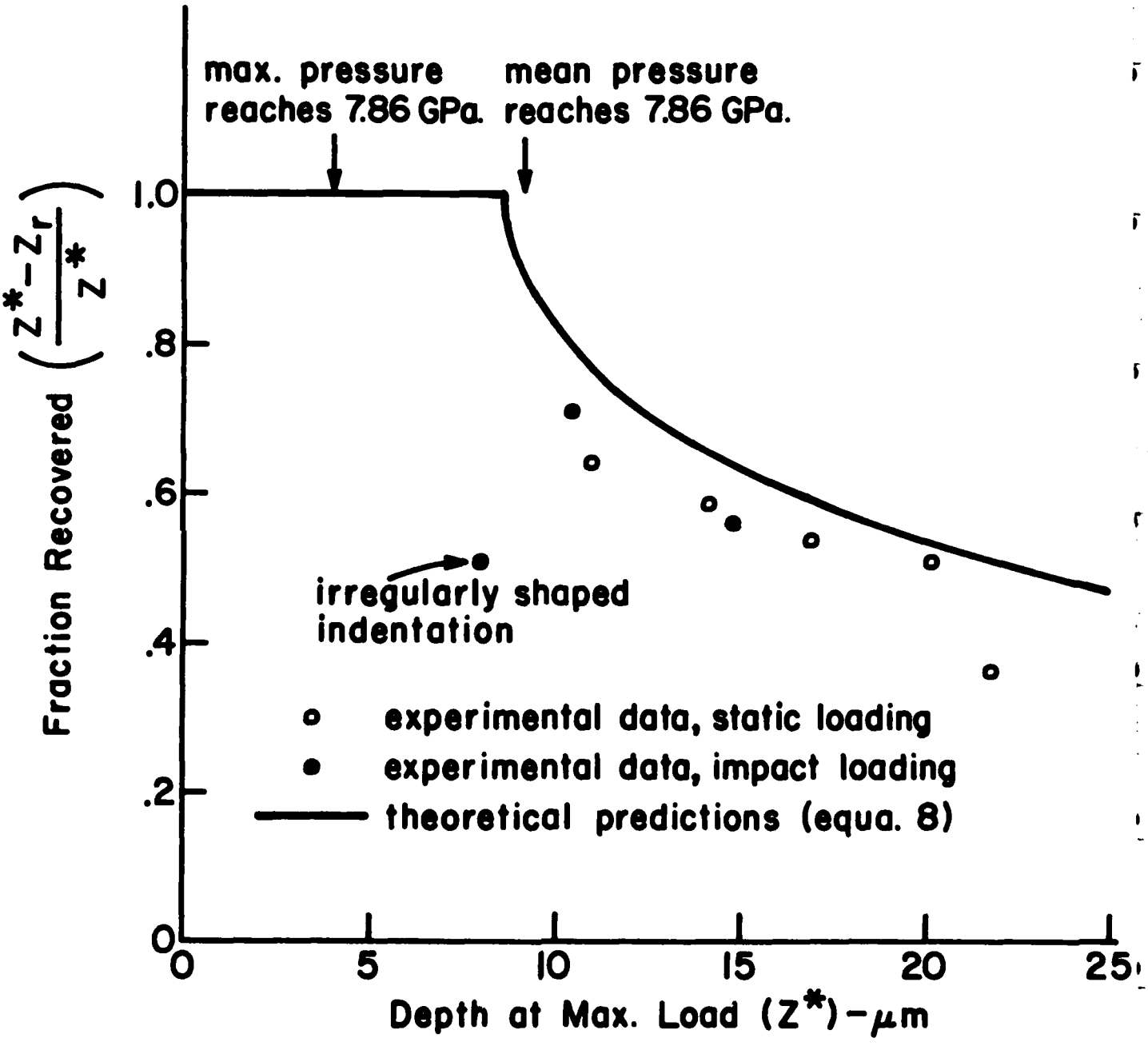

Figure 3 Fraction recovered vs depth at maximum load for static indentations in MgF_2 (WC sphere 1.59 mm diam.)

indentations may be induced for $Z^* > 4$ μm, it is clear that equation (8) overestimates the fraction recovered in the range $4 < Z^* < 8.6$ μm. However, the experimental data may extrapolate to total recovery at $Z^* = 4$ μm, where plastic deformation is first expected to occur.

Impact loading

Except at low impact velocities, extensive chipping removed much of the indentation surfaces so that the specimens were not suitable for measuring the recovered indentation depth. Therefore available data are limited to three data points mainly at low velocities. By substituting Z^* and Z_r in equation (8), the dynamic hardness was estimated. The results are given in Table 1 and plotted in Figure 2. The fraction recovered was also calculated and plotted in Figure 3. Because the elastic recovery is somewhat less than expected for a material of this hardness and Young's modulus, the dynamic hardness values and the fraction recovered are lower than might have been expected.

The kinetic energies of the impacts can be estimated from the mass and velocity of the impacting sphere as well as from the depth Z^* of the indentation. Results from both methods are compared in Figure 4. At low impact velocities the kinetic energies, calculated using equation (8), are close to the values calculated from the mass and impact velocity. In this velocity range good indentations with little chipping are formed. Therefore, the measurements of the indentation radii and the estimates of Z^* should be reliable. Furthermore, the elastic-plastic mechanism of indentation formation and energy absorption is consistent with the assumptions of the analysis. Therefore, the model can be used to estimate the impact energy at low velocities. At

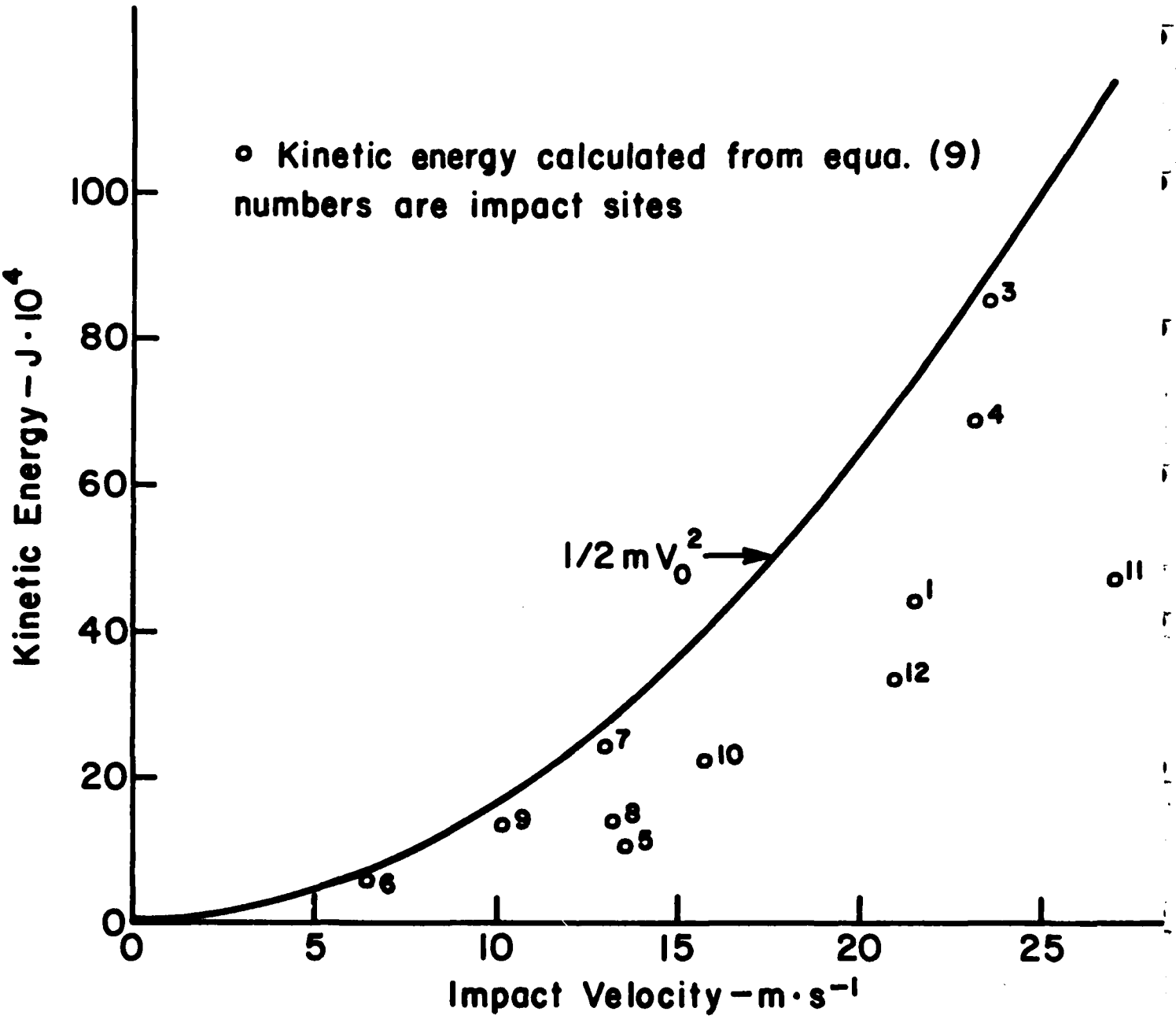

Figure 4 Kinetic energy vs impact velocity for impacts of 1.59 mm diameter tungsten carbide spheres on MgF_2.

higher velocities considerable chipping, lateral cracking and crushing are observed. The chipping introduces uncertainty into the measurement of the indentation radii which in turn affects the estimates of Z*. It appears that in some cases in which the sides of the indentation have been chipped away, r_i has been underestimated leading to underestimates of Z*. Because the kinetic energies depend on Z^{*2}, the resulting errors can be large.

In principle it should be possible to derive equations for the rebounding kinetic energy and the coefficient of restitution using the Lawn and Howes approach. However, in view of the scatter in the impact kinetic energy data, this approach seems unpromising in this case. However, the measured impact and rebounding velocities were used to calculate the coefficients of restitution as shown in Figure 5. The coefficient of restitution (e) decreases gradually with increasing impact velocity in contrast to the Lawn and Howes prediction of a constant value for impacts of pyramidal indenters. This difference can be explained, at least in part, by the fact that at low impact velocities spheres are expected to have high coefficients of restitution because there is little or no plastic deformation. At higher impact velocities the fraction of the kinetic energy loss due to plastic deformation increases, thus decreasing the coefficient of restitution. It is expected that this tendency will be moderated to some extent by the increase in dynamic hardness with impact velocity.

The log kinetic energy loss varies linearly with log impact velocity as shown in Figure 6. The slope is 2.61, a value very similar to the value 2.6 predicted by Hunter[11] for elastic impacts of spheres on flat plates. Except perhaps at 6.25 $m \cdot s^{-1}$ impact velocity, cracks were

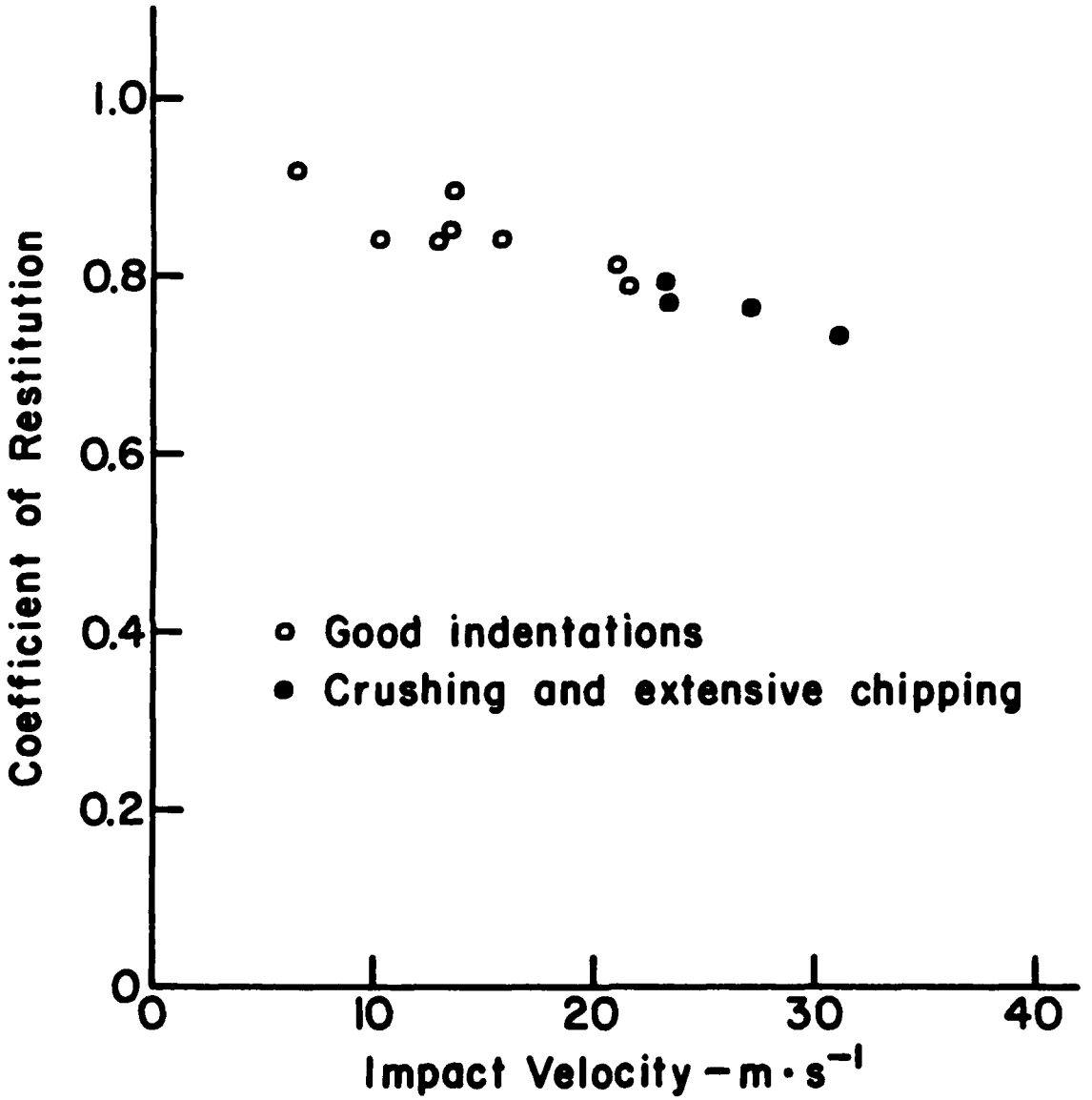

Figure 5 Coefficient of restitution vs impact velocity, MgF_2 Plate, 1.59 mm diameter WC sphere.

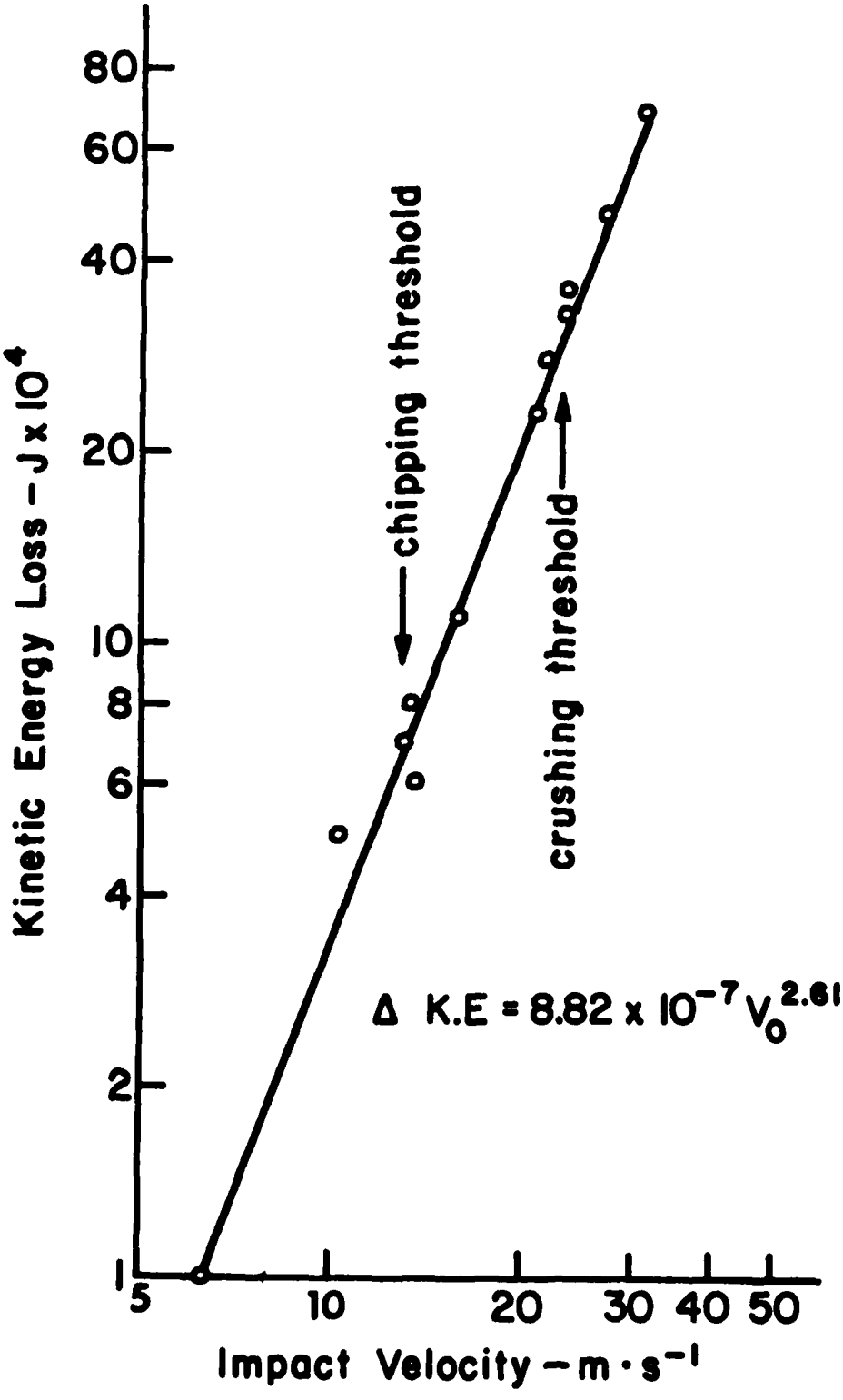

Figure 6 Kinetic energy loss vs impact velocity for impacts of 1.59 mm diameter WC spheres on MgF_2.

observed at all of the impact sites. The threshold velocities for chipping (10 $m \cdot s^{-1}$) and crushing (23 $m \cdot s^{-1}$) are marked on the curve. One might have expected that additional loss mechanisms such as chipping and crushing would cause increasing kinetic energy loss over that expected but this was not observed. Apparently, because these mechanisms depend on the elastic stress field, the energy losses are partitioned among the available mechanisms. Earlier observations[12] involving crushing in a viscoelastic material gave a different result in which the slope increased at the crushing threshold, probably because of friction losses that do not depend on the elastic field.

The results in Figure 6 are also significant in terms of elastic recovery. One might have thought, for example, that relief of the residual stresses induced during elastic recovery by chipping might increase the extent of elastic recovery, thus increasing the coefficient of restitution and decreasing kinetic energy loss in those specimens. Instead, the results seem to indicate that the details of the recovery process are not important.

IV. CONCLUSIONS

The existence of other damage mechanisms in addition to plastic deformation at the indentation is not in itself a decisive reason for not applying the Lawn and Howes[4] approach to analysis of the recovery at indentations formed by static or impact loading by spheres. In fact, an analysis for spheres based on their approach yielded predictions that were confirmed in several respects by static and impact loading experiments on MgF_2. The principal difficulties were practical problems like

measuring the indentation radius when part or all of the sides of the indentation have been removed by chipping and measuring the depth of the indentation in the presence of a raised specimen surface caused by lateral cracking.

In MgF_2, the contact pressure was approximately constant over the range of loads used in the static loading experiments. The fraction of the indentation depth that is recovered decreased with increasing static load as predicted by the theory. This result differs from the constant value obtained previously by Lawn and Howes for static pyramidal indentations in a wide variety of materials.

In impact experiments, elastic recovery is similar to that in static loading experiments. The coefficient of restitution decreases with increasing impact velocity reflecting at least in part the decrease in the fraction of the indentation depth that is recovered, with increasing impact velocity. The slope of the log kinetic energy loss vs. log impact velocity curve was 2.61 in excellent agreement with Hunter's[11] prediction for elastic impacts where the losses are mainly due to stress waves. The presence of different loss mechanisms such as plastic deformation, chipping and crushing did not vary the slope of this curve. Apparently, the energy losses for the mechanisms deriving their energy from the elastic field are subject to a partitioning process so that if one mechanism requires more energy, other mechanisms must be limited.

ACKNOWLEDGEMENTS

The writers are pleased to acknowledge the cooperation of Professor Carlo G. Pantano and of personnel at the Materials Research Laboratory at Penn State University, the contributions of their associates at Ceramic Finishing Co., and the sponsorship of the Office of Naval Research.

REFERENCES

1. J. J. Petrovic, L. A. Jacobson, P. K. Talty and A. K. Vasudevan, "Controlled Surface Flaws in Hot-Pressed Si_3N_4," J. Amer. Ceram. Soc. 58 (3-4) 113-116 (1975).

2. D. B. Marshall and B. R. Lawn, "Residual Stress Effects in Sharp Contact Cracking; I, Indentation Fracture Mechanics," J. Mater. Sci. 14 (8) 2001-2012 (1979).

3. H. P. Kirchner and E. D. Isaacson, "Residual Stresses in Hot-Pressed Si_3N_4 Grooved by Single Point Grinding," J. Amer. Ceram. Soc. 65 (1) 55-60 (1982).

4. B. R. Lawn and V. R. Howes, "Elastic Recovery at Hardness Indentations," J. Mater. Sci. 16, 2745-2752 (1981).

5. N. A. Stillwell and D. Tabor, "Elastic Recovery at Conical Indentations," Proc. Phys. Soc. (London) 78, 169-179 (1961).

6. D. Tabor, "The Hardness of Metals," Oxford at the Clarendon Press (1951).

7. K. L. Johnson, "The Correlation of Indentation Experiments," J. Mech. Phys. Solids 18, 115-126 (1970).

8. H. P. Kirchner and T. J. Larchuk, "Load/Radial Crack Size Relations for Static Indentations in Zinc Sulfide," J. Amer. Ceram. Soc. 64 (2) C27-28 (1981).

9. H. P. Kirchner and T. J. Larchuk, "Comparisons of Static and Impact Loading Damage in Zinc Sulfide," To be published in J. Amer. Ceram. Soc.

10. Eastman Kodak Company Publication U-72 (1971).

11. S. C. Hunter, "Energy Absorbed by Elastic Waves During Impact," J. Mech. Phys. Solids 5, 162-171 (1957).

12. H. P. Kirchner and R. M. Gruver, "Localized Impact Damage in a Viscous Medium (Glass)," from Fracture Mechanics of Ceramics, Vol. 3, Edited by R. C. Bradt, D. P. H. Hasselman and F. F. Lange, Plenum, New York (1978) pages 365-377.

EFFECT OF MECHANICAL IMPEDANCE ON THE DISTRIBUTION OF STRESS WAVE ENERGY DURING PARTICLE IMPACT

by

D. M. Richard
H. P. Kirchner

CERAMIC FINISHING COMPANY
P. O. Box 498, State College, Pa. 16801

ABSTRACT

Stress wave energy is the principal energy loss mechanism in elastic impacts on firmly supported targets and is a significant loss mechanism in other cases. In this paper, Hunter's analysis is extended to the case in which the mechanical impedance of the impacting particle is finite. Expressions are derived for the total stress wave energy and the stress wave energies in the target and the impacting particle. These expressions are used to explore the effect of the impedance on the efficiency of an impact and the stress wave energy. The theoretical results are compared with measurements of the coefficient of restitution for impacts on a glass.

AD-A120 952 LOCALIZED IMPACT DAMAGE IN CERAMICS(U) CERAMIC 2/2
FINISHING CO STATE COLLEGE PA H P KIRCHNER ET AL.
31 AUG 82 N00014-74-C-0241

UNCLASSIFIED F/G 11/2 NL

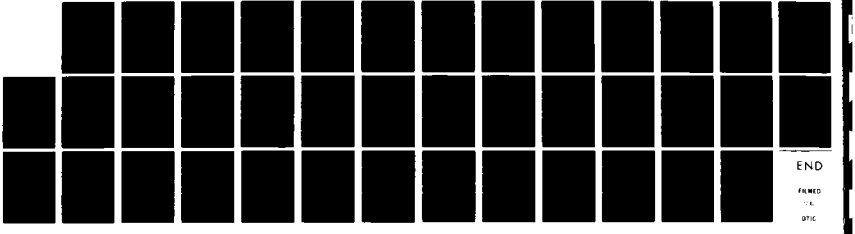

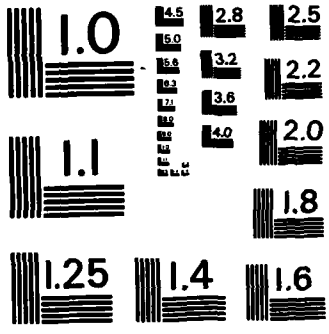

MICROCOPY RESOLUTION TEST CHART
NATIONAL BUREAU OF STANDARDS-1963-A

I. INTRODUCTION

Some theories of impact assume that the stress wave energy is negligible[1]. This assumption enables one to directly derive the velocity dependence of important characteristics such as load, contact time and depth of damage. However, if one analyzes the energy losses during impact on firmly supported targets, the stress wave energy is an essential factor, especially in an elastic situation where it represents the only significant loss.

The present analysis is concerned with extension of Hunter's[2] analysis of the stress wave energy in a semi-infinite solid to the case of a real impact in which the mechanical impedance of the impacting particle is not assumed to be infinite. This analysis is followed by an inquiry into the role of the impedance of the target and the particle on the efficiency of an impact and its relation to the energy of the stress waves. The theoretical results were compared, to the extent possible, using experimental data for the coefficient of restitution for impacts at various velocities on glass at various temperatures[3].

II. EXTENSION OF HUNTER'S ANALYSIS

Hunter[2] derived an expression for the stress wave energy stored in a target after impact by a spherical projectile. The derivation assumed the radiation impedance* of the projectile to be infinite in the same way as Miller and Pursey[4,5] assumed a perfect oscillator in their analysis of the field and radiation impedance of mechanical radiators.

However, in real impact situations, the radiation impedance of an impacting particle (i.e. the radiator) is finite. If a stress is applied to the particle, a displacement will appear within it, and stress waves will propagate. Thus, part of the stress wave energy, produced by impact, is induced in the particle.

To derive an expression for the stress wave energy induced in the particle, one can follow a derivation similar to that of Miller and Pursey[4] for a semi-infinite solid. This approach is reasonable. Indeed, Love[6] has shown the similarities in the elastic behavior of a half plane and a disk. Therefore, one can expect such similarities to come into play when comparing a sphere and a semi-infinite solid.

Miller and Pursey's[4] derivation describes the case where a circular disk of finite radius vibrates normally to the free surface of a semi-infinite solid. For these conditions, they derive the expression for the displacement of the free surface of the solid. Then they determine the energy carried by the stress waves thus produced and compute the partitioning

---

*The radiation impedance is defined as the ratio of the stress to the mean displacement velocity under the radiator in the direction of the applied stress[4].

of this energy among the various types of waves (compressional, shear and surface waves)[5]. Hunter generalized the results of Miller and Pursey to cover the problem of transient pulses. Using the expression for the normal displacement of the free surface of a semi-infinite body subjected to a uniform periodic surface pressure $pe^{i\omega t}$ acting over a surface of radius (a), the mean surface displacement ($\bar{u}$) over the circle of contact (contact area of impact) was obtained, by Fourier synthesis, for a pressure pulse of arbitrary profile p(t) [2]. This result was a key to determining the stress wave energy produced in the target during impact which is given by*

$$W_t = \frac{2\,\tau\, m_p^{-1/5}\, R_p^{3/5}\, g^{-6/5}}{\rho_t\, c_{0t}^3} V_0^{3/5}\,(\tfrac{1}{2}\, m_p\, V_0^2) \qquad (1)$$

For a spherical particle, the derivation will follow the same pattern described in the above paragraph.

As Miller and Pursey[4] did, one can write the expression relating the components of the displacement (u_i) to the dilatation (div $\vec{U} = \Delta$) and the distortion ($\vec{rot}\ \vec{U} = \vec{W}$), as well as the partial differential equations characteristic of the dilatation and the distortion. The expressions for the stress across the free surface as functions of the displacement complete the set of equations necessary to solve the problem.Φ Hankel's transform[7,8] was used to change the partial differential equations to differential equations. In the case of a semi-infinite solid, this transformation is

---

*See Appendix A for definitions of symbols.

ΦThese relationships are written in a cylindrical system of coordinates with the origin at the center of the contact area and the z axis extending from this origin along the diameter of the particle (Fig. 1) as in the case (z) of Reference 4.

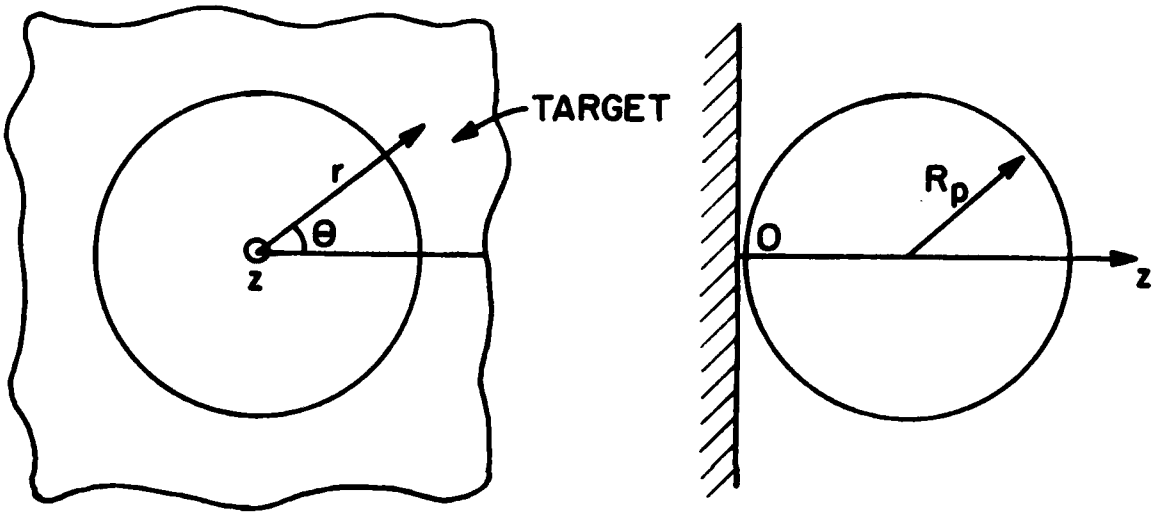

Figure 1. System of coordinates used in the derivation (center is at the center of the contact area. System (θ,r) parallel to the target and axis Z coinciding with the diameter of the particle and with origin O).

relatively simple but complications occur in the spherical case because application of Hankel's transform to a derivative involves introduction of boundary conditions. These boundary conditions are such that the surface of the sphere is free of stress outside the contact area. Under these conditions, remembering cylindrical symmetry, use of Hankel's transform implies introduction of bulk dilatation and bulk distortion of the sphere and their derivatives. In effect, in the treatment of the stress waves in a sphere, the partial differential equations are transformed into non-homogenous differential equations (see Appendix B). These equations could probably be solved but since the analysis of the bulk deformation of a particle is beyond the scope of this particular investigation, this problem was avoided by assuming a rigid sphere (based on the distinction that stress waves are properties of the medium and bulk deformation is a property of the body*). This assumption enables one to equate to zero the second member of the differential equations characteristic of the stress waves in the sphere and, in consequence, to use the results for a semi-infinite solid to describe these stress waves in a sphere. In order to determine the stress wave energy in the particle, we can relate it to the amount of stress wave energy in the target through the notion of intensity. The intensity of an elastic wave is defined as the mean power transmitted per unit of surface[9]. For the target, this intensity

---

*Such an assumption is comparable to the assumption of a non-bending plate.

will be equal to the stress wave energy divided by the time of contact (t_c) and the contact area (πa^2)

$$I_t = \frac{W_t}{t_c \pi a^2} \quad (Jm^{-2}s^{-1}) \tag{2}$$

This wave intensity is known to be equal to the applied stress squared divided by the characteristic impedance of the medium ($\rho_t c_{0t}$)[9].

Therefore, one can write for the target

$$I_t = \frac{W_t}{t_c \pi a^2} = \frac{p^2}{\rho_t c_{0t}} \tag{3}$$

Similary, for the particle

$$I_p = \frac{W_p}{t_c \pi a^2} = \frac{p^2}{\rho_p c_{0p}} \tag{4}$$

As p, t_c and πa^2 are the same for the target and particle, they can be eliminated yielding

$$W_p = W_t \left(\frac{\rho_t c_{0t}}{\rho_p c_{0p}}\right) \tag{5}$$

Therefore, Hunter's formula can be extended as

$$W_s = W_t \left(1 + \frac{\rho_t c_{0t}}{\rho_p c_{0p}}\right) \tag{6}$$

in which W_t is given by equa. (1). This equation shows that the impedance ratio between the target and the particle has a significant effect on the impact characteristics.

III. EFFECT OF THE IMPEDANCE RATIO ON THE PARTITIONING OF STRESS WAVE ENERGY

If one assumes the particle to have infinite impedance, one derives the results found by Hunter [2], namely

$$W_s = W_t \tag{7}$$

If one assumes the particle and the target to have the same characteristic impedance, one should find that the total stress wave energy is twice that induced in the target. Kirchner and Gruver[10] obtained experimental results consistent with this expectation for impacts of glass spheres on glass plates for which the target and particle have the same characteristic impedance. Similarly, this result implies a better match between Hunter's theory and the data of Tillet[11]. In that case the experimental values for the coefficient of restitution are lower than predicted by Hunter's theory. Introduction of a finite impedance ratio implies a larger stress wave energy loss, hence a lower coefficient of restitution.

The distribution of the stress wave energy between the particle and the target varies substantially depending on the properties of the particular materials. Letting (n) be the ratio of the characteristic impedance of the target to that of the particle, equa. (6) becomes

$$W_s = W_t \quad (1 + n) \tag{8}$$

$$\frac{W_t}{W_s} = \frac{1}{1 + n} \tag{9}$$

and

$$\frac{W_p}{W_s} = \frac{n}{1 + n} \tag{10}$$

Table I gives the percentages of the total stress wave energy in the target and the particle for the realistic range of (n). These data have practical importance in some cases. For example, ceramic armor with a high Young's modulus (i.e. a high characteristic impedance) is likely to have a high impedance compared to a given projectile so that substantial stress wave energy is induced in the projectile, increasing the likelihood that the projectile will be destroyed by reflected stress waves. Similarly, in the case of IR windows, high characteristic impedance is a desirable property for the same reason.

TABLE I

PERCENTAGES OF THE TOTAL STRESS WAVE ENERGY IN THE PARTICLE AND TARGET FOR VARIOUS VALUES OF n

$n = \frac{\rho_t c_{0t}}{\rho_p c_{0p}}$	Stress Wave Energy in the Target %	Stress Wave Energy in the Particle %
0.2	83	17
0.4	71	29
0.6	63	37
0.8	56	44
1	50	50
2	33	67
3	25	75
4	20	80
5	17	83
6	14	86

IV. THE EFFECT OF TARGET AND PARTICLE IMPEDANCE ON THE AMOUNT OF STRESS WAVE ENERGY PRODUCED DURING IMPACT

Before analyzing the expression for total stress wave energy developed in Section II (equa. (6)), it is enlightening to analyze in detail Hunter's formula (equa. (1)) in terms of impedance. A simple substitution of the value of the target impedance

$$Z_t = \sqrt{E_t \rho_t} = \rho_t c_{0t} \tag{11}$$

in equation (1) yields

$$W_t = \frac{2\tau m_p^{-1/5} R^{3/5} g^{-6/5} \rho_t^{2} V_o^{3/5}}{Z_t^{3}} \left[\tfrac{1}{2} m_p V_o^2\right] \tag{12}$$

This expression cannot be reduced to a simple function of the target impedance $W_t = f(Z_t)$. Thus, it must be analyzed as a multivariate function dependant upon impedance, density and elastic modulus of both target and projectile, or formally

$$W_t = f(Z_t, E_t, E_p, \rho_t, \rho_p) \tag{13}$$

To evaluate the behavior of such a function, a study of its projections in various planes is necessary. a. First the projectile and the incoming velocity are kept constant ($E_p = 50\ 10^9$ N/m^2, $\rho_p = 2000$ kg/m^3 $V_o = 80$ m/s $R = .001$m), thus insuring constant incoming energy. With this constraint, the density and elastic constant of the

target are independantly varied within a range centered around the projectile characteristics

$$1000 < \rho_t < 3000 \quad K_g\ m^{-3}$$

$$30 \cdot 10^9 < E_t < 70 \cdot 10^9 \quad N\ m^{-2}$$

The variations of the resulting stress wave energy in the target (W_t) are then plotted as a function of the density and the elastic constant of the target (Fig. 2a and Fig. 2b). These graphs show a behavior consistent with simple wave mechanics; an increase in the density (i.e. mass) yields more stress wave energy in the form of inertia. On the contrary, an increasing elastic constant decreases the potential for displacement (particle velocity) and thus, decreases the energy of the stress wave.

Fig. 2c shows the variation of the stress wave energy in the target (W_t) as a function of the target impedance. The variations at constant elasticity or constant density are easily traced on this graph. This plot also shows that the spread of possible values of the stress wave energy varies with the impedance, as a relatively larger target impedance yields less variability than a smaller one. This effect is due to the relative importance of the target density and elastic modulus in the impedance, which favors the elastic modulus at high impedance and favors the density at low impedance.

b. To complete the analysis of the stress wave energy in the target, a similar evaluation of Hunter's equation must be made for a constant target. However, to allow comparison with the previous analysis, one must keep the same incoming energy. As a consequence, one must vary the incoming

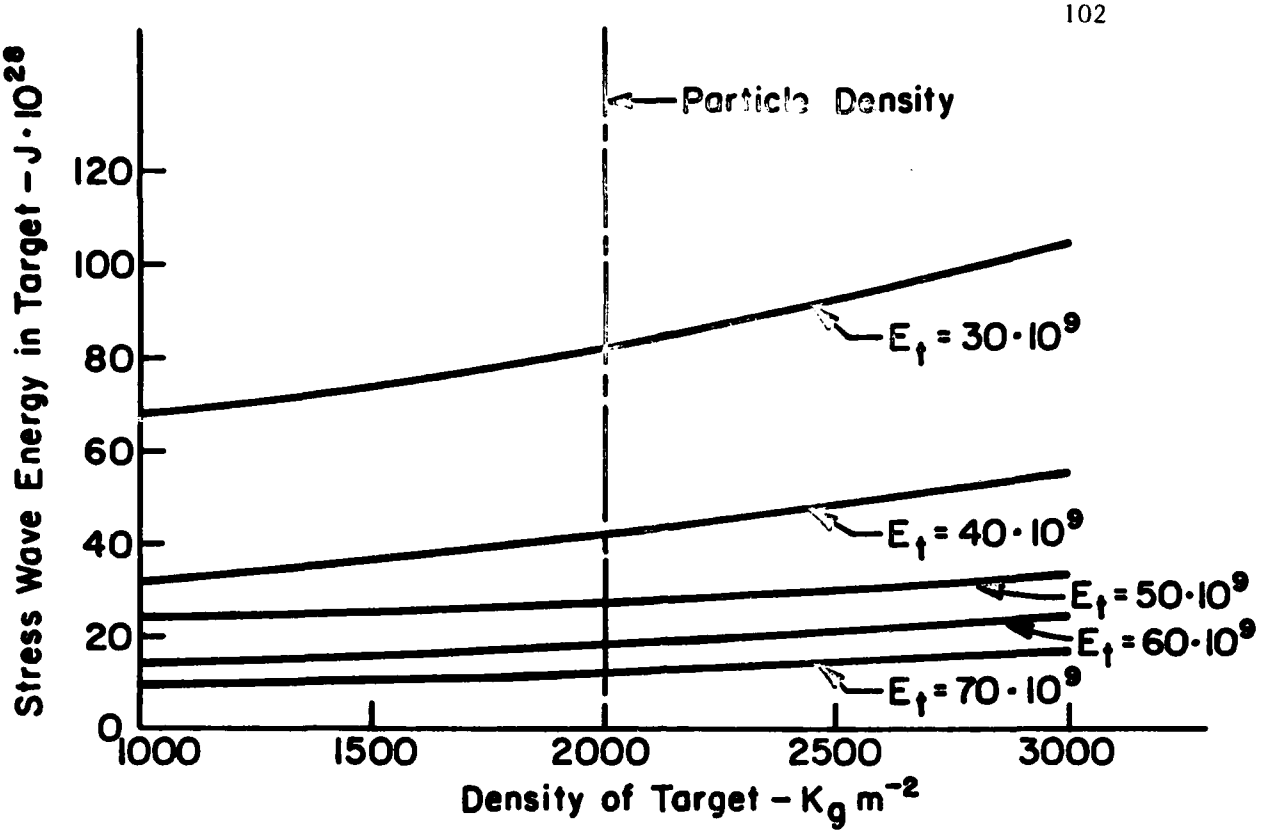

Figure 2a. Stress wave energy in target vs. target density for fixed particle properties and impact energy.

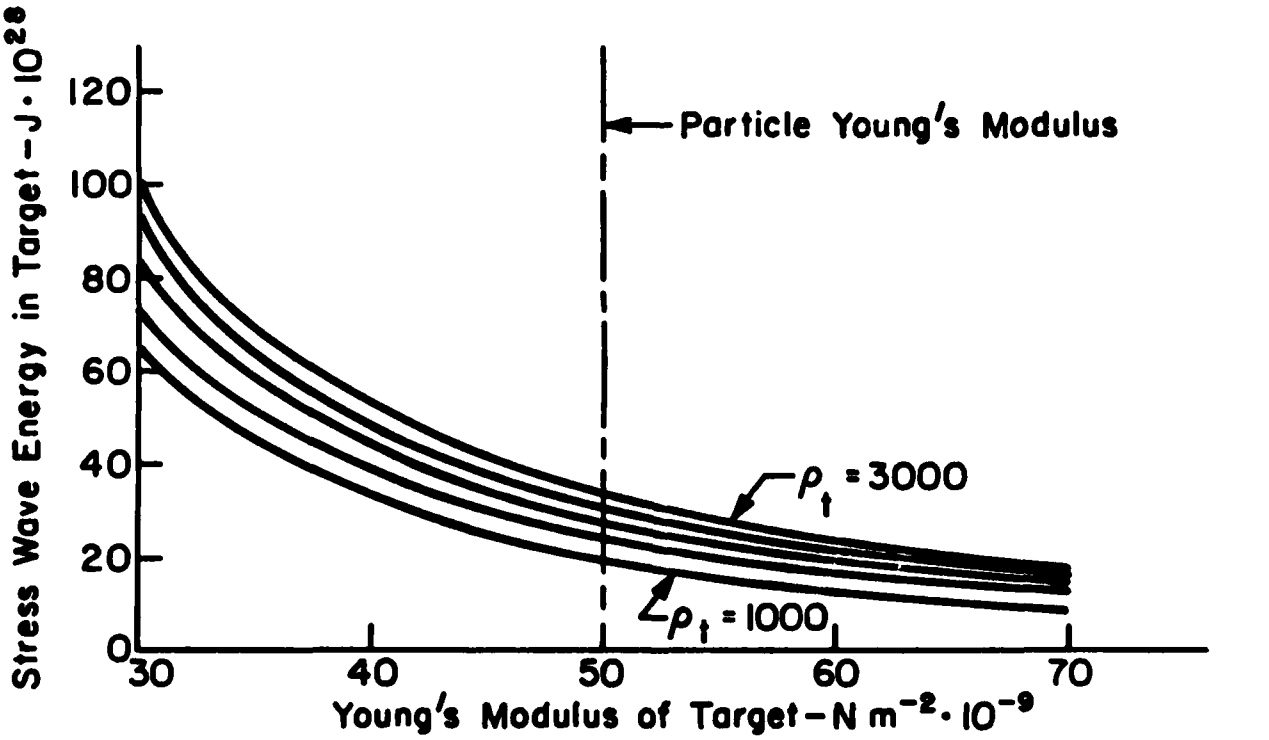

Figure 2b. Stress wave energy in target vs. Young's modulus of target for fixed particle properties and impact energy.

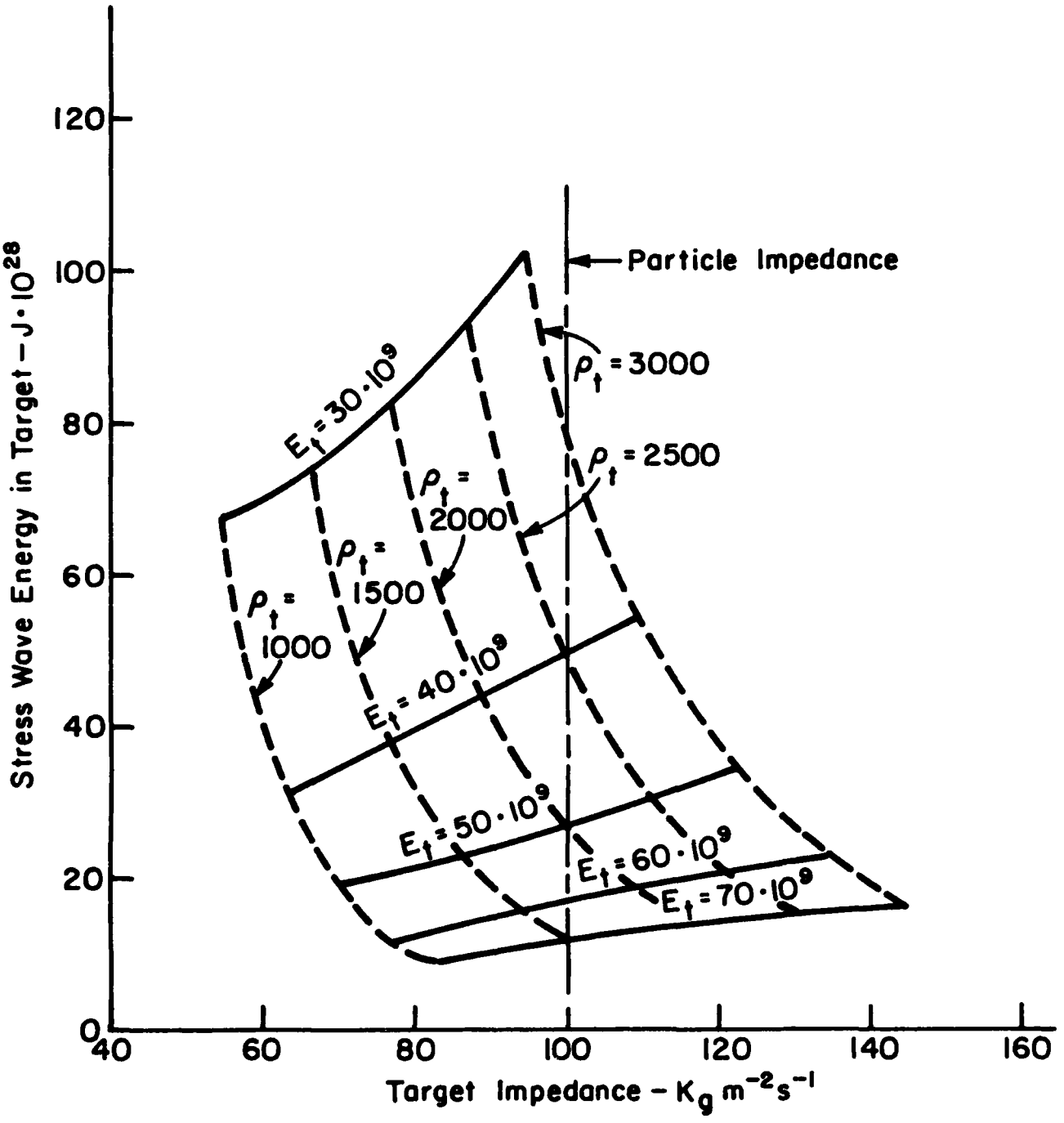

Figure 2c. Stress wave energy in target vs. target impedance for fixed particle properties and impact energy.

velocity with the varying particle density according to

$$V_1 = V_o\sqrt{\frac{\rho_o}{\rho_1}} \qquad (14)$$

where V_o and ρ_o are the velocity and density of the particle in the previous analysis. With this minor change, the analysis proceeds as before (Fig. 3a, 3b and 3c). There the plot of the stress wave energy shows little variation with density and a decreasing variation with the elastic constant. One must remark, however, that the energy developed in that case is somewhat lower than in the previous case; in particular, the level of energy varies when the characteristics of the target and the particle are interchanged.

When the total stress wave energy is considered, two cases must be distinguished (Fig. 4a and 4b):

a. If the particle characteristics are kept constant and the target characteristics are taken as equal to those of the particle, then the total stress wave energy is double that in the target. As the target impedance decreases, the total stress wave energy becomes less than double the target stress wave energy and, conversely, as the impedance of the target increases, the total stress wave energy is more than double that of the target. The overall effect is a reduction in the variation of spread of possible values for the stress wave energy for various target impedances that were observed earlier (Fig. 2c).

b. When the target characteristics are kept constant, the effect of the impedance ratio is reversed: low relative particle impedance yielding a ratio of total stress wave energy to target stress wave energy larger than 2 while a high relative particle impedance yields a ratio lower than 2.

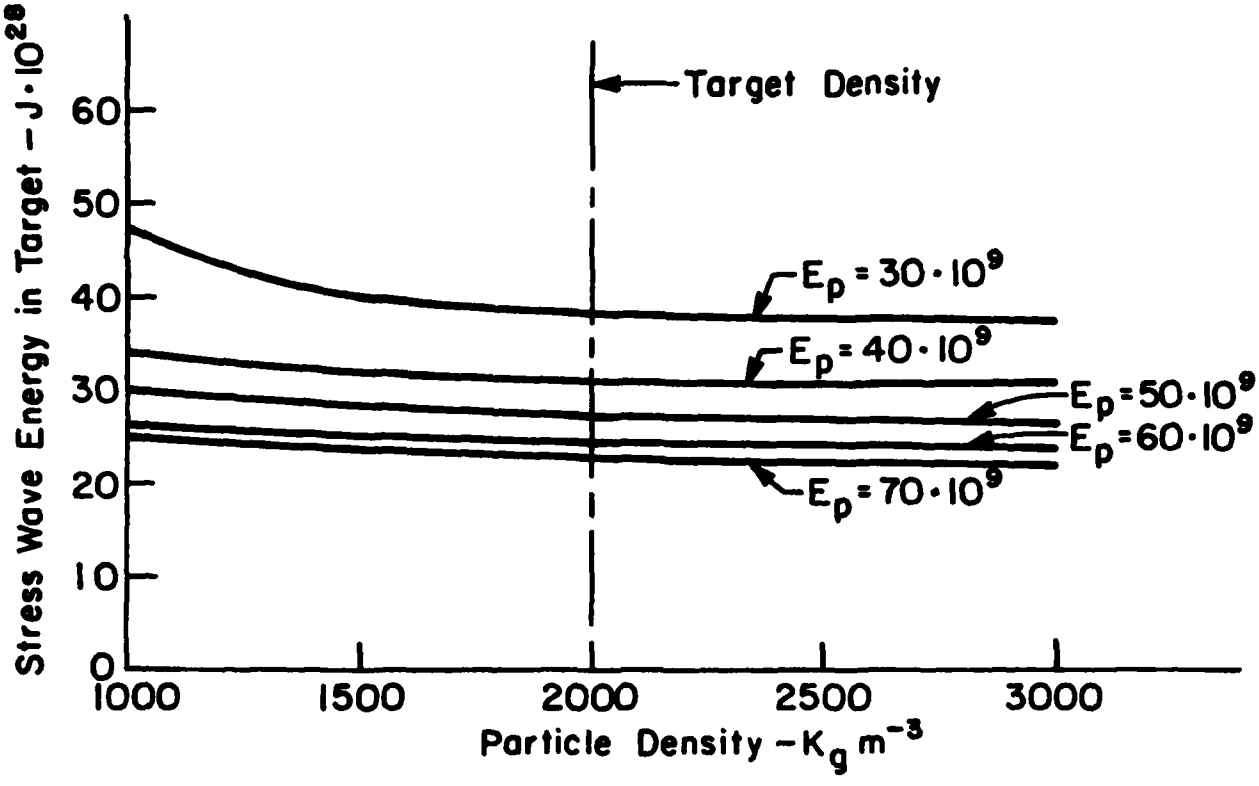

Figure 3a. Stress wave energy in target vs. particle density for fixed target properties and impact energy.

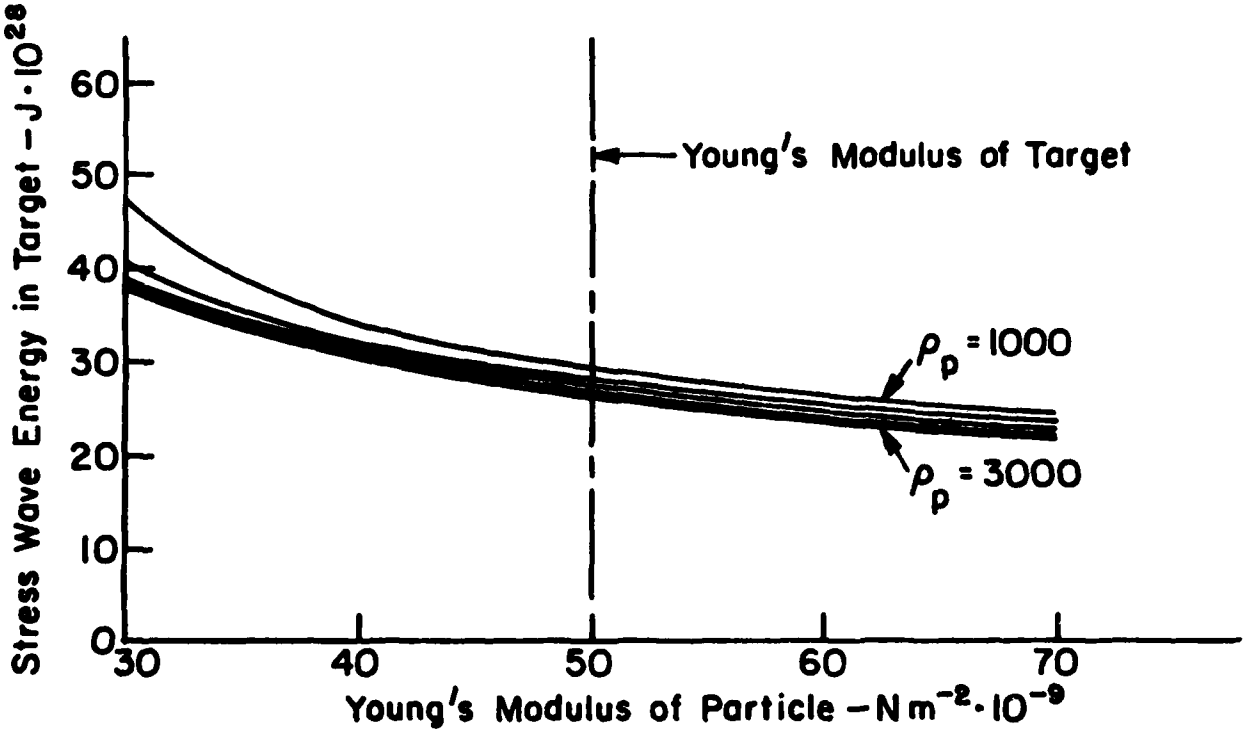

Figure 3b. Stress wave energy in target vs. Young's modulus of particle for fixed target properties and impact energy.

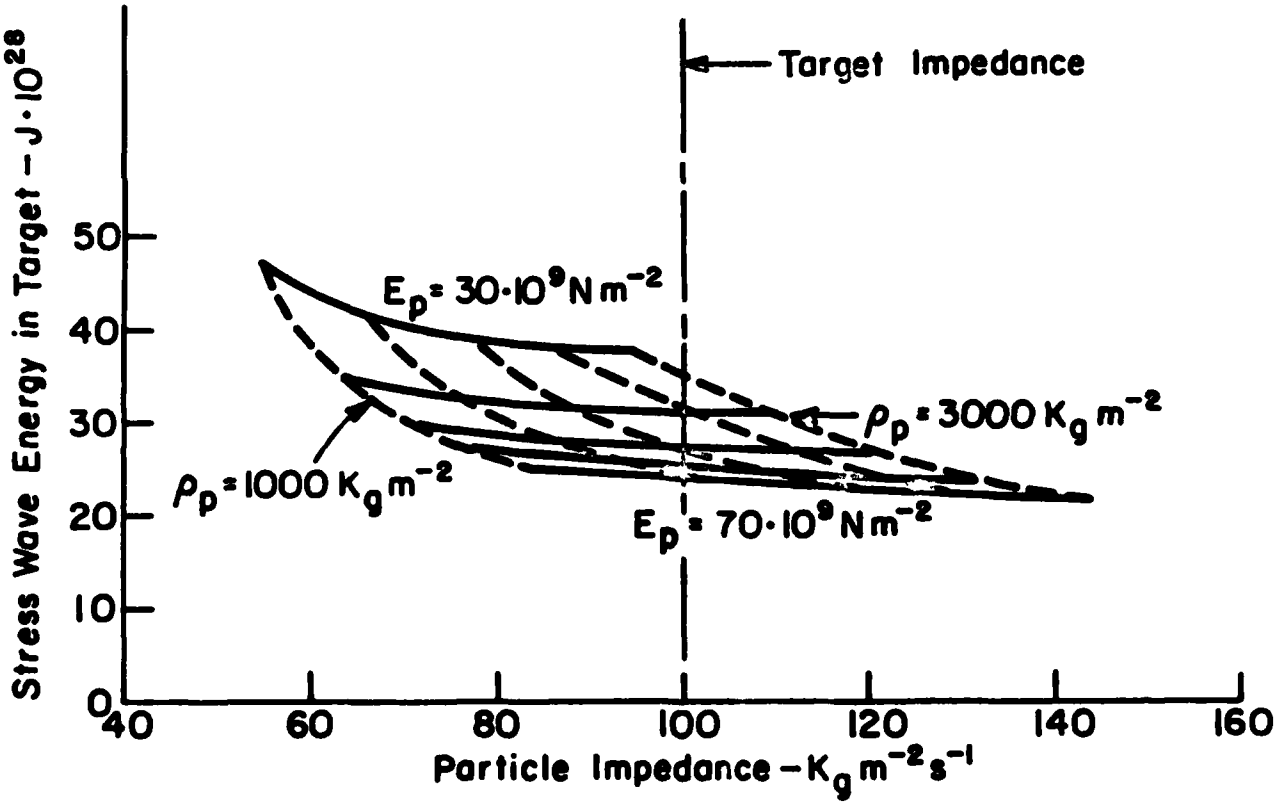

Figure 3c. Stress wave energy in target vs. particle impedance for fixed target properties and impact energy.

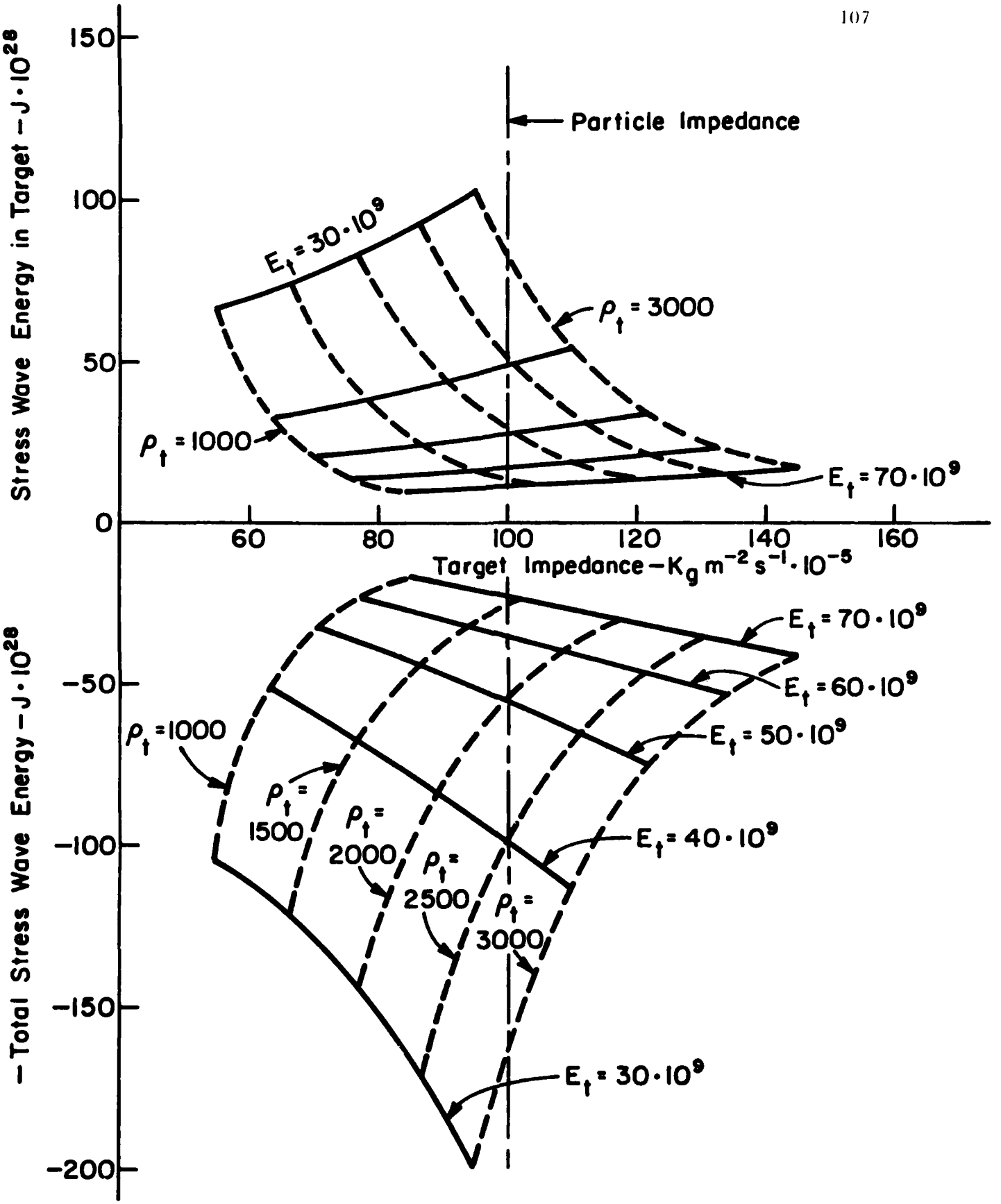

Figure 4a. Comparison of the stress wave energy in the target and total stress wave energy for fixed particle properties.

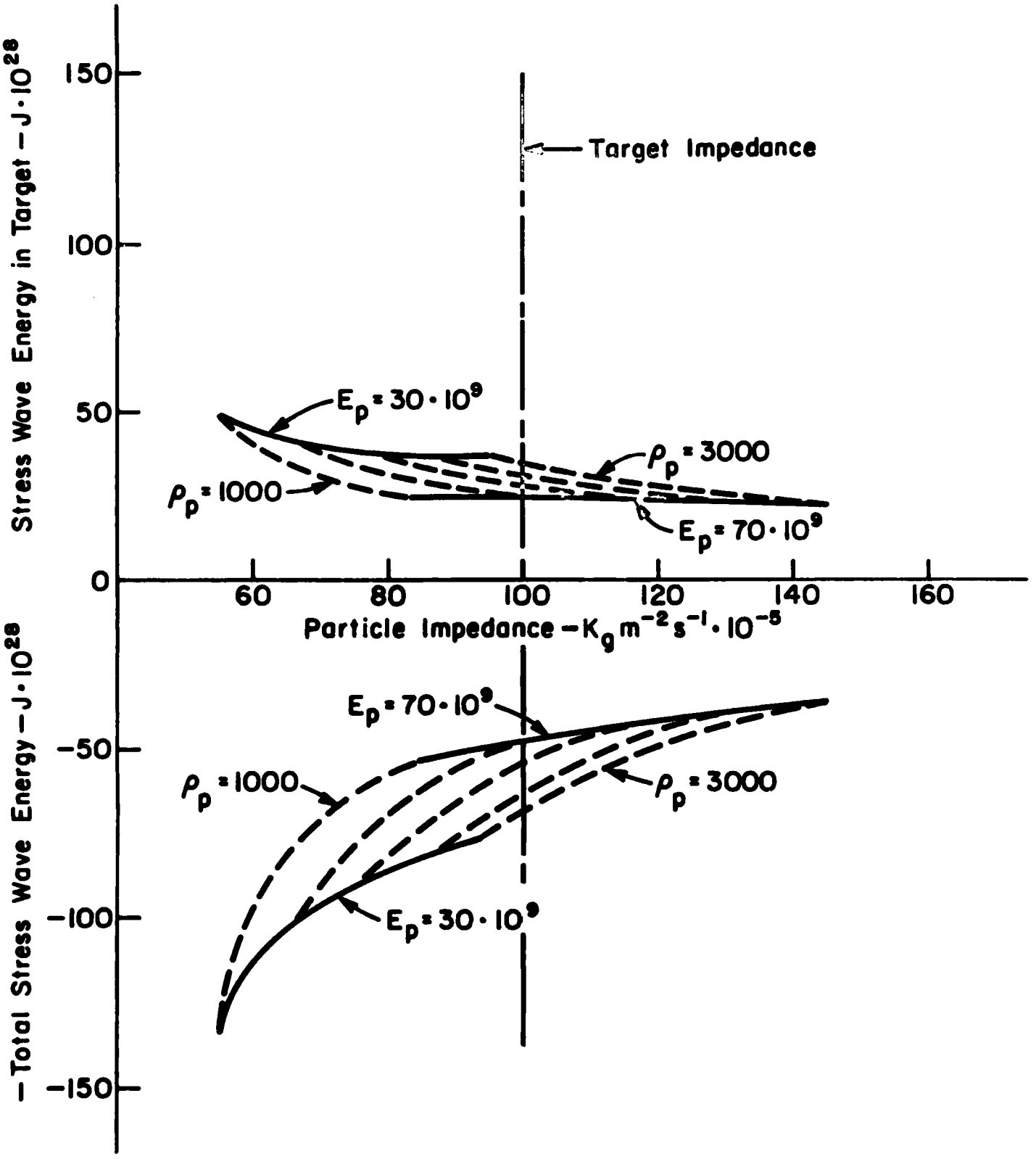

Figure 4b. Comparison of the stress wave energy in the target and the total stress wave energy for fixed target properties and impact energy.

In conclusion, the analysis of the variations of the total stress wave energy due to impact shows a very complex dependency upon target and projectile characteristics; in particular, these variations are very different when the impedance is varied at constant elasticity and when varied at constant density. In fact these variations are opposite. Furthermore, it can be noted that the asymmetry of the problem (i.e. non equivalence of energy when target and projectile characteristics are interchanged) is inherent to Miller and Pursey[11] derivation. The introduction of the impedance ratio tends to temper this asymmetry but, further investigations into the mechanics of the contact should be made to permit a physical explanation of this phenomenon.

V. COMPARISON OF THE THEORY WITH EXPERIMENTS USING GLASS

Kirchner and Gruver[3] determined the coefficient of restitution for impacts of glass spheres, 3mm in diameter, on firmly supported soda lime glass plates. They found that, at room temperature, the coefficient of restitution remained above 0.9 over a wide range of impact velocities (Figure 5). As shown in Figure 6, the present theory which assumes only stress wave energy losses yields similar results. The effect of the temperature dependence of density, Young's modulus and Poisson's ratio, was investigated using data of Duchateau and co-workers[12]. Assuming only stress wave energy losses, the effect of the variations in these properties with temperature on the coefficient of restitution is small (Figure 6). The energy loss varies as the square of the coefficient of restitution. The variation at 525°C is less than that at 440°C because the Poisson's ratio decreases sharply around the annealing temperature (500 - 550°C)[12].

These variations due to the stress wave energy losses do not account for the large decreases in coefficient of restitution observed at high velocities at 440 and 525°C. Therefore, the explanation based on increased crushing[3] remains the only explanation available. At higher temperatures 650 and 720°C, which are above the softening point, the variation of the coefficient of restitution with velocity is different from that observed at lower temperatures. Lower coefficients of restitution (higher energy losses) are observed at low impact velocities but the decreases are not

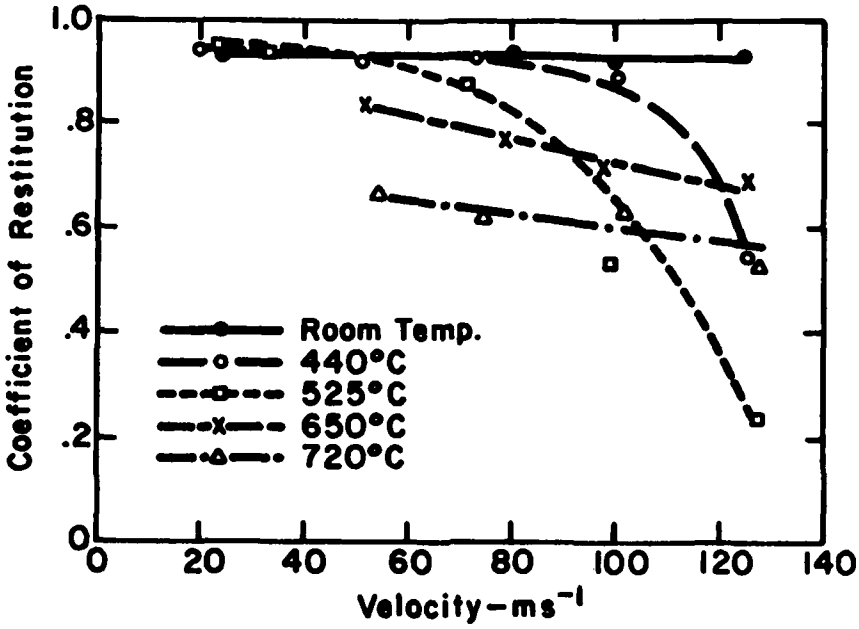

Figure 5. Coefficient of Restitution vs. Impact Velocity at various temperatures.

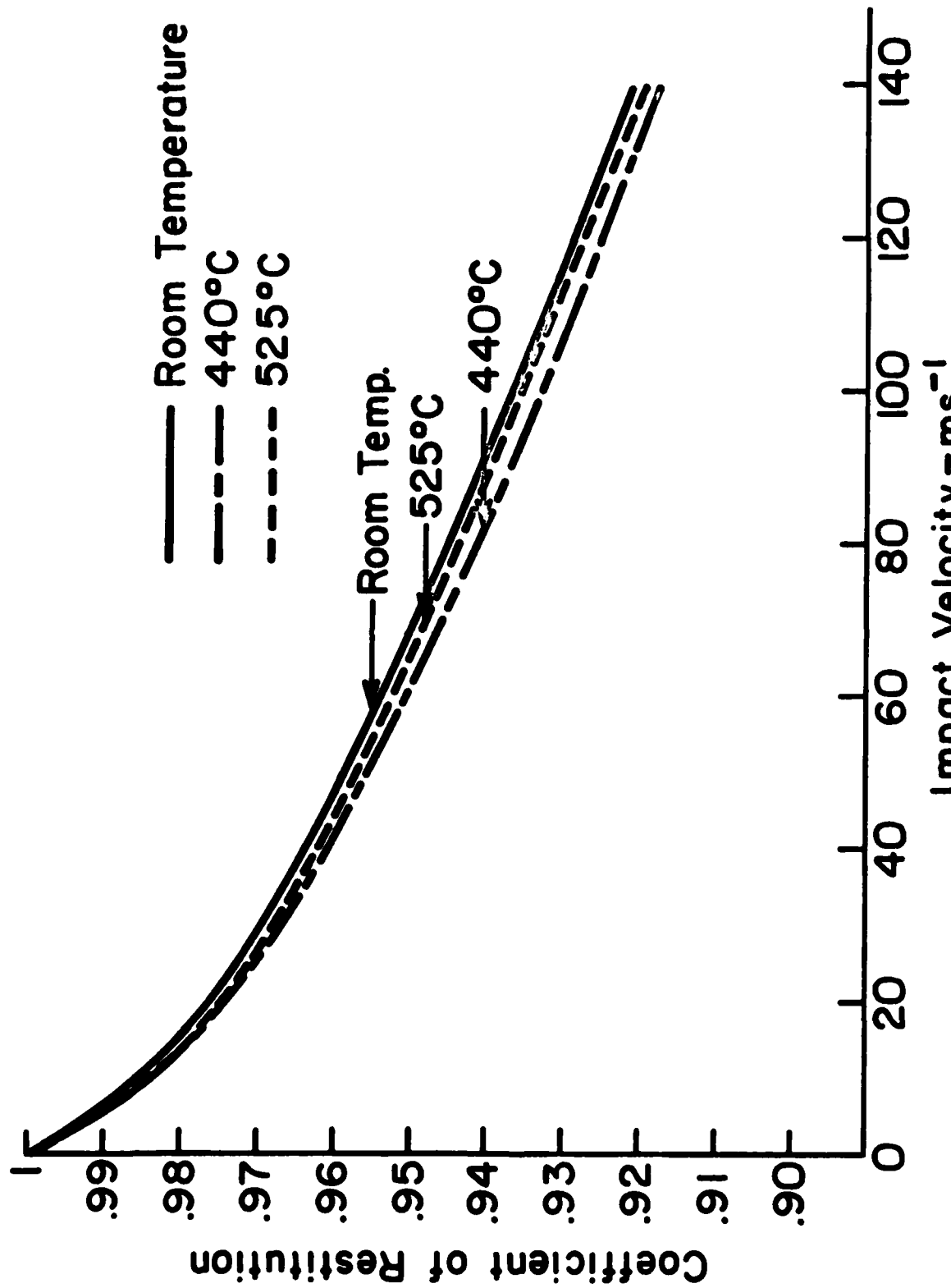

Figure 6. Coefficient of Restitution vs. Impact Velocity for impacts of glass spheres on glass plates at room temperature, 440°C and 550°C assuming only stress wave energy losses, data from Duchateau(12) and Doremus (13).

as great at higher velocities. At these higher temperatures, the glass deforms viscoelastically to form indentations. Because there is no threshold velocity or yield point for this viscoelastic deformation, the effects of the resulting energy losses are observed at all velocities. Therefore, it is reasonable to conclude that this change in shape of the coefficient of restitution vs. impact velocity curves is the result of the introduction of the indentation energy loss mechanism at temperatures above the softening point.

APPENDIX A

LIST OF SYMBOLS

a	Radius of the area of contact
c_{11}	Compressional elastic constant of the medium
c_{44}	Shear elastic constant of the medium
c_{0p}	Velocity of a longitudinal wave in a thin rod made of the same material as the impacting particle ($=\sqrt{E_p/\rho_p}$)
c_{0t}	Velocity of a longitudinal wave in a thin rod made of the same material as the target ($=\sqrt{E_t/\rho_t}$)
E_p	Young's modulus of the particle
E_t	Young's modulus of the target
$F_0(\xi)$	$(2\xi^2 - \gamma^2)^2 - 4\xi^2 (\xi^2 - 1)(\xi^2 - \gamma^2)^{\frac{1}{2}}$ (eq (1))
g	$\frac{1 - \sigma_t^2}{E_t} + \frac{1 - \sigma_p^2}{E_p}$ (eq (1))
$\vec{grad}$	gradient operator
$g_m(\zeta)$	Hankel's transform of order m
I_p	Wave intensity in the particle
I_t	Wave intensity in the target
$J_m(\cdot)$	Bessel's function of order m(mεQ)
K_1	$\omega(\rho_t/c_{11})^{\frac{1}{2}}$
K_2	$\omega(\rho_t/c_{44})^{\frac{1}{2}}$
m_p	Mass of the particle
m	Order of Bessel's function
n	Index characteristic of impedance ratio ($\rho_t c_{0t}/\rho_p c_{0p}$)

APPENDIX A (continued)

p	Applied stress
Q	Set of rational numbers
r	Radial dimension of a cylindrical system of coordinates
R_p	Radius of the particle
$\overrightarrow{rot}$	Rotational operator
t_c	Contact time between target and particle
$\vec{U}$	Vector displacement
u_r	Radial component of the displacement
u_θ	Angular component of the displacement
u_z	Axial component of the displacement
V_o	Impact velocity
v	Partial function for integration by parts
W_p	Stress wave energy in particle
W_t	Stress wave energy in target
W_s	Total stress wave energy
w	Partial function for integration by parts
Z_t	Target impedance
Z_p	Particle impedance
z	Axial dimension of a cylindrical system of coordinates
$\overline{zz}$	Axial stress at the free surface of the sphere
$\widehat{zr}$	Radial stress at the free surface of the sphere

APPENDIX A (continued)

γ	$\left[\frac{2(1-\sigma_t)}{(1-2\sigma_t)}\right]^{\frac{1}{2}}$ (eq (d))
Δ	dilatation (= divergence $\vec{U}$ = div $\vec{U}$)
ζ	Hankel's variable
θ	Angular dimension of a cylindrical system of coordinates
λ	Lamé constant
μ	Lamé constant
ξ	Dummy variable for integration
ρ_p	Density of the particle
ρ_t	Density of the target
σ_p	Poisson's ratio of the particle
σ_t	Poisson's ratio of the target
τ	$(1.068)^5 \quad (1 + \sigma_t) \quad (\frac{1-\sigma_t}{1-2\sigma_t})^{\frac{1}{2}} \; (\frac{16}{15})^{6/5} \; \beta(\sigma_t)$
ω	Angular frequency of a periodic phenomenon
∇^2	Laplacian operator $= \frac{1}{r}\frac{\partial}{\partial r}\left(r\frac{\partial}{\partial r}\right) + \frac{1}{r^2}\frac{\partial^2}{\partial \theta^2} + \frac{\partial}{\partial z^2}$ in a cylindrical system of coordinates

APPENDIX B

EQUIVALENCE OF THE STRESS WAVE ENERGY OF A SEMI-INFINITE SOLID AND SPHERE

Starting from the equation of elasticity

$$c_{11} \overrightarrow{\text{grad}}\, \Delta - c_{44} \overrightarrow{\text{rot}}\, \vec{W} = \rho_t \frac{\partial^2 \vec{U}}{\partial t^2} \tag{15}$$

in which $\vec{U}$ is the vector displacement

$\Delta = \text{div}\, \vec{U}$ is the dilation

$\vec{W} = \overrightarrow{\text{rot}}\, \vec{U}$ is the distortion

$c_{11} = \lambda + 2\mu$ linear combinations of the

$c_{44} = \mu$ Lamé constants λ and μ

To account for the time dependence, we assume the dependence on time to be harmonic so that (15) becomes

$$c_{11} \overrightarrow{\text{grad}}\, \Delta = c_{44} \overrightarrow{\text{rot}}\, \vec{W} + \rho_t \omega^2 \vec{U} = 0 \tag{16}$$

This equation projected on the axes z and r of a cylindrical system gives two of the equations necessary for the solution of the problem of stress waves in a sphere.

Taking the divergence and the curl of equation (16) yields two additional equations respectively characteristic of Δ and $\vec{W}$. Then, writing the stress across the free surface gives the last two required equations. These six equations are listed as follows:

$$c_{11} \frac{\partial \Delta}{\partial r} + c_{44} \frac{\partial W}{\partial z} + \rho_t \omega^2 u_r = 0 \tag{17}$$

$$c_{11} \frac{\partial \Delta}{\partial z} + \frac{c_{44}}{r} \frac{\partial (rW)}{\partial r} + \rho_t \omega^2 u_z = 0 \tag{18}$$

$$c_{11} \nabla^2 \Delta + \rho_t \omega^2 \Delta = 0 \tag{19}$$

$$\frac{\partial}{\partial r} \left(\frac{1}{r} \frac{\partial (rW)}{\partial r}\right) + \frac{\partial^2 W}{\partial z^2} + K_2^2 W = 0 \text{ with } K_2 = \omega \sqrt{\frac{\rho_t}{c_{44}}} \tag{20}$$

$$\frac{\rho \omega^2 \widehat{zz}}{c_{44}^2} = \frac{\partial}{\partial r} \left(r \frac{\partial W}{\partial r}\right) - \frac{\mu^2(\mu^2-2)}{r} \frac{\partial}{\partial r} \left(r \frac{\partial \Delta}{\partial r}\right) = \mu 4 \frac{\partial^2 \Delta}{\partial z^2} \tag{21}$$

$$\frac{\rho \omega^2 \widehat{zr}}{c_{44}^2} = \frac{\partial}{\partial r} \left(\frac{1}{r} \frac{\partial (rW)}{\partial r}\right) - 2\mu^2 \frac{\partial^2 \Delta}{\partial r \partial z} - \frac{\partial^2 W}{\partial z^2} \tag{22}$$

with $\mu^2 = \frac{c_{11}}{c_{44}}$.

To solve these equations one must eliminate r. This is done by the Hankel transform defined as

$$g_m(\zeta) = \int_0^\infty f(r) r \, J_n(r\zeta) \, dr \tag{23}$$

and its inverse

$$f(r) = \int_0^\infty g_m(\zeta) \, \zeta \, J_m(r\zeta) \, d\zeta \tag{24}$$

where $J_m(r\zeta)$ is a Bessel function of the mth order. Thus, the Hankel transform replaces the function f(r) by its transform $g_m(\zeta)$ independent of r. One further advantage of the Hankel's transform is to change a differentiation into a multiplication as in the case of Laplace's or

Fourier's transforms, and hence, change a partial differential equation with two variables into a differential equation. In fact, to take the transform of the derivative of f with respect to r

$$\int_0^\infty \frac{\partial f(r)}{\partial r} \, r \, J_m(r\zeta) \, dr \tag{25}$$

one must do an integration by parts by writing

$$v = r \, J_m(r\zeta) \tag{26a}$$

$$dw = \frac{\partial f(r)}{\partial r} \, dr \tag{26b}$$

which by differentiation of (26a)[14] and integration of (26b) gives

$$dv = \zeta r \, J_{m-1}(r\zeta) \, dr \tag{27a}$$

$$w = f(r) \tag{27b}$$

which combined with (26a) and (26b) gives the value of the integral (25)

$$\int_0^\infty \frac{\partial f(r)}{\partial r} \, r \, J_m(r\zeta) \, dr = \left[f(r) \, r \, J_m(r\zeta)\right]_0^\alpha - \zeta \int_0^\infty f(r) \, r \, J_{m-1}(r\zeta) \, dr \tag{28}$$

or

$$g_{m-1}\left(\frac{\partial f}{\partial r}\right) = \left[f(r) \, r \, J_m(r\zeta)\right]_0^\alpha - \zeta g_{m-1}(f) \tag{29}$$

As stated earlier, the Hankel transform has changed the derivative $g_m \frac{\partial f}{\partial r}$ into a multiplication $\zeta g_{m-1}(f)$ but it has also introduced the boundary conditions $\left[f(r) \, r \, J_m(r\zeta)\right]_0^\alpha$. In the case of a semi-infinite

solid these boundary conditions vanish. In the case of a sphere, they are a function of the bulk displacement and bulk distortion of the sphere. These displacements are due to the deformability of the sphere which allows the bulk vibrations of the sphere[15]. However, when the sphere is small, as in the case of particle impact, the frequency of the bulk vibrations is high so that they cannot be excited by the relatively low frequency impact pulse. Therefore, in most cases, these bulk vibrations can be neglected. If, in addition, we assume that no plastic deformation occurs in the sphere upon impact, the boundary conditions introduced by the Hankel's transform vanish as in the case of a semi-infinite solid. The derivation of the expression for the displacement thus follows that of Miller and Pursey[11].

ACKNOWLEDGMENTS

The authors are pleased to acknowledge the contributions of their associates at Ceramic Finishing Company and the sponsorship of the Office of Naval Research.

REFERENCES

1. H. Hertz "On the Contact of Elastic Solids" from Miscellaneous Papers, MacMillan and Co. Ltd., London (1896) p. 146.

2. S. C. Hunter "Energy Absorbed by Elastic Waves During Impact," J. Mech. Phys. Solids 5 162-171 (1957).

3. H. P. Kirchner and R. M. Gruver "Localized Impact Damage in a Viscous Medium" from Fracture Mechanics of Ceramics, Vol. 3, Flaws and Testing, Edited by R. C. Bradt, D. P. H. Hasselman and F. F. Lange, Plenum Publishing Corporation, New York (1978) p. 365.

4. G. F. Miller and H. Pursey "The Field and Radiation Impedance of Mechanical Radiators on the Free Surface of a Semi-Infinite Isotropic Solid," Proc. Roy. Soc. A223, 521-541 (1954).

5. G. F. Miller and H. Pursey "On the Partition of Energy Between Elastic Waves in a Semi-Infinite Solid," Proc. Roy. Soc. A233 55-69 (1955).

6. A. E. H. Love "Mathmatical Theory of Elasticity," Cambridge University Press, Cambridge (1920).

7. J. Mills "Integral Transform in Applied Mathmatics," Cambridge Univerisity Press, Cambridge (1971).

8. S. Columbo "La Transformation de Mellin et de Hankel," Application a la Physique Mathematique, Centre National de la Recherche Scientifique, Paris (1959).

9. P. M. Morse and K. V. Ingard "Theoretical Acoustics," McGraw-Hill Book Company, New York (1968).

10. H. P. Kirchner and R. M. Gruver "The Effect of Localized Damage on Energy Losses During Impact" Material Science and Engineering 33, 101-106 (1978).

11. J. P. A. Tillet "A Study of the Impact of Spheres on Plates," Proc. Phys. Soc. B, 67, 667 (1954).

12. J. Duchateau, C. Georgeon, M. Schneegans "Etude des Caracteristiques de Propagation des Ultra-Sons dans les Milieux Vitreux. Applications aux mesures de Quelques Proprieter Physiques des Verres" from Communications Scientifiques et Techniques. 1. Sujet Scientifiques et Recherches de Base. Congres International du Verre Versailles 27 Septembre-2 Octobre 1971, Edite par P. Institut de Verre Paris (1971), p.573.

13. R. H. Doremus "Glass Science," John Wiley & Sons, New York (1973).

14. G. N. Watson "A Treatise on the Theory of Bessel Functions," Cambridge University Press, Cambridge (1922).

15. E. Schreiber, O. L. Anderson and N. Soga "Elastic Constants and their Measurement," McGraw-Hill Book Company, New York (1973).

BASIC DISTRIBUTION LIST

Technical and Summary Reports

Organization	No. of Copies
Defense Documentation Center Cameron Station Alexandria, Virginia 22314	(12)
Office of Naval Research Department of the Navy Arlington, Virginia 22217	
Attn: Code 471	(1)
Code 102	(1)
Code 470	(1)
Commanding Officer Office of Naval Research Branch Office 495 Summer Street Boston, Massachusetts 02210	(1)
Commanding Officer Office of Naval Research Branch Office 536 South Clark Street Chicago, Illinois 60605	(1)
Office of Naval Research San Francisco Area Office One Hallidie Plaza Suite 601 San Francisco, CA 94102	(1)
Naval Research Laboratory Washington, D.C. 20390	
Attn: Code 6000	(1)
Code 6100	(1)
Code 6300	(1)
Code 6400	(1)
Code 2627	(1)
Naval Air Development Center Code 302 Warminster, Pennsylvania 18974 Attn: Mr. F. S. Williams	(1)
Naval Air Propulsion Test Center Trenton, New Jersey 08628 Attn: Library	(1)
Naval Construction Batallion Civil Engineering Laboratory Port Hueneme, California 93043 Attn: Materials Division	(1)
Naval Electronics Laboratory Center San Diego, California 92152 Attn: Electron Materials Sciences Division	(1)
Naval Missile Center Materials Consultant Code 3312-1 Point Mugu, California 93041	(1)
Commanding Officer Naval Surface Weapons Center White Oak Laboratory Silver Spring, Maryland 20910 Attn: Library	(1)
David W. Taylor Naval Ship R&D Center Materials Department Annapolis, Maryland 21402	(1)
Naval Undersea Center San Diego, California 92132 Attn: Library	(1)
Naval Underwater System Center Newport, Rhode Island 02840 Attn: Library	(1)
Naval Weapons Center China Lake, California 93555 Attn: Library	(1)
Naval Postgraduate School Monterey, California 93940 Attn: Mechanical Engineering Dept.	(1)
Naval Air Systems Command Washington, D.C. 20360	
Attn: Code 52031	(1)
Code 52032	(1)
Code 320	(1)

BASIC DISTRIBUTION LIST (Cont'd)

Organization	No. of Copies
Naval Sea System Command Washington, D.C. 20362 Attn: Code 035	(1)
Naval Facilities Engineering Command Alexandria, Virginia 22331 Attn: Code 03	(1)
Scientific Advisor Commandant of the Marine Corps Washington, D.C. 20380 Attn: Code AX	(1)
Naval Ship Engineering Center Department of the Navy CTR BG #2 3700 East-West Highway Prince Georges Plaza Hyattsville, Maryland 20782 Attn: Engineering Materials and Services Office, Code 6101	(1)
Army Research Office Box CM, Duke Station Durham, North Carolina 27706 Attn: Metallurgy & Ceramics Div.	(1)
Army Materials and Mechanics Research Center Watertown, Massachusetts 02172 Attn: Res. Programs Office (AMXMR-P)	(1)
Air Force Office of Scientific Research Bldg. 410 Bolling Air Force Base Washington, D.C. 20332 Attn: Chemical Science Directorate Electronics and Solid State Sciences Directorate	(1) (1)
Air Force Materials Lab (LA) Wright-Patterson AFB Dayton, Ohio 45433	(1)
NASA Headquarters Washington, D.C. 20546 Attn: Code RRM	(1)
NASA Lewis Research Center 21000 Brookpark Road Cleveland, Ohio 44135 Attn: Library	(1)
National Bureau of Standards Washington, D.C. 20234 Attn: Metallurgy Division Inorganic Materials Division	(1) (1)
Defense Metals and Ceramics Information Center Battelle Memorial Institute 505 King Avenue Columbus, Ohio 43201	(1)
Director Ordnance Research Laboratory P.O. Box 30 State College, Pennsylvania 16801	(1)
Director Applied Physics Laboratory University of Washington 1013 Northeast Fortieth Street Seattle, Washington 98105	(1)
Metals and Ceramics Division Oak Ridge National Laboratory P.O. Box X Oak Ridge, Tennessee 37380	(1)
Los Alamos Scientific Laboratory P.O. Box 1663 Los Alamos, New Mexico 87544 Attn: Report Librarian	(1)
Argonne National Laboratory Metallurgy Division P.O. Box 229 Lemont, Illinois 60439	(1)

SUPPLEMENTARY DISTRIBUTION LIST

Technical and Summary Reports

Organization	No. of Copies
Dr. W.F. Adler Effects Technology Inc. 5383 Hollister Avenue P.O. Box 30400 Santa Barbara, CA 92105	(1)
Dr. G. Bansal Battelle 505 King Avenue Columbus, OH 43201	(1)
Dr. R. Bratton Westinghouse Research Lab. Pittsburgh, PA 15235	(1)
Dr. A.G. Evans Rockwell International P.O. Box 1085 1049 Camino Dos Rios Thousand Oaks, CA 91360	(1)
Mr. E. Fisher Ford Motor Co. Dearborn, MI	(1)
Dr. P. Gielisse University of Rhode Island Kingston, RI 02881	(1)
Dr. M.E. Gulden International Harvester Company Solar Division 2200 Pacific Highway San Diego, CA 92138	(1)
Dr. D. P. H. Hasselman Virginia Polytechnic Institute and State University Dept. of Materials Engineering Blacksburg, VA. 24061	(1)
Mr. G. Hayes Naval Weapons Center China Lake, CA 93555	(1)
Professor A.H. Heuer Case Western Reserve University University Circle Cleveland, OH 44106	(1)
Dr. R. Hoagland Battelle 505 King Avenue Columbus, OH 43201	(1)
Dr. R. Jaffee Electric Power Research Institute Palo Alto, CA	(1)
Dr. P. Jorgensen Stanford Research Institute Poulter Laboratory Menlo Park, CA 94025	(1)
Dr. R.N. Katz Army Materials and Mechanics Research Center Watertown, MA 02171	(1)
Dr. H. Kirchner Ceramic Finishing Company P.O. Box 498 State College, PA 16801	(1)
Dr. B. Koepke Honeywell, Inc. Corporate Research Center 500 Washington Avenue, South Hopkins, MN 55343	(1)
Mr. Frank Koubek Naval Surface Weapons Center White Oak Laboratory Silver Spring, MD 20910	(1)
E. Krafft Carborundum Co. Niagara Falls, NY	(1)

BASIC DISTRIBUTION LIST (Cont'd)

Organization	No. of Copies
Brookhaven National Laboratory Technical Information Division Upton, Long Island New York 11973 Attn: Research Library	(1)
Library Building 50 Room 134 Lawrence Radiation Laboratory Berkeley, California	(1)
Dr. J. D. Buch Prototype Development Assoc., Inc. 1740 Garry Avenue, Suite 201 Santa Ana, CA 92705	(1)
Dr. B. Budiansky Harvard University Department of Engineering and Applied Science Cambridge, MA 02138	(1)
Professor H. Conrad University of Kentucky Materials Department Lexington, KY 40506	(1)
Dr. A. Cooper Case Western Reserve University Materials Department Cleveland, OH 44106	(1)
Dr. I. Finney University of California Berkeley, CA 94720	(1)
Mr. A. A. Fyall Royal Aircraft Establishment Farnborough, Hants UNITED KINGDOM	(1)
Dr. R. Jaffee Electric Power Research Institute Palo Alto, CA	(1)
Dr. L. Rubin Aerospace Corporation P.O. Box 92957 Los Angeles, CA 90009	(1)
Dr. G. Schmidt Air Force Materials Laboratory Wright-Patterson AFB Dayton, OH 54533	(1)
Dr. D. A. Shockey Stnaford Research Institute Poulter Laboratory Menlo Park, CA 94025	(1)
Mr. T. Derkus TRW Cleveland, OH 44117	(1)
Dr. S. Hart Naval Research Laboratory Washington, DC 20375	(1)
Professor G. Kino Stanford University Palo Alto, CA 94305	(1)
Dr. J. Krumhansl Physics Department Cornell University Ithica, NY 14850	(1)
Dr. R. E. Loehman University of Florida Ceramics Division Gainesville, FL 32601	(1)
Dr. D. Mulville Office of Naval Research Code 474 800 North Quincy Street Arlington, VA 22217	(1)
Dr. N. Perrone Office of Naval Research Code 474 800 North Quincy Street Arlington, VA 22217	(1)
Dr. J. R. Rice Brown University Division of Engineering Providence, RI 02912	(1)

SUPPLEMENTARY DISTRIBUTION LIST (Cont'd)

Organization	No. of Copies
Dr. S.A. Bortz IITRI 10 W. 35th Street Chicago, IL 60616	(1)
Dr. Stan Wolf Division of Materials and Science Department of Energy Washington, DC 20545	(1)
Dr. W.G.D. Frederick Air Force Materials Laboratory Wright-Patterson AFB Dayton, OH 45433	(1)
Dr. P. Land Air Force Materials Laboratory Wright-Patterson AFB Dayton, OH 45433	(1)
Mr. K. Letson Redstone Arsenal Huntsville, AL 35809	(1)
Dr. S. Freiman Naval Research Laboratory Code 6363 Washington, DC 20375	(1)
Director Materials Sciences Defense Advanced Research Projects Agency 1400 Wilson Boulevard Arlington, VA 22209	(1)
Dr. James Pappis Raytheon Company Research Division 28 Seyon Street Waltham, MA 02154	(1)
Major W. Simmons Air Force Office of Scientific Research Building 410 Bolling Air Force Base Washington, DC 20332	(1)
Dr. P. Becher Naval Research Laboratory Code 6362 Washington, DC 20375	(1)
Mr. L.B. Weckesser Applied Physics Laboratory Johns Hopkins Road Laurel, MD 20810	(1)
Mr. D. Richerson AiResearch Manufacturing Company 4023 36th Street P.O. Box 5217 Phoenix, AZ 85010	(1)
Dr. H.E. Bennett Naval Weapons Center Code 3818 China Lake, CA 93555	(1)
Mr. G. Denman Air Force Materials Laboratory Code LPJ Wright-Patterson AFB Dayton, OH 45433	(1)
Dr. D. Godfrey Admiralty Materials Laboratory Polle, Dorset BH16 6JU UNITED KINGDOM	(1)
Dr. N. Corney Ministry of Defense The Adelphi John Adam Street London WC2N 6BB UNITED KINGDOM	(1)

SUPPLEMENTARY DISTRIBUTION LIST (Cont'd)

Organization	No. of Copies
Dr. F.F. Lange Rockwell International P.O. Box 1085 1049 Camino Dos Rios Thousand Oaks, CA 91360	(1)
Dr. J. Lankford Southwest Research Institute 8500 Culebra Road San Antonio, TX 78284	(1)
Library Norton Company Industrial Ceramics Division Worcester, MA 01606	(1)
State University of New York College of Ceramics at Alfred University Attn: Library Alfred, NY 14802	(1)
Dr. L. Hench University of Florida Ceramics Division Gainesville, FL 32601	(1)
Dr. N. MacMillan Materials Research Laboratory Pennsylvania State University College Park, PA 16802	(1)
Mr. F. Markarian Naval Weapons Center China Lake, CA 93555	(1)
Dr. Perry A. Miles Raytheon Company Research Division 28 Seyon Street Waltham, MA 02154	(1)
Mr. R. Rice Naval Research Laboratory Code 6360 Washington, D.C. 20375	(1)
Dr. J. Ritter University of Massachusetts Department of Mechanical Engineering Amherst, MA 01002	(1)
Professor R. Roy Pennsylvania State University Materials Research Laboratory University Park, PA 16802	(1)
Dr. R. Ruh AFML Wright-Patterson AFB Dayton, OH 45433	(1)
Mr. J. Schuldies AiResearch Phoenix, AZ	(1)
Professor G. Sines University of California, Los Angeles Los Angeles, CA 90024	(1)
Dr. N. Tallan AFML Wright-Patterson AFB Dayton, OH 45433	(1)
Dr. T. Vasilos AVCO Corporation Research and Advanced Development Division 201 Lowell Street Wilmington, MA 01887	(1)
Mr. J.D. Walton Engineering Experiment Station Georgia Institute of Technology Atlanta, GA 30332	(1)
Dr. S.M. Widerhorn Inorganic Materials Division National Bureau of Standards Washington, DC 20234	(1)

SUPPLEMENTARY DISTRIBUTION LIST (Cont'd)

Organization	No. of Copies
Dr. L.M. Gillin Aeronautical Research Laboratory P.O. Box 4331 Fisherman's Bend Melbourne, VIC 3001 AUSTRALIA	(1)
Dr. R. A. Tanzilli General Electric Company Reentry and Environmental Systems Division 3198 Chestnut Street Philadelphia, PA 19101	(1)
Professor John Field University of Cambridge New Cavendish Laboratory Cambridge, UNITED KINGDOM	(1)
Dr. B. R. Lawn National Bureau of Standards Washington, D. C. 20234	(1)